POLITECNICO DI MILANO

DEPARTMENT OF CIVIL AND ENVIRONMENTAL ENGINEERING

MASTER OF SCIENCE IN

CIVIL ENGINEERING FOR RISK MITIGATION

Lateral Response of Single and Groups of Fixed Head Piles

Author:

Kasra Majdanishabestari

Matricola: 872111

Supervisor:

Prof. Roberto Paolucci

Co-Supervisors:

Ing. Bruno Becci

Dr. Ali Güney Özcebe

ACADEMIC YEAR 2018/2019

Abstract

Being a fundamental part of the family of soil-structure interaction (SSI) engineering problems, soil-piled foundation-structure interaction constitutes an important part of everyday practice in civil, structural, and geotechnical engineering. While the behavior of the system under gravity conditions are rather well consolidated, estimation of ultimate lateral capacity is still often disregarded.

As a current state of practice, there are already well-developed complete methodologies based on p-y curves that are able to predict with a good accuracy the whole response of single piles (e.g. Naggar and Bentley, 2000). Furthermore, p-y curves approach is already implemented into various design guidelines (e.g. ASCE Guidelines, 1984). The group effects on each pile (taking into account of "shadowing effects") in piled foundations are traditionally represented by p-multipliers (e.g. Brown et al., 1988).

In this thesis, first a numerical campaign of laterally loaded pile groups with fixed head conditions, and hybrid model is presented. By means of commercial code FLAC3D (continuum model) and SeismoStruct2018 (p-y curve approach model), responses of single piles as well as the foundations are thoroughly studied and verified by considering a variety of different geometrical and constitutive parameters. As the outcome, a compilation of foundation group efficiency factors is assembled based on the results of the numerical analyses. Then, a simple-to-apply design method in the estimation of foundation group efficiency factor is proposed, which is based on the extension of classical Broms method. Comparisons of foundation group efficiency factors computed through theoretical and numerical means show reasonably close agreement. Finally, a worked example regarding the application of the proposed simplified method is implemented in a spreadsheet.

Keywords: single pile, pile group, p–y method, group reduction factor, soil–pile interaction, continuum model, hybrid model, ultimate lateral capacity, simplified method

Acknowledgements

First, I would like to thank my supervisor professor Dr. Roberto Paolucci and co-supervisor professor and researcher Dr. Ali Güney Özcebe and to express my gratitude to Ing. Bruno Becci for all their dedication and exceptional guidance during the development of this investigation. Special thanks to ITASCA consulting company for providing a Full-License FLAC3D software by the educational purpose, CEAS s.r.l Company for providing me their super-computers, data and organizing tutorial classes by their expert Ing. Marco Carni to improve my FLAC3D skills at Harpa-Ceas.

Given the fact that my co-supervisor Dr. Özcebe is a post-doc researcher at Università degli Studi di Pavia, Department of Civil Engineering and Architecture - DICAr, I would like to also thank this institution.

Academic license of SeismoStruct2018 provided by Seismosoft is kindly acknowledged.

Lovely and huge thanks go to my mother Parivash Amirfiroozkoohi, my Father Saeid Majdanishabestari and my Brother Babak Majdanishabestari for all their support during this time and to my family and friends as well for all you best wish that have given to me.

A big thank you goes to all my colleagues and classmates with whom I have shared lectures, studies, and experiences, to all professors from who I have learned many things that have made me a better person and professional as well.

…and thanks to all my special persons in the past, the present… and the future.

Contents

Lateral Response of Single and Group of Fixed Head Piles Subjected to Lateral Loads:

Figures

CHAPTER 1
INTRODUCTION

All engineering structures involve some type of structural element with direct contact with ground. When external forces act on these systems, structural and soil displacements at foundation level must show compatibility so as to satisfy the stability condition. The process in which the response of the soil influences the motion of the structure and the motion of the structure influences the response of the soil is termed as soil-structure interaction or SSI (Luco, 1982).

Under gravity-only conditions, SSI is considered to be static and fundamentally along vertical direction. Once a lateral force component is present (such as wind and earthquakes), horizontal SSI emerges to impose a key importance. As a matter of fact, damage sustained in recent earthquakes, such as the 1995 Kobe earthquake, have also highlighted that the seismic behavior of a structure is highly influenced not only by the response of the superstructure, but also by the response of the foundation and the ground as well. Hence, the modern seismic design codes, such as standard specifications for concrete structures: seismic performance verification JSCE 2007 stipulate that the response analysis should be conducted by taking into consideration a whole structural system including superstructure, foundation and ground.

Depending on the soil conditions, structural and loading configurations, foundation system may desire the installation of piles that will not only impose a lateral inertial interaction at slab level, but also a kinematic interaction between the surrounding soil both at slab level and along the length of the piles.

Overall, the theoretical framework lateral kinematic interaction between the foundation system and soil is well established (traditionally through p-y curves) for single pile case (like large-diameter caisson foundations). On the other hand, group effect of closely spaced foundation systems is still a topic of ongoing research.

The main scope of this thesis is to present a numerical dataset and a theoretical framework investigating the monotonic load-displacement relation of fixed-head closely spaced foundation systems utilizing elastic and elasto-plastic hypotheses for the piles. The organization of the specified chapters will be as follows:

- Chapter 2: Background information on the use of piles and definition of the p-y curves
- Chapter 3: Lateral response of single pile, row of piles and pile groups and background information and failure modes
- Chapter 4: Numerical case studies presenting the response of single piles under linear and nonlinear pile response through 3D numerical analysis and p-y approach through Commercial code FLAC3D and SeismoStruct2018
- Chapter 5: Numerical case study of a 3x3 pile group under linear and nonlinear pile response modeled by FLAC3D and SeismoStruct2018, calculation of the group effect factor from the results obtained
- Chapter 6: An extensive numerical dataset toward the definition of a new group efficiency proposal and simplified method
- Chapter 7: A proposal for closed form assessment of group effect
- Chapter 8: Conclusions

CHAPTER 2
GENERAL USE OF PILES

2.1 Pile foundations usage

Pile foundations are structural members traditionally used to support the gravity (i.e. vertical) loads (Das, 2016) to transmit the load of the superstructure to the lower resistant layers of the soil. Two most common cases of pile group use are summarized as below:

- **Weak soil layer at surface:** Weak layer cannot support the weight of the building, so the loads of the building must bypass this layer and be transferred to the layer of stronger soil or rock that is below the weak layer. Such transfer mechanism may be through skin friction (in friction piles) and/or through tip resistance (in end piles);

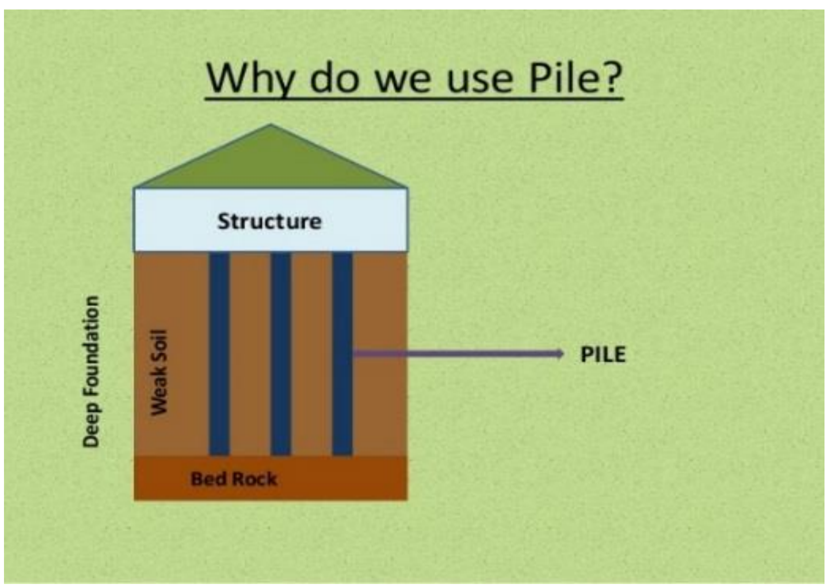

Figure 2-1 Weak soil layer at surface (Chellis, 1951)

- **Heavy weighted superstructures on the foundation:** In certain situations, even if the soil layers do not show weakness, their bearing capacity may not be enough to support very heavy superstructures exerting significant vertical pressures to superficial soil layers, such as in the case of high-rise structure foundations.

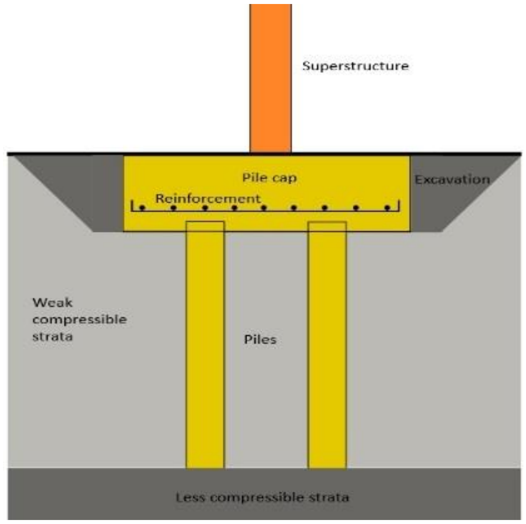

Figure 2-2 High concentrated load on foundations (Chellis, 1951)

There are two fundamental types of piles as end bearing and friction piles. Selection of pile type is dependent both on distribution of the soil layers and/or economic aspects of the engineering project under consideration. Below, definitions of such systems are described (Chellis, 1951)

- **Friction piles**: Pile transfers the load of the building to the soil across the full height of the pile, by friction. In other words, the entire surface of the pile, which is cylindrical in shape, works to transfer the forces to the soil.

- **End bearing piles**: In end bearing piles (as in Figure 1-right), the bottom end of the pile rests on a layer of especially strong soil or rock. The load of the building is transferred through the pile to the strong layer. In a sense, this pile acts like a column embedded in the soil. The key principle is that the bottom end rests on the surface which is the intersection of a weak and strong layer. The load therefore bypasses the weak layer and is safely transferred to the strong layer.

2.2 Lateral response of the piles

Piles are not only subjected to vertical loadings coming from the superstructure, but also to lateral loads coming from inclined loads, wind, waves, earthquakes, etc. It has been noticed in the past that piles have faced major damages due to lateral loads (McVay., et al., 1995). For laterally loaded piles, two types of failure mechanism are usually considered. The first type of failure mechanism usually occurs at relatively shallow depths involves the failure of a wedge of soil in front of the pile with a gap forming behind the pile. The second type of failure mechanism occurs at greater depth and represented by plastic flow of the soil around the pile as it deflects laterally. The depth at which these two failure mechanisms predict the same ultimate soil resistance is known as critical depth (Zcr). The ultimate soil resistance up to critical depth varies with depth but below critical depth it is taken constant. (Randolph & Susan, 2011). Development of p-y curves for monopiles in Clay using Finite Element Model Plaxis 3D Foundation.

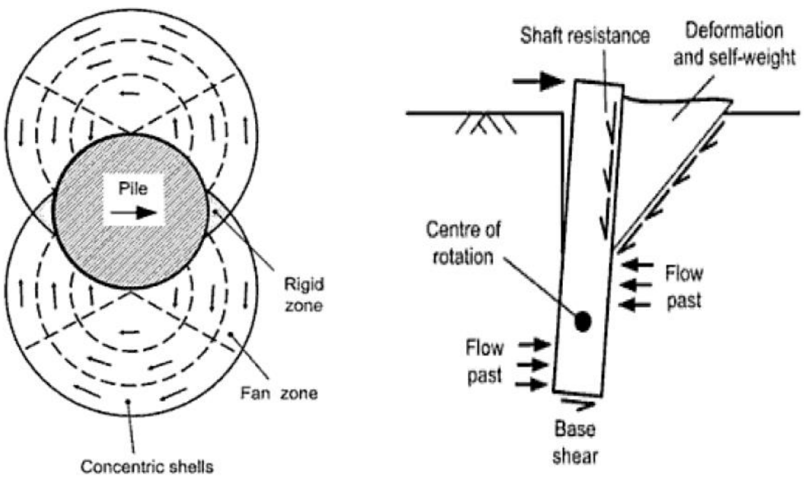

Figure 2-3 Lateral Response of the Pile (Randolph & Susan, 2011)

Currently, there are already code-based simplified approaches based on p-y curves able to predict with a good accuracy the whole response of the single piles (e.g. Naggar and Bentley, 2000). Furthermore, considering the relative motion of a cylindrical geometry with respect to surrounding soil, similar type of p-y curves approach is already implemented into various design guidelines (e.g. ASCE Guidelines, 1984).

2.3 P-Y curves method:

The p-y analysis is a numerical model that simulates the soil resistance as predefined nonlinear springs, where p is the soil pressure per unit length of the pile and y is the pile deflection. The soil is represented by a series of nonlinear p-y curves that vary with depth and soil type. The p-y curve for a particular point on a foundation depends on many factors, such as:

- Soil type

- Type of loading (static, dynamic, monotonic, cyclic or combinations thereof)
- Foundation diameter and cross-sectional shape
- Coefficient of friction between foundation and soil
- Depth below the ground surface
- Head boundary conditions
- Foundation construction methods
- Group interaction effects.

The influence of these factors is not well established, so it has been necessary to develop p-y curves empirically by back-calculating them from full-scale load tests. Soil reactions can be modelled by means of uncoupled non-linear elastoplastic "springs", accounting for permanent pile deflections and even for possible softening behavior of the soil. Each soil layer is assumed to be independent of each other. Continuity of displacement is then only due to structural bending stiffness (e.g. Naggar and Bentley, 2000).

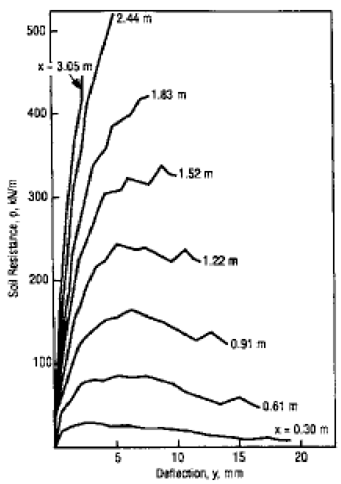

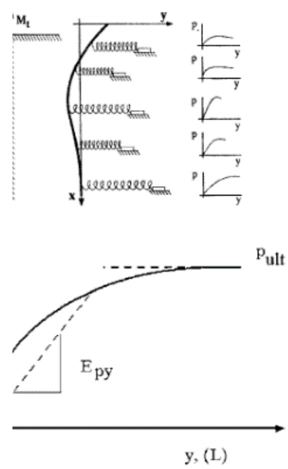

Figure 2-4 p-y curve and definition of independent springs

The accuracy of such empirical methods depends upon the data from which it was developed. The reliability of the approach is based on the number of tests (Kramer, 1988). The most commonly used p-y curve criteria (Matlock, 1970) is based on a very limited number of tests. The slope of p-y curve at any deflection represents the tangent soil stiffness at that deflection. The ratio p/y at any deflection represents the secant soil stiffness corresponding to that deflection (Kramer, 1988). The reference displacement (yc) is taken as the displacement of pile that will occur at 50% of the ultimate soil resistance. The ultimate soil resistance occurs at a displacement of yu and beyond these remains' constant for ideally plastic clays (Kodikara, Haque, & Lee,2010).

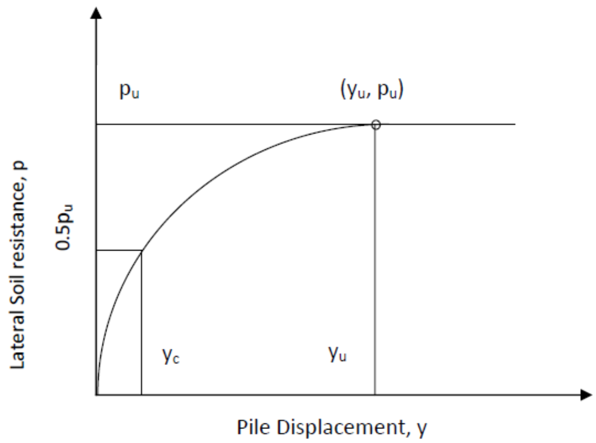

Figure 2-5 Typical p-y curve and parameters

The p-y method is a method of analyzing the ability of deep foundations to resist loads applied in the lateral direction. This method uses the finite difference method and p-y graphs to find a solution. P-y graphs are graphs which relate the force applied to soil to the lateral deflection of the soil. In another words, the p-y analysis is a numerical model that simulates the soil resistance as predefined nonlinear springs, where p is the soil pressure per unit length of the pile and y is the pile deflection. In essence, non-linear springs are attached to the foundation in place of the soil. The springs can be represented by the following equation:

$P = k*y$

where k is the non-linear spring stiffness defined by the p-y curve, y is the deflection of the spring, and p is the force applied to the spring. The p-y curves vary depending on soil type.

2.4 Group of Piles:

Depending on its position in the group, the behavior of a pile within a pile group may differ substantially from that of a pile alone. There would be also different kind of failure for group of the piles illustrated below (McVay., et al., 1995). Engineers will usually group a few piles together, and top them with a pile cap. A pile cap is a very thick cap of concrete that extends over a small group of piles, and serves as a base on which a column can be constructed. The load of this column is then distributed to all the piles in the group.

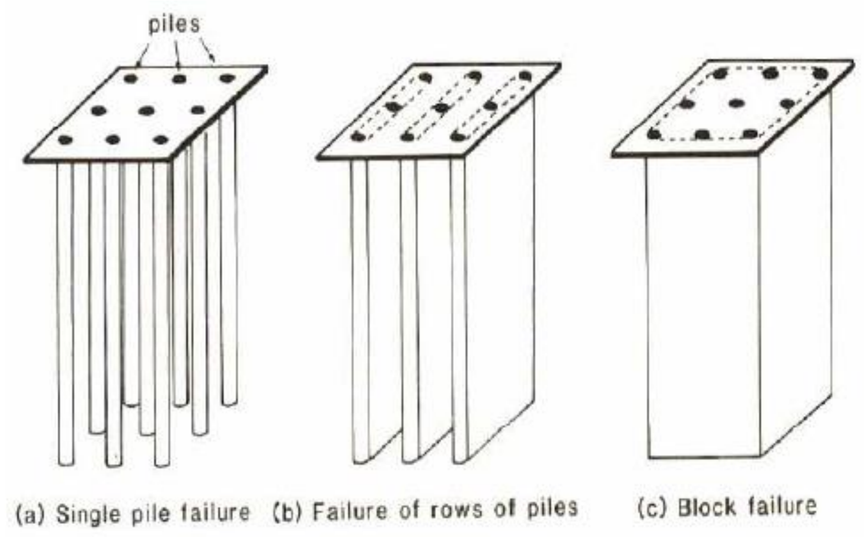

Figure 2-6 Group of piles related failure modes (Viggiani., et al., 2012)

2.4.1 Effect of Pile Group:

Brown approach is one of the methods for considering effects of pile group. In this approach, the single pile's p portion of the p-y curve is multiplied by a constant, which accounts for the group interaction effects. This concept is concise and is simple to incorporate into any numerical code that employs p-y curves to represent lateral pile response, i.e., GROUP (Reese., et al., 1990) and FLPIER (McVay., et al., 1996b). These methods have been shown to be very effective in predicting 3 x 3 laterally loaded pile groups (Brown., et al., 1988; McVay., et al., 1995). With increasing of the pile spacing, efficiency increases, where increasing length of the pile improves efficiency very low where lateral load subjected to the piles, increases the axial resistance.

To predict the response of a large pile group (Le., 5, 6, 7, etc. rows), experimental data on such behavior must be available, so that the p-multiplier factors for each row can be back-computed through analytical means. The response of every different rows would be different and so we would have less p multiplier for those which have less contribution in resistance, where this contribution is function of pile spacing. *p-y* curves for sand do a good job of matching the lateral resistance versus displacement of single piles, and (Brown et al., 1988) *p-y* multiplier approach does a good job of matching the total group load and individual row distribution up to larger displacements. In loose and medium dense sands, it is found that an individual row’s contribution to a group's lateral resistance did not change with size of the group, only with its row position. Lateral resistance of the group of the piles is independent of the soil density.

2.4.2 Edge effect:

In the pile group, each pile pushes against the soil in front of it, creating a shear zone in the soil. These shear zones begin to enlarge and overlap as the lateral load increases. More overlapping occurs if the piles are closely spaced to each other. This effect of overlapping zones of influence between piles in the same row is so called "Edge effect."

Piles in groups will undergo significantly more displacement for a given load per pile than will a single isolated pile. Although piles in the leading row of a group may sometimes have load versus deflection curves similar to that for a single pile, piles in trailing rows will exhibit significantly lower load versus displacement curves.

2.4.3 Shadow effect:

Apparently, as closely spaced pile groups move laterally, the failure zone for individual piles overlap as shown in Fig.2-8. The tendency for a pile in a trailing row to exhibit less lateral resistance because of the pile in front of it is commonly referred to as "shadowing effect." (Larkela, 2008). This shadowing effect becomes less significant as the spacing between piles increases and is relatively unimportant for spacing greater than about six pile diameters center to center based on model tests (Cox., et at., 1984).

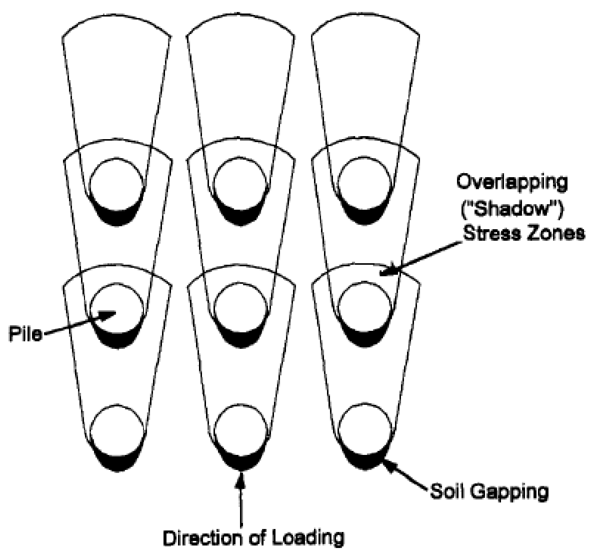

Figure 2-7 Shadow effect

CHAPTER 3
LATERAL RESPONSE OF THE SINGLE PILE AND GROUP OF PILES

It has been decades that pile foundation systems are used in order to increase the bearing capacity of the foundation as well as lateral resistance to the horizontal loadings such as seismic loads, wind and so on.

Design of pile groups subjected to relevant lateral forces is still challenging task for designers. While several design approaches are available and widely used to assess pile groups behavior under lateral loadings which are quite lower than ultimate group capacity, in contrast a limited number of methods are available to reliably assess ultimate capacity.

A review of existing literature on this topic reveals that available theoretical or experimental studies on ultimate lateral capacity of pile groups are quite limited mainly due to the intrinsic complexities of this problem which is governed by a tight interaction between geotechnical and structural aspects.

3.1 Soil pressure on a single isolated pile:

In order to better understand the group effect of piles, first the behavior of single pile is needed to be well understood. Depending on the source type of the loading, individual piles may be either (i) active or (ii) passive. In active loading piles, relative deformation between the pile and surrounding soil is primarily because of the motion of the pile, whereas in passive piles relative deformation between the pile and the surrounding soil is caused by unstable soil yielding around the shaft. Cubrinovski., et al., (2006; 2009) clearly explains the difference between active and passive pile deformation modes as illustrated in Figure 3-1.

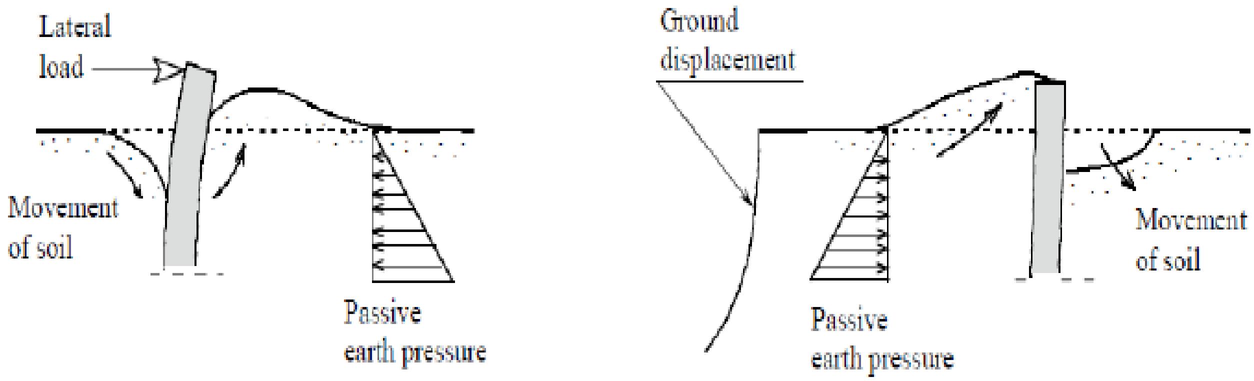

Figure 3-1 Difference between active (left) and passive (right) piles (Cubrinovski et al. 2006; 2009)

Broms (1964) figured out that the soil resistance mobilized in front of the shaft can be related to the passive resistance of the soil wedge whose geometry depends on pile diameter. Many different researchers, later, confirmed this phenomenon through experimental and numerical approaches (Reese., 1992; Cubrinovski., et al., 2006; Poulos., 1995; and many others).

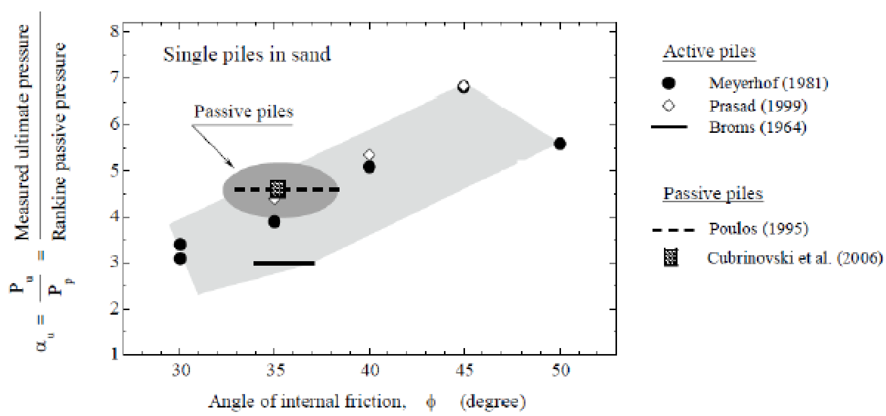

Figure 3-2 Ultimate soil pressure acting on isolated piles (Cubrinovski., et al., (2006))

Broms, (1964) found out that α Kp is the modified passive pressure acting in front of the pile; where α is between 3 and 5, recommending the selection of lower bound value of 3 in the practice of the ordinary design situations. As also discussed by Cubrinovski et al. (2009), this assumption may be quite under conservative when the pile is loaded passively as for example in lateral spreading problems. Cubrinovski et al., (2006; 2009) have shown the range of a coefficient as a function of internal friction angle used by several researchers.

Viggiani (1981) studied the response of pile passively loaded moving soil on a stable layer. Both of the layers are purely cohesive. According to the plastic moment, length of the pile and thickness, strength properties of the cohesive layers, six different mechanisms are categorized. Figure 3-3 shows the failure mechanisms in which only soil fails.

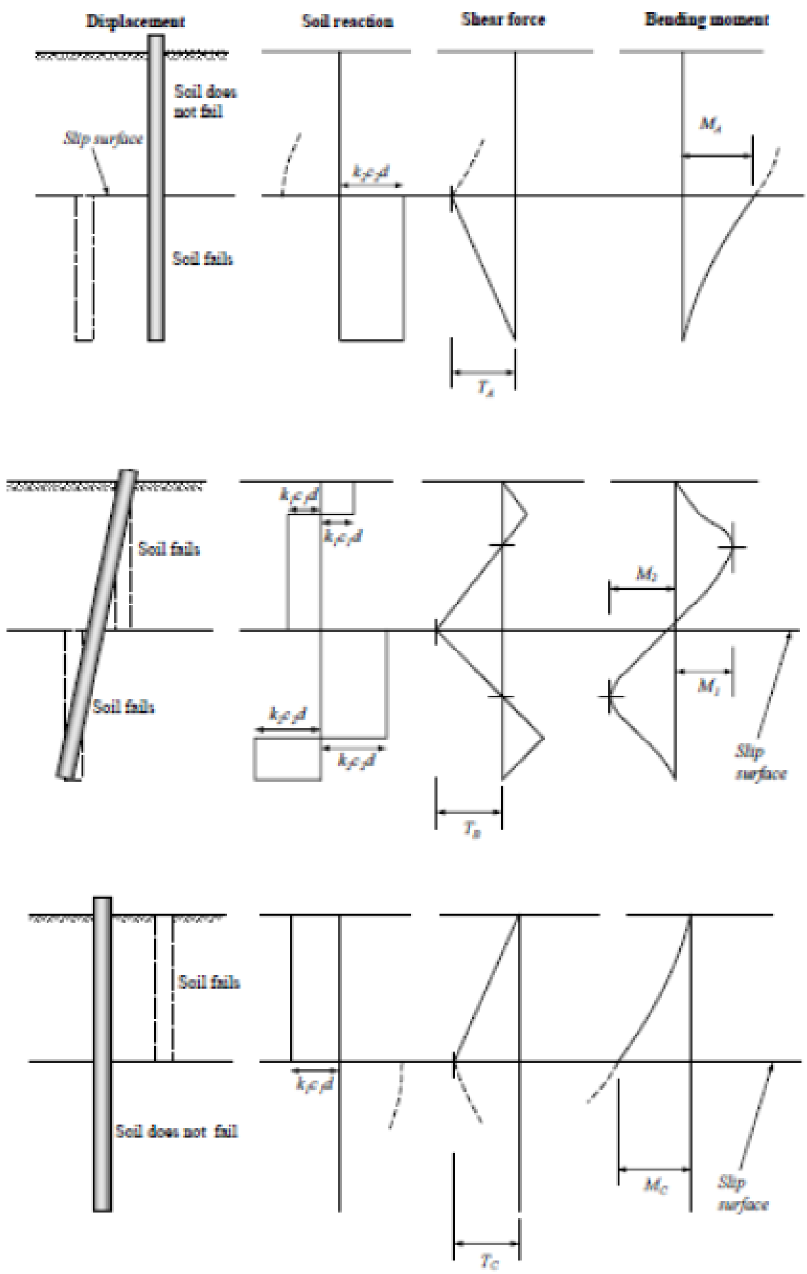

Figure 3-3. Failure modes of pile-supported passively moving soil (Viggiani, 1981).

3.2 Lateral Response of the Pile Group:

Lateral pile response is typically analyzed using finite-difference models of the pile along with nonlinear springs to represent the resistance provided by the soil. The load-displacement curves for the soil are known as *p-y* curves, where *p* is the horizontal soil resistance (force per length) and *y* is the horizontal displacement. Generic *p-y* curves have been developed for soft clays, stiff clays, and sands and have been widely incorporated in computer models (Matlock., 1970; Reese et al. 1974, 1975). For closely spaced piles, Brown et al. (1987) proposed that the *p-y* curve for a pile in a group can be obtained using p-multipliers *(P_M)* to reduce all the p-values on a single pile *p-y* curve, as shown in Fig. 3-4. With this approach, it is possible to reduce the computed load-carrying capacity of the piles in a group relative to the single pile capacity (Rollins., et al., 2002).

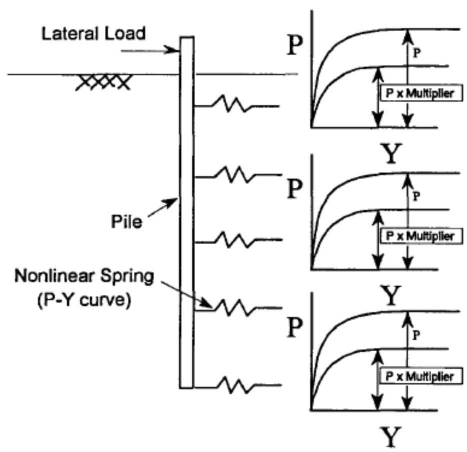

Figure 3-4 Definition of p-multiplier (P_m) in the Winkler Model (Rollins., et al., 2002)

In this approach, one of the most common methods of accounting for interaction effects in pile groups is to modify the single pile p–y curves using a p-multiplier for each row of piles in the group, with higher values for leading row and lower values for trailing rows. The leading and trailing rows interchange during seismic loading; therefore, sometimes an average p-multiplier is used for all piles in the group. This average p-multiplier is called the group reduction factor. Group reduction factors have been established from experimental data from static loading tests on small pile groups, mostly 3 × 3 groups with free pile head conditions and center-to-center pile spacings of about 3 pile diameters. To study the group reduction factors in 3 × 3 to 6 × 6 square pile groups subjected to static loading continuum simulations can be used. However, the study shows that design guidelines such as the American Association of State Highway and

Transportation Officials (AASHTO) and Federal Emergency Management Agency (FEMA) P-751 overestimate the group reduction factors, hence the lateral resistance, in larger pile groups and larger spacings, especially for fixed pile head conditions (Rollins., et al., 2002).

3.2.1 Group reduction factor calculation:

The group reduction factor is a uniform factor applied to all p–y curves in the group to yield the same pile head deflection as measured in a test or calculated from a continuum model. The process for obtaining the group reduction factor at a prescribed pile head deflection is depicted in Fig. 3-5. This method follows the procedure described by Rollins et al. (2006), except that they used data from a field test rather than data from analysis, as in this study. The load–deflection curve for the pile group in Fig. 3-5 a is computed using the continuum model. The load corresponding to a prescribed deflection of this model is then applied to the p–y model in Fig. 3-5 b (Finn., et al., 2014).

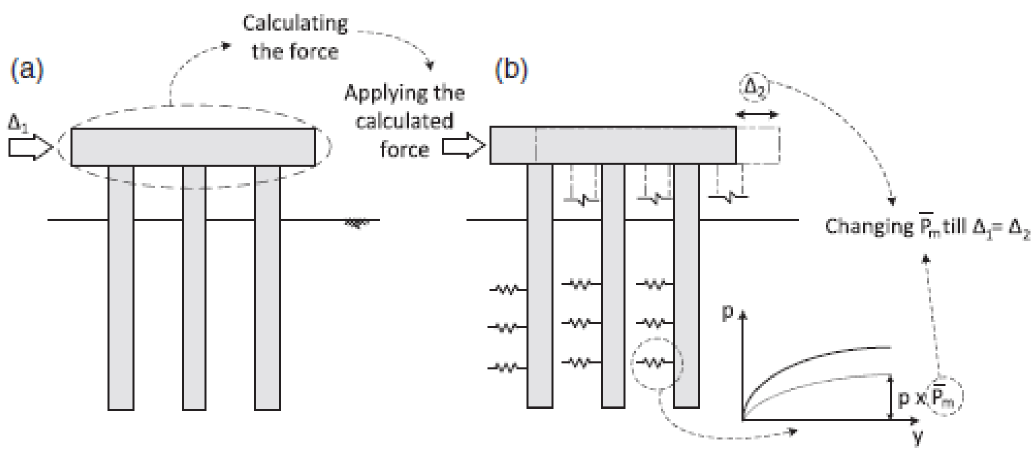

Figure 3-5 Methodology for calculating group reduction factor using (a) continuum and (b) p–y models.P_m, group reduction factor (Finn., et al., 2014)

Group reduction factors can be obtained using experimental studies such as full-scale load tests. It is, however, very difficult and expensive to perform a full-scale test on a pile group. The capacity of the loading equipment also limits the size of the pile group that can be tested. Therefore, full-scale tests are usually carried out on small pile groups with close spacings. Centrifuge tests are a useful alternative to full-scale tests and can be used to study the group reduction factors (e.g., McVay et al. 1995, 1998). Most of the pile group experiments were performed on 3 × 3 free-head pile groups with the center-to-center spacing of three pile diameters (D) and pile head deflections of up to 5 cm. Because p-multipliers were typically derived from free-head pile group tests, there are some uncertainties regarding their applicability for fixed-head conditions that are more routinely encountered in engineering practice where a pile cap is used (Rollins and Sparks, 2002). The literature review also shows the lack of a comprehensive study on the group reduction factor for larger pile groups, various pile spacing, pile head conditions, and soil properties. The limitations in the available experimental database justify using three-dimensional numerical simulations to study the effects of these different parameters on the group reduction factor (Finn., et al., 2014).

In 1995, McVay., et al, conducted centrifuge tests on single and 3 x 3 pile groups having three-diameter (3D) and five-diameter (5D) spacings. In all of the tests, the piles were driven and laterally loaded in flight without stopping the centrifuge. The piles simulated 432 mm diameter by 13 m long hollow circular piles founded in medium loose *(Dr*- 33 %) and medium dense *(Dr* = 55 *%)* sands. Results of the tests showed that the ratio of lateral resistance of a group to a single pile, I.e. efficiency, was independent of soil density. The group efficiency at 3D spacing was 0.74, whereas at 5D spacing the group efficiency was 0.94. Due to their comparison between results obtained from the test and approximation by P multiplier, points on the graph obtained as shown (McVay., et al., 1995)

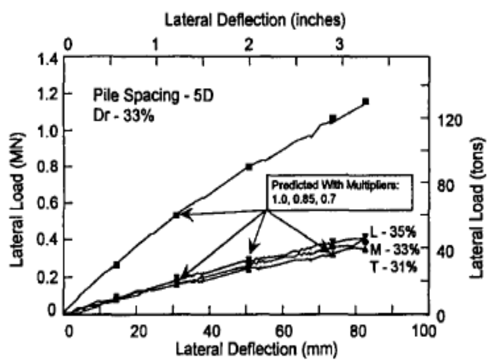

Figure 3-6 Test results vs P-multiplier approximation (McVay., et al., 1995)

3.3 Lateral-Pile Displacement due to the Applied Lateral Loads:

Estimation of lateral-pile displacement due to externally applied (i.e., active) pile loading is often achieved using load-transfer *p*-*y* curves, where *p* is the lateral-pile pressure; and *y* is the lateral-pile displacement, together with a finite-difference solution of the pile-bending equations as is called the subgrade-reaction method. Many publications discuss *p*-*y* curves for single piles and general soil conditions (e.g., American Petroleum Institute (API)., 1987). Adapting single-pile *p*-*y* curves for use in pile groups by considering pile-soil-pile interaction effects is more problematic, although attempts have been made to introduce stiffness and pressure factors empirically (e.g., Brown- and Shie., 1991). Previous workers used load-transfer curves obtained for active lateral-pile loading, i.e., *p-y* curves for cases when piles are passively loaded by lateral-soil movements for example, those caused by adjacent surcharge loading (Poulos., 1973; Byrne., et al., 1984; and Frank., 1981). Springman (1989) and Stewart et al. (1994) used a relationship developed from an analysis of a single pile in an arbitrary-sized zone of elastic soil (Baguelin., et al., 1977); the French design methods use *p-y* curves for active loading determined by pressure meter testing (Frank., 1981). The pile-load-transfer curves suitable for prediction of pile pressures due to active pile displacement *(p-y)* and passive soil displacement *(p-8)* are different. *p-y* curves, suitable for use during passive lateral-pile loading, assume local plane-strain soil deformation around the piles and are dependent only on the local soil behavior, the pile diameter, and spacing. *p-y* curves also depend on 3D global soil behavior, which varies with pile geometry and pile-pressure distribution.

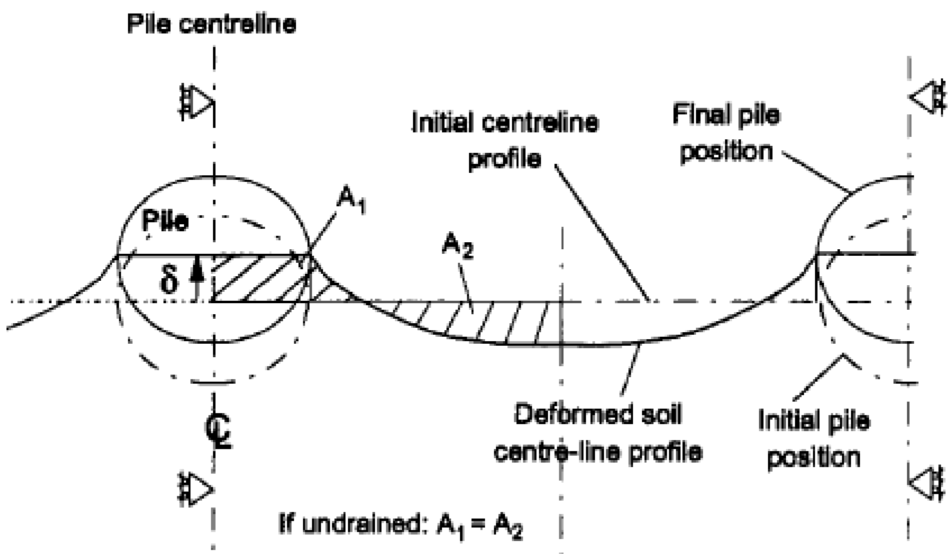

Figure 3-7 Different stages of pile lateral displacement (Bransby., 1996))

Hence, *p-y* curves depend on the mode of pile-head loading and the overall pile-group geometry as well as the global and local soil properties, as observed by previous research workers. Determination of *p-y* curves from knowledge of soil behavior will require consideration of all these effects. This may allow rational estimation of *p-y* curves for pile groups to be made directly from knowledge of soil-element behavior and pile group geometry, without recourse to 3D finite-element analysis or empiricism (Bransby., 1996).

3.4 Lateral Load Design by P-Y Curves:

Lateral load design considerations are of considerable importance for deep foundations. Most lateral load investigations have been performed on isolated single piles, although piles are most frequently used in groups. Consequently, there exists a lack of knowledge concerning pile group effects, despite the significance of closely spaced pile interaction. To date, only a few full-scale lateral load group tests of deep foundations have been performed due to cost limitations (Brown., et al., 1988). Alternatively, small-scale centrifugal model tests can be used. A widely acceptable solution for lateral load design in piles is the *p-y* approach; that is, a Winkler or a subgrade reaction approach that utilizes a beam-column on an elastic foundation with nonlinear springs to transfer the load from the pile to the soil. These springs represent the total soil resistance at a particular depth to the lateral displacement of a horizontally loaded pile. Empirical recommendations to establish *p-y* curves are based on the results of full-scale tests, with a close agreement between results obtained from experiments and theoretical solutions. Currently, the laterally loaded group design scenario consists of (1) obtaining pile *p-y* relationships either from a lateral load test or inferred from in-situ tests; and (2) applying *p-y* "multipliers" to adjust the single pile results to account for group shadowing effects. Consequently, two problems face a designer; specifically, (1) characterization of the soil properties to develop the *p-y* relationships; and (2) selection of the group *p-y* multipliers.

3.4.1. Full scale test published by Pedro and Frank Townsend (1997):

Pedro and Frank in 1997 performed a test on group of fixed head piles (16 piles) on Roosevelt bridge where they considered 10 piles as sacrificial piles and 6 piles as reaction piles. Reaction piles were in instrumented by inclinometers and strain gauges, applying lateral loading around 4500 kN on sacrificial piles and measuring the results on reaction piles.

The pre-driving in-situ tests mentioned before were used directly or indirectly for the determination of *p-y* curves, and the soil properties, friction angle, unit weight, and subgrade modulus, used were estimated indirectly through SPT and CPT tests.

The bending moments were fitted to third-order polynomial equations using least-squares polynomial regression. The deflection, *y*, was obtained by double integration, and the soil reaction, *p*, was determined by double differentiation of the moment curves. Inclinometer measurements were used as a complement to obtain integration constants, Le., pile head rotation and deflection. The pile response is dictated by the cracking moment. FLPlER method for nonlinear prestressed concrete piles very accurately predicts the post-cracking behavior, where uses a discrete element model in which the nonlinear material behavior is modeled via input or default material stress-strain curves (Hoit., et al., 1996). The soil modulus (coefficient of subgrade reaction) dominates the initial part of the load-deflection curve, while the ultimate soil resistance of the upper layer influences load-deflection at larger displacements with a transition between both conditions.

Dilatometer methods provide a good approximation in the initial linear region, while Robertson's PMT method is good in the large deformation region. The DMTIPMT method tries to join both methods with good results. The procedures of Reese., et al. (1974) or O'Neill (1983) can provide very good approximations if the correct parameters are taken-for this case, a high modulus of subgrade reaction and relatively low angle of internal friction. The SPT *p-y* curve method also provides a good approximation due to the fact that it is related to the procedure of Reese., et al. with the conditions established before.

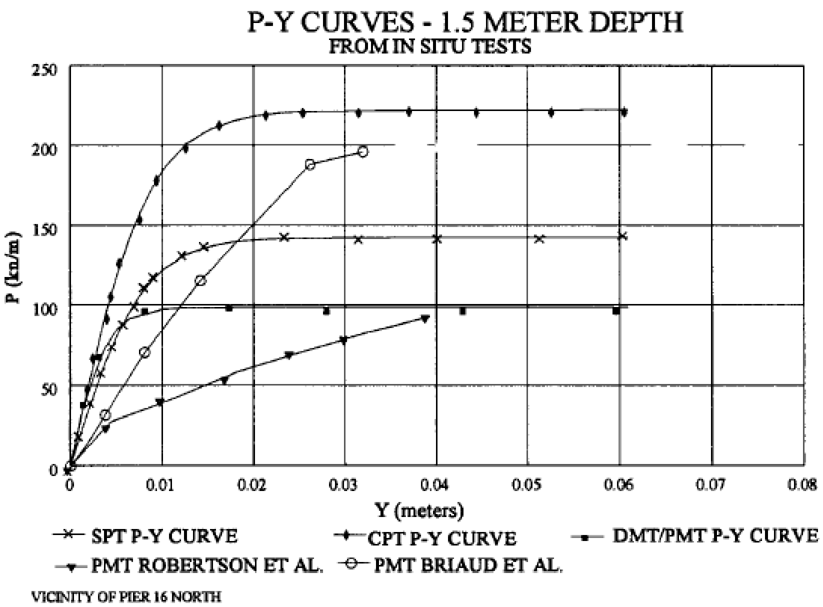

Figure 3-8 P-Y Curve From IN-SITU Test (Pedro., et al., 1997)

The average pile group response was softer than the single pile response. However, the single pile test can be a good indicator of the pile group behavior. The average of the leading row piles behaved similarly to a single pile and took more load than the average of the piles in the trailing rows. Also, outside piles took more load than inner piles within a row, possibly due to a shadow effect and pile driving sequence. The *p-y* multipliers work well to account for the group effect. They have reasonable agreement with the centrifuge results of McVay., et al., (1995) and the pile group of Brown et al. (1988). The overall *p*-*y* multiplier for the group was 0.55 for the test pile group and 0.8, 0.7, 0.3, and 0.3 for the leading, middle leading, middle trailing, and trailing rows, respectively. The maximum bending moments for the leading row is higher than for the trailing rows. However, all were within a 15% range. The Reese et al. (1974) recommendations for *p*-*y* curves in sandy layers are very reasonable for the calculation of ultimate soil resistance using the estimated friction angles for the SPT values. However, it appears that the estimated coefficient of subgrade reaction is conservative (Pedro., et al., 1997).

CHAPTER 4
NUMERICAL CASE STUDY RESPONSE OF SINGLE PILES UNDER LINEAR AND NON-LINEAR PILE RESPONSE THROUGH 3D NUMERICAL ANALYSIS AND P-Y APPROACH

To attempt a rational selection of governing parameters of the proposed procedure, a set of benchmark results would be necessary. However, in our best knowledge, it is quite hard to access enough experimental data covering relevant conditions for practical applications. Therefore, we considered performing continuum-based couple soil-structure interaction analyses by FLAC3D (Itasca 2018) and carry out its p-y spring-based engineering approximation through the use of SeismoStruct 2018 software (Seismosoft 2018). There are approaches and equations used for this modeling inside the software as well as analytical solutions which would be described in the following.

4.1 Approach description and Background for the equation of FLAC3D:

FLAC3D is a numerical modeling code for advanced geotechnical analysis of soil, rock, and structural support in three dimensions, which is used in analysis, testing, and design by geotechnical, civil, and mining engineers. It is designed to accommodate any kind of geotechnical engineering project where continuum analysis is necessary. FLAC3D utilizes an explicit finite difference formulation that can model complex behaviors not readily suited to FEM codes, such as: problems that consist of several stages, large displacements and strains, non-linear material behavior and unstable systems (even cases of yield/failure over large areas, or total collapse). The numerical scheme relies on a finite difference nodal formulation of the fluid continuity equation. The formulation can be paralleled to the mechanical constant stress formulation (presented in Finite Difference Approximation to Space Derivatives) that leads to the nodal form of Newton's law.

4.1.1 Highlighted Features:

- Large-strain simulation of continua, with interfaces or slip-planes to represent distinct interfaces along which slip and/or separation may occur, thereby simulating the presence of faults, joints, or frictional boundaries
- Explicit solution scheme that gives stable solutions to unstable physical processes
- Twelve built-in material models: the "null" model, three elasticity models, and eight plasticity models

It is noted that pile elements in FLAC3D are modelled with hollow brick elements with hollow circular geometry, hence, under full plasticity condition plastic moment is of the real reinforced concrete cross-section is recovered. Due to this reason, elasto-plastic rule with Von-Mises yield surface (with proper cohesion) is selected. On the other hand, for soil zones classical Mohr-Coulomb yield surface is used. Both of the cases rely on elasto-plasticity implemented in FLAC3D, which is discussed through Von-Mises yield surface in Section 4.1.2.

4.1.2 Composite Failure Criterion and Flow Rule:

The failure criterion used for this FLAC3D model is a composite Drucker-Prager criterion with tension cutoff as sketched in the (τ, σ) representation of Figure 4-3. The failure envelope $f(\tau, \sigma) = 0$ is defined, from point A to B on the figure, by the Drucker-Prager failure criterion $f^s = 0$, with

$$f^s = \tau + q_\phi \sigma - k_\phi$$

and, from B to C, by the tension failure criterion $f^t = 0$, with

$$f^t = \sigma - \sigma^t$$

where q_ϕ , k_ϕ are positive material constants, and σ^t is the tensile strength for the Drucker-Prager model. Note that, for a material whose property q_ϕ is not equal to zero, the maximum value of the tensile strength is given by

$$\sigma^t_{max} = \frac{k_\phi}{q_\phi}$$

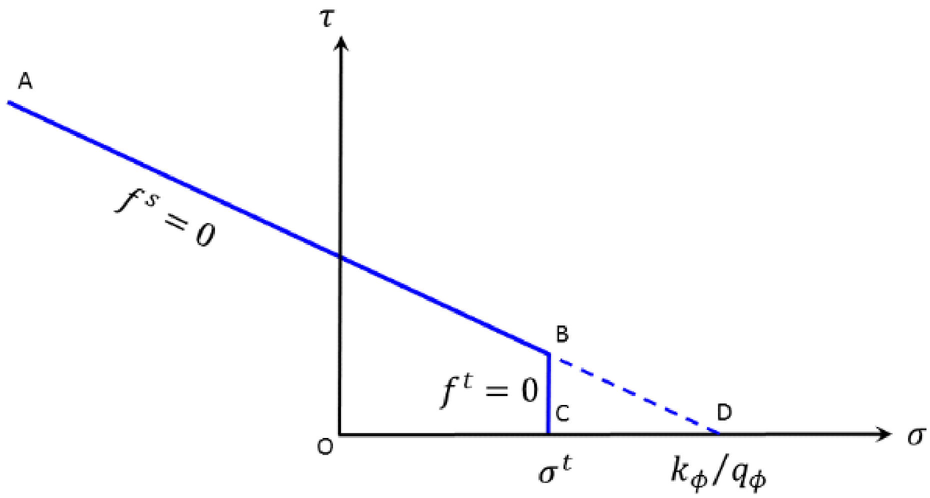

Figure 4-1 FLAC3D Drucker-Prager failure criterion (Itasca FLAC3D User Manual 2018)

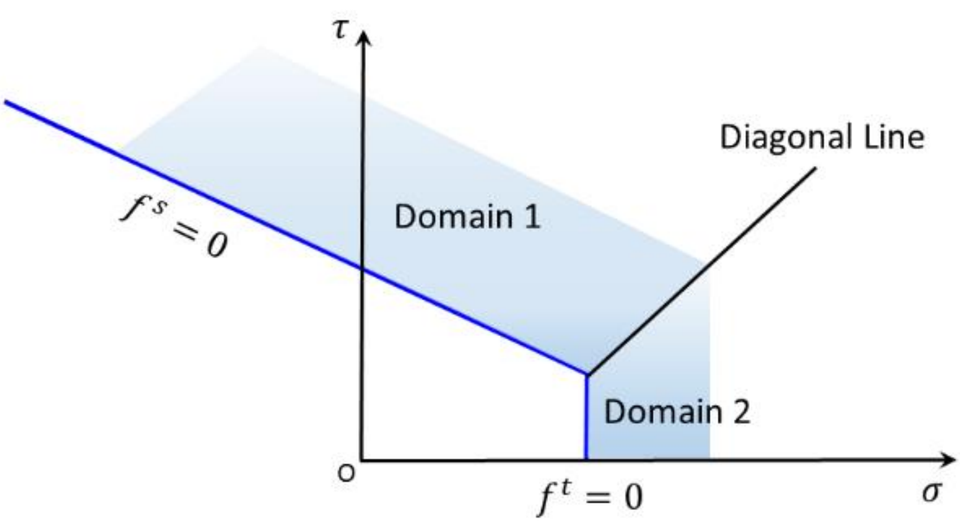

Figure 4-2 Drucker-Prager model—domains used in the definition of the flow rule. (Itasca FLAC3D User Manual 2018)

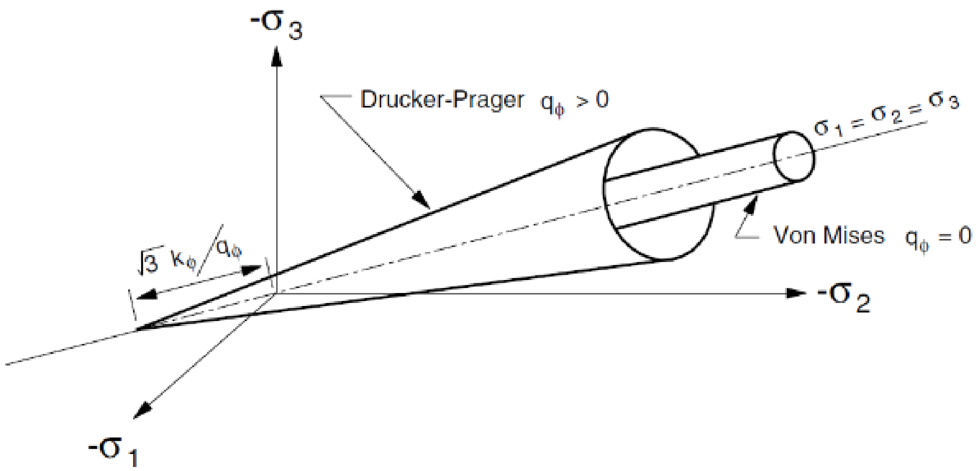

Figure 4-3 Drucker-Prager and von Mises yield surfaces in principal stress space (Itasca FLAC3D User Manual 2018)

4.1.3 Drucker-Prager Model:

The failure envelope for this model involves a Drucker-Prager criterion with tension cutoff. The position of a stress point on this envelope is controlled by a non-associated flow rule for shear failure, and an associated rule for tension failure (Itasca FLAC3D User Manual 2018).

Generalized Stress and Strain Components:

The generalized stress vector [σ] involved in the definition of the Drucker-Prager model has two components (n = 2): the tangential stress, τ, and mean normal stress, σ, defined as:

$$\tau = \sqrt{\frac{1}{2} s_{ij} s_{ij}} \quad , \quad \sigma = \frac{\sigma_{kk}}{3}$$

where the Einstein summation convention applies, and [s] is the deviatoric-stress tensor. The components of the associated generalized strain increment vector Δ[ε] are the shear-strain increment, Δ[γ], and volumetric-strain increment, Δε, introduced as:

$$\Delta\gamma = \sqrt{2\Delta e_{ij} \Delta e_{ij}} \quad , \quad \Delta\varepsilon = \Delta\varepsilon_{kk}$$

where Δe is the incremental deviatoric-strain tensor.

4.1.4 Incremental Elastic Law:

The incremental expression of Hooke's law, in terms of the generalized stress and stress increments, has the form

$\Delta\tau = G\Delta\gamma^e$

$\Delta\sigma = K\Delta\varepsilon^e$

where K and G are the bulk and shear modulus, respectively.

4.2 Model: Single Pile FLAC3D Model (Surrounding Soil Included):

After verification of the numerical and analytical solutions now we can model the surrounding soil and as matter of time for calculation just half of the problem modeled which is symmetric and a circular hollow section pile with 1m outer diameter and 0.9m internal diameter considered. Such model includes following main components:

- A uniform soil layer with Mohr-Coulomb constitutive model is assigned (Figure 3-14) with dimensions of 25m from center and top of the soil modeled with the Properties of the soil as: Cohesion: 0^o , Friction(ϕ): 30^o , Bulk modulus(K): $8.3*10^4$ [kN/m^2] Shear modulus(G): $3.9*10^4$ [kN/m^2] where E = 9KG/(3K+G), therefore: Young modulus: 10^5 [kN/m^2];
- Figure 3-15. prescribed boundary condition at pile top as we have fixed-head pile;
- Piles (o single pile) which are modelled as elastic by using a cohesion of Drucker Prager 100 times more than the typical one in order to increase the yielding criteria of the failure and to can check the results by Seismostruct in elastic region, 40 vertical Nodes of Meshing considered in every 0.5 meter along the pile (Figure 3-14);
- A slip interface between pile and soil, whose resistance is assigned through a friction angle 30^o considering Drucker-Prager model which is mentioned above (Figure 3-16).
- At the top of the piles, fixed head support condition is modelled by prescribing same lateral movement $\bar{u}$ to all the grid points of a portion of piles projecting above soil surface and called “Stem”.

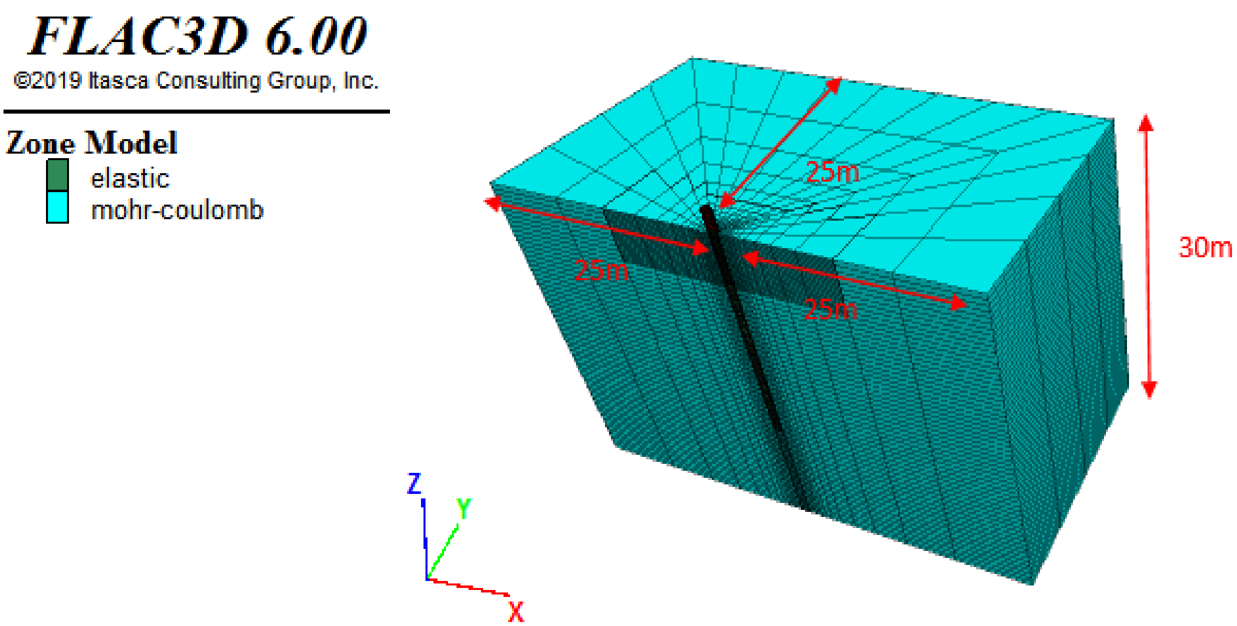

Figure 4-4 Dimensions and constitutive models

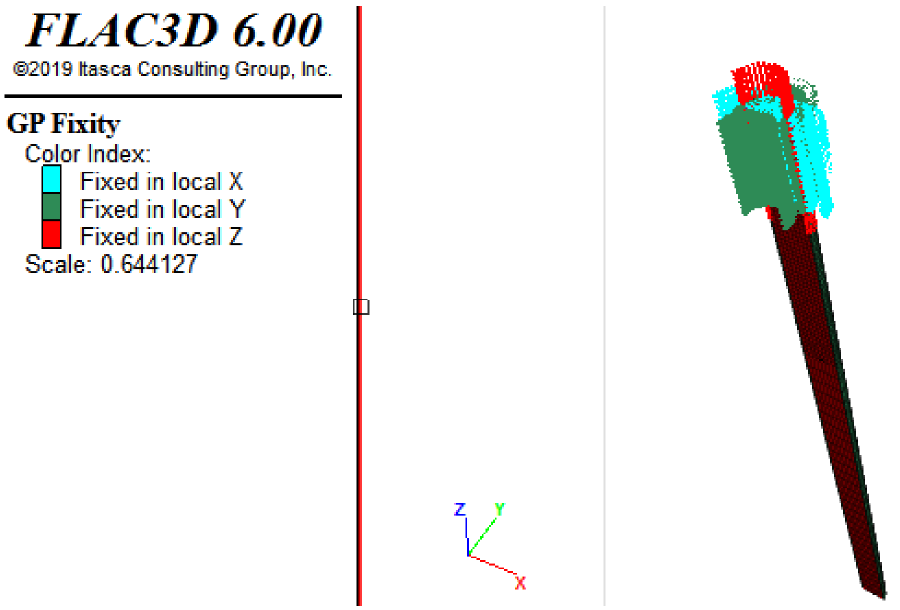

Figure 4-5 Boundary condition of the pile top (fixed head)

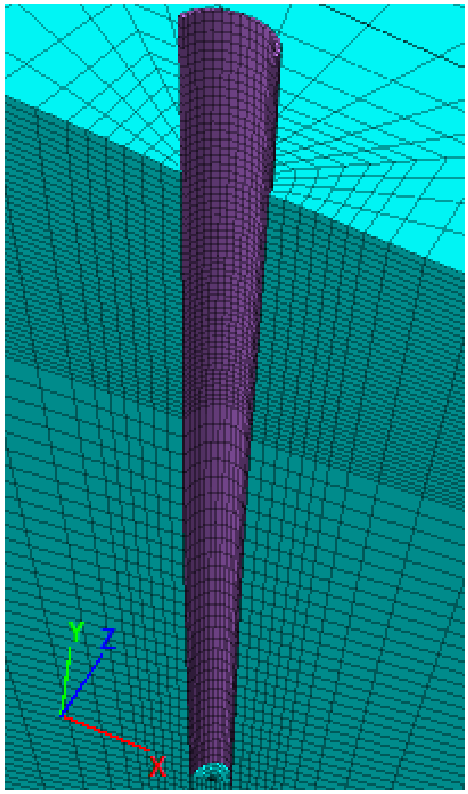

Figure 4-6 Slip Interface

For each pile pattern, including single pile conditions, a FLAC3D analysis has been performed, according with following sequence:

1) Set up of initial at rest condition by assigning an initial K0 stress field
2) Insertion of piles (and their interface)
3) Progressive increase of top displacement $\bar{u}$, with 4 increments of 1, 1, 3 and 5 cm each, up to a final displacement of 10 cm applied in x direction and states saved as 1cm, 2cm, 5cm and 10 cm of velocity (displacement applied).
4) By using fish coding features of the software total reaction acted on the pile extracted

Such procedure is accomplished by means of the nonlinear explicit pseudo-dynamic integration scheme offered by FLAC3D, by simply applying prescribed velocities as units of displacement for a suitable number of steps. Between each displacement increment, additional cycles with null velocities are performed, until overall top reaction (i.e. the resultant of all the lateral reactions where lateral displacement is assigned) is stabilized. In this study, only 1000 mm dia., 20 m long concrete piles are considered, in a granular dry soil.

4.3 FLAC3D Results (Elastic Pile Material)

4.3.1 **State at 1cm Displacement applied:**

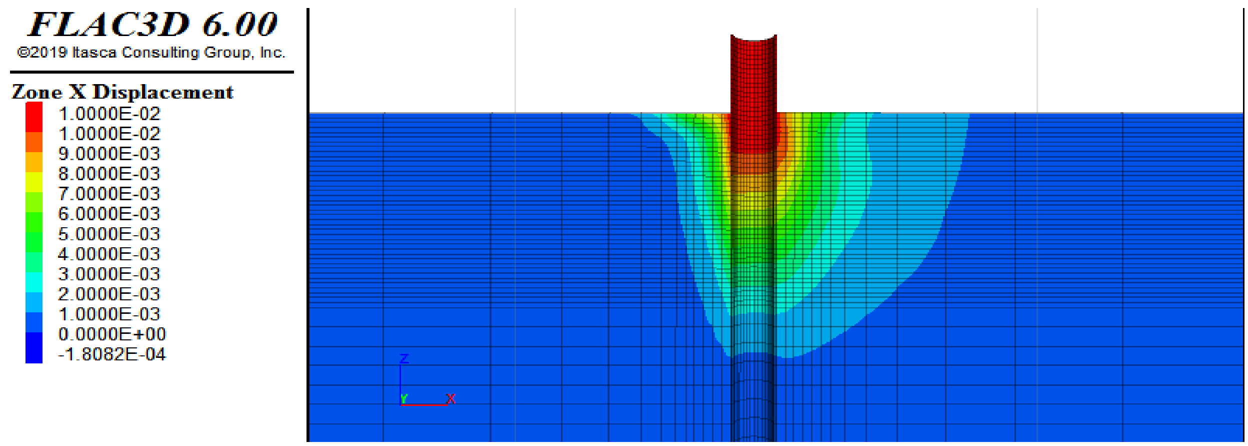

Figure 4-7 Zone x-displacement at 1cm Displacement applied

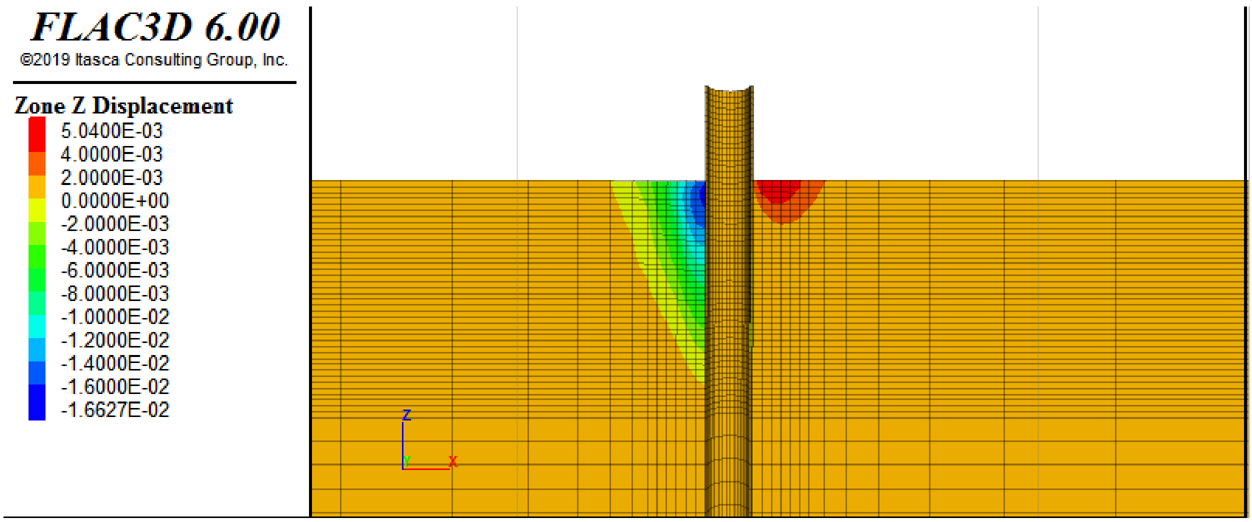

Figure 4-8 Zone z-displacement at 1cm Displacement applied

From the (Figure 4-8) it worth to mention that we can see the soil at left side of the pile has negative value of the z-displacement which means the soil behind the pile is going down and the soil in front of the pile where it is the direction of the forced velocity (displacement) has positive value and going up this is more clear by using command in FLAC3D as large strain on, which can shows us this phenomenon but not at this stage which has very small value at stage of 1cm and to be shown in the last stage (10cm). it should be noted that acting conditions behind the pile are quite evident whereas passive conditions in front of the pile are not activated for small displacements.

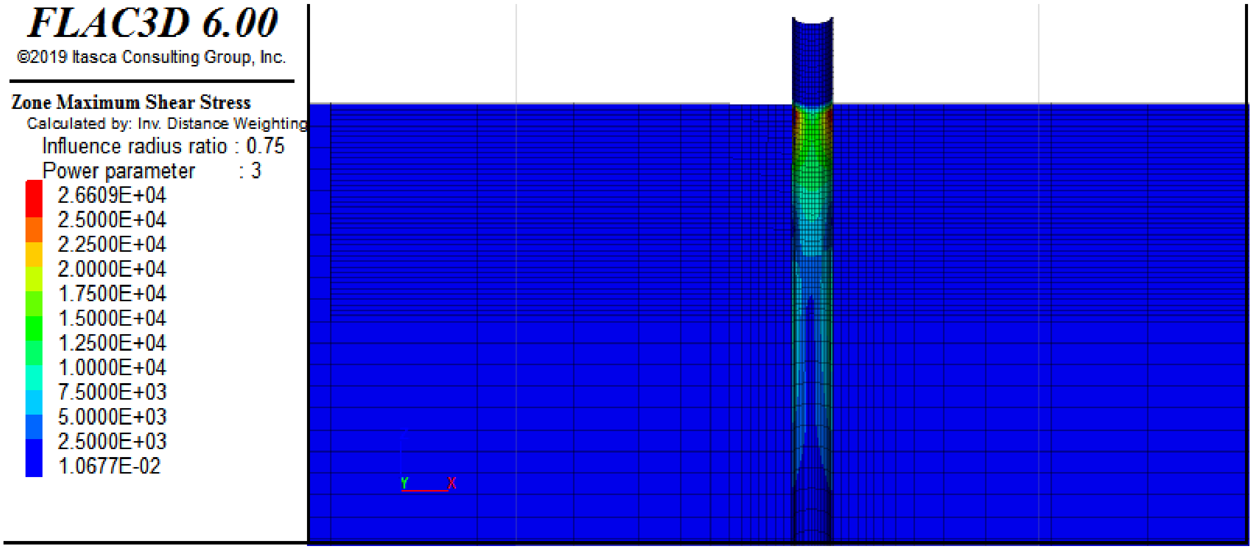

Figure 4-9 Zone Maximum Shear Stress at 1cm Displacement applied

4.3.2 State at 2cm Displacement applied:

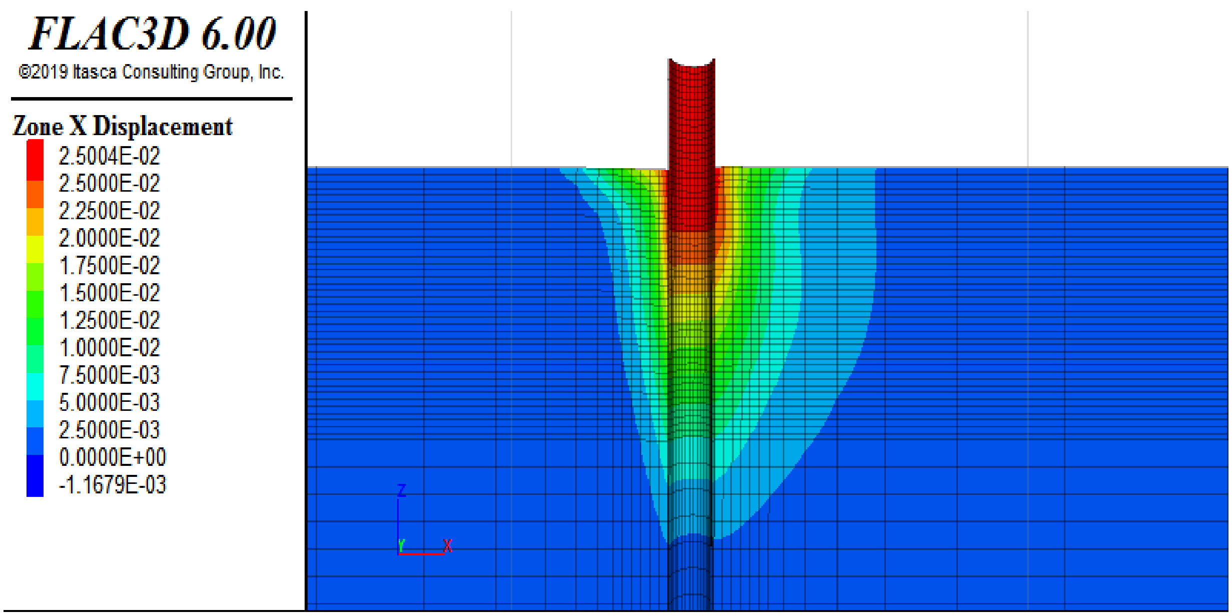

Figure 4-10 Zone x-displacement at 2cm Displacement applied

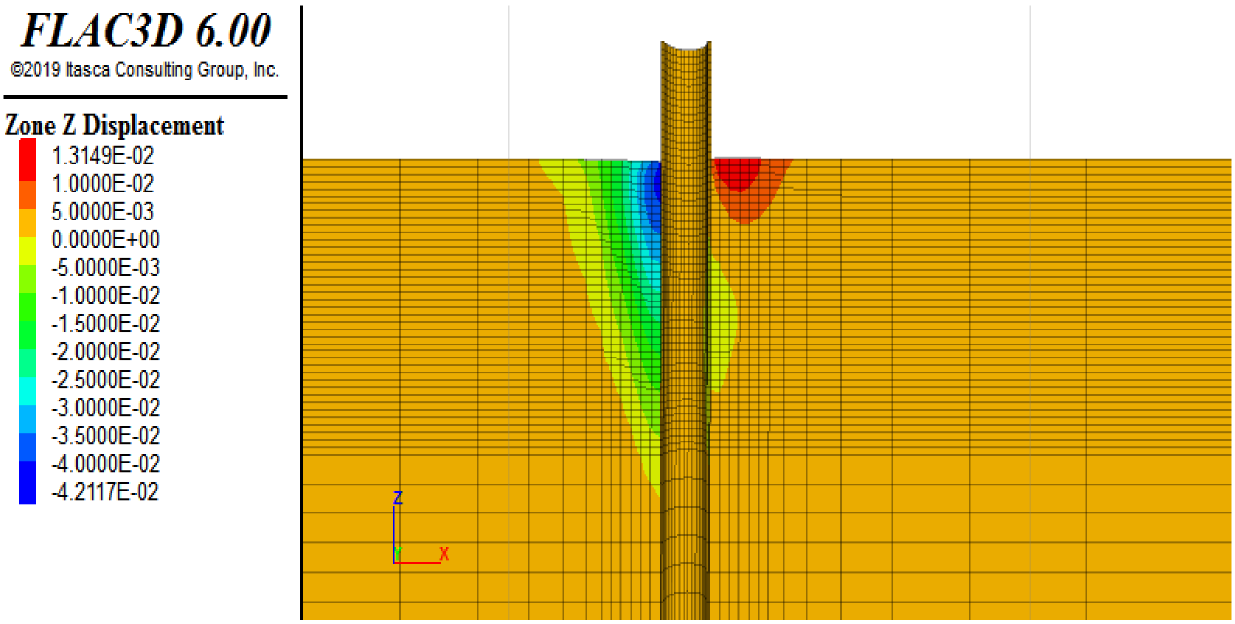

Figure 4-11 Zone z-displacement at 2cm Displacement applied

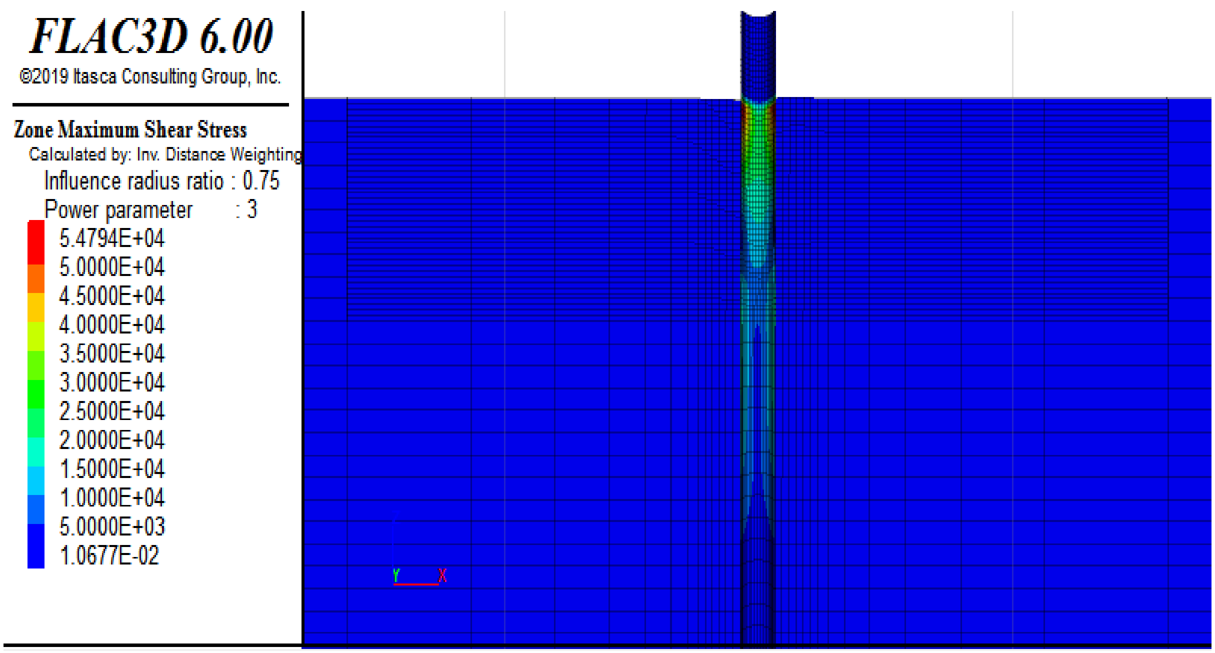

Figure 4-12 Zone Maximum Shear Stress at 2cm Displacement applied

4.3.3 State at 5cm Displacement applied:

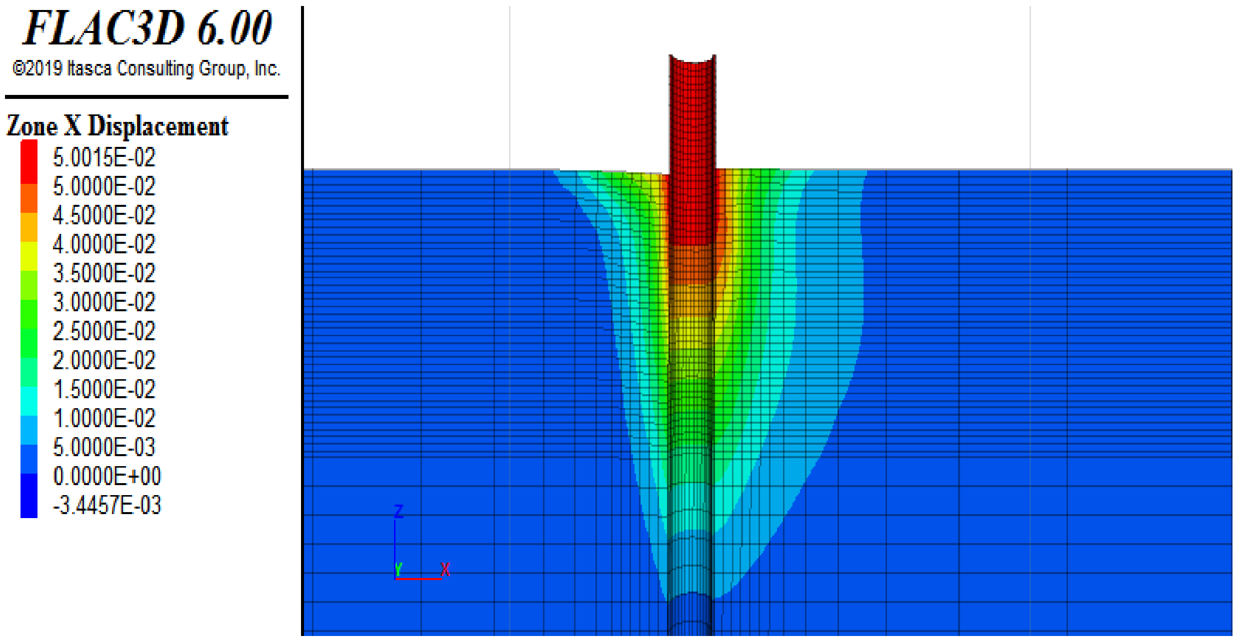

Figure 4-13 Zone x-displacement at 5cm Displacement applied

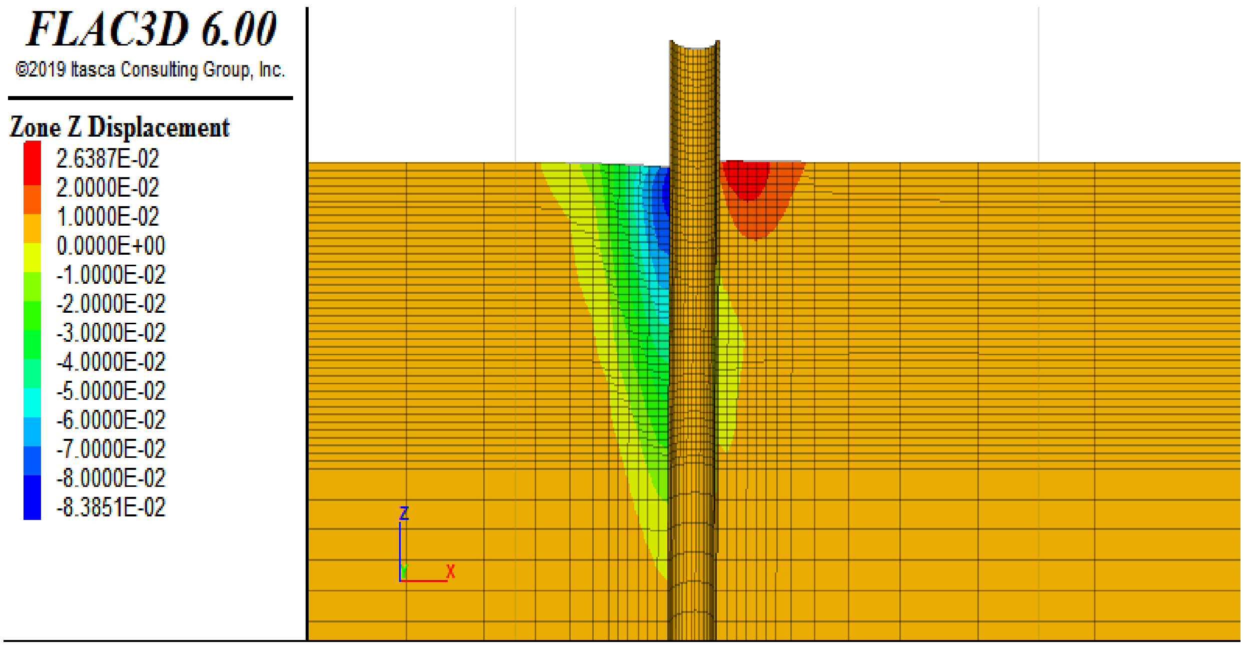

Figure 4-14 Zone z-displacement at 5cm Displacement applied

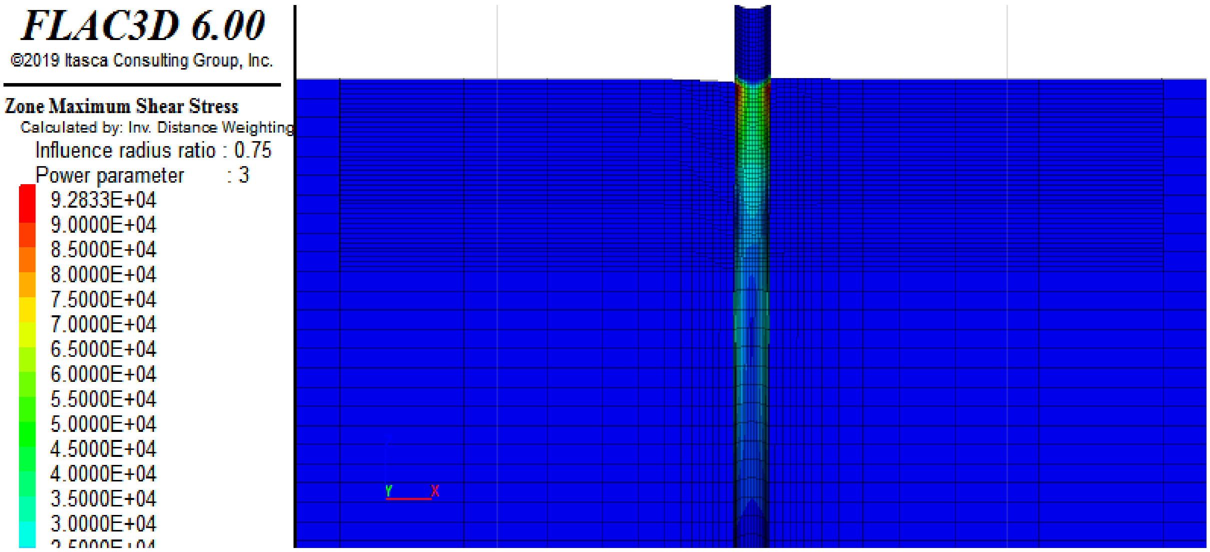

Figure 4-15 Zone Maximum Shear Stress at 5cm Displacement applied

As we can see from the graph, at the end of the state (1cm) the value of the total reaction acting on top of the pile is $-1.3*10^3$ kN/m^2.

4.3.4 State at 10cm Displacement applied:

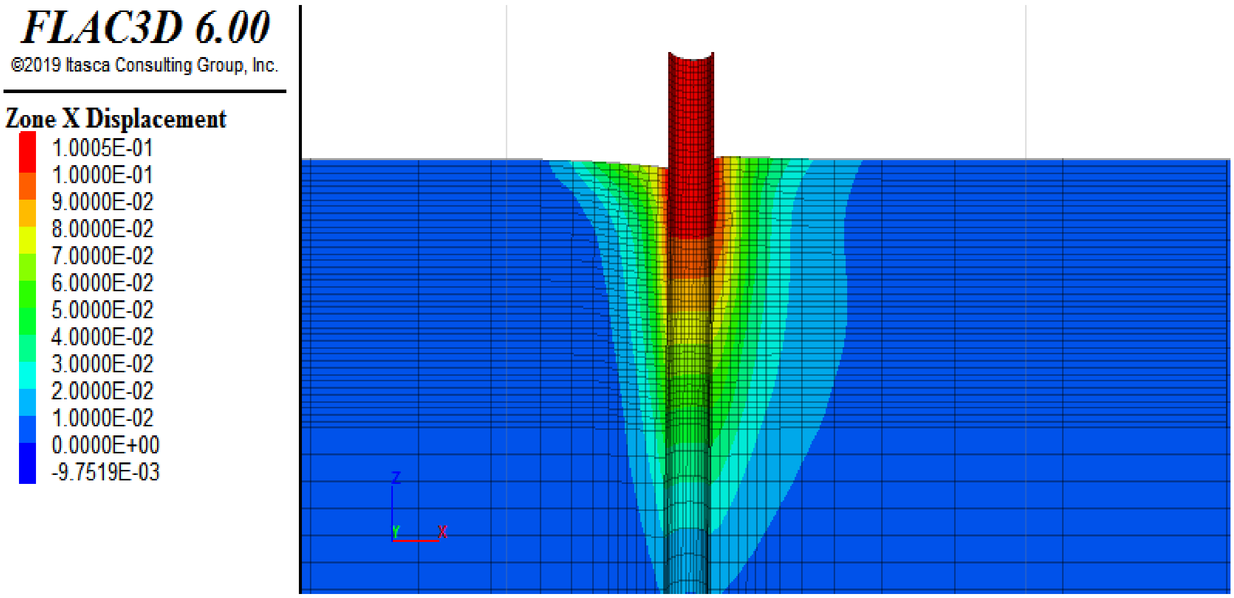

Figure 4-16 Zone x-displacement at 10cm Displacement applied

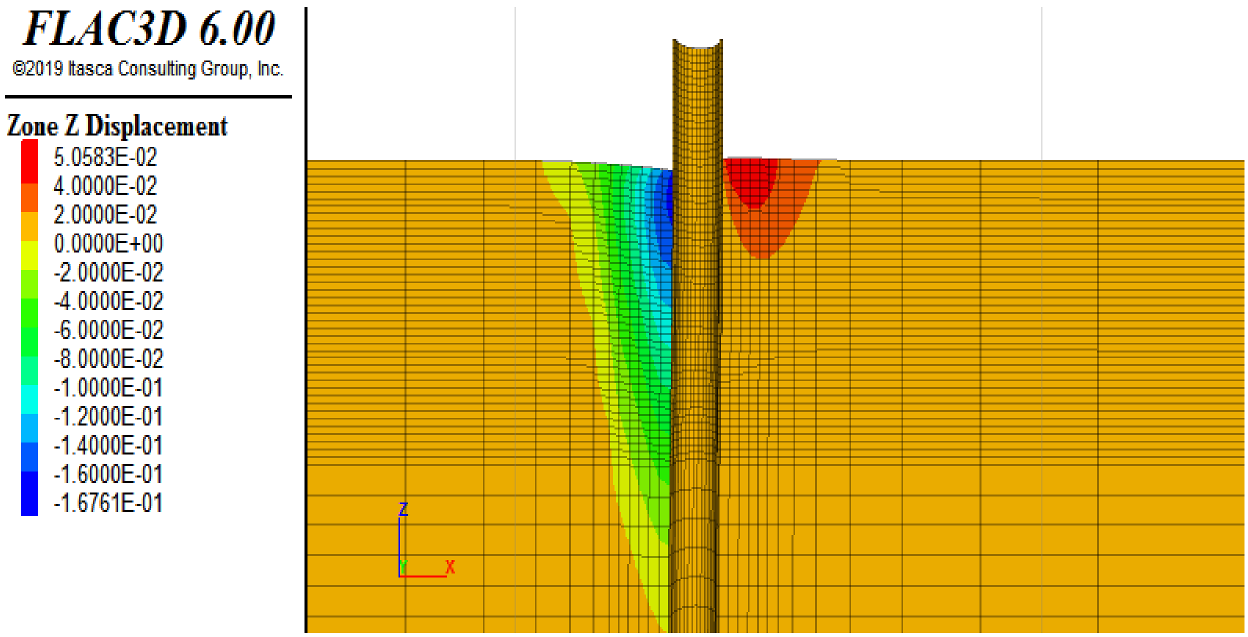

Figure 4-17 Zone z-displacement at 10cm Displacement applied

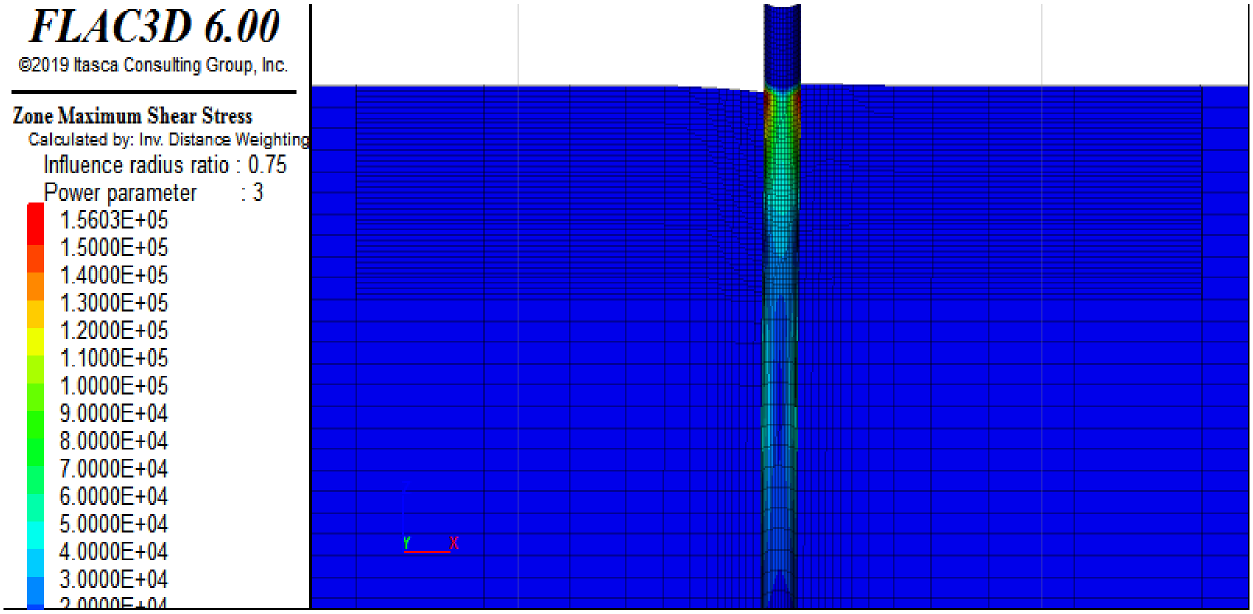

Figure 4-18 Zone Maximum Shear Stress at 10cm Displacement applied

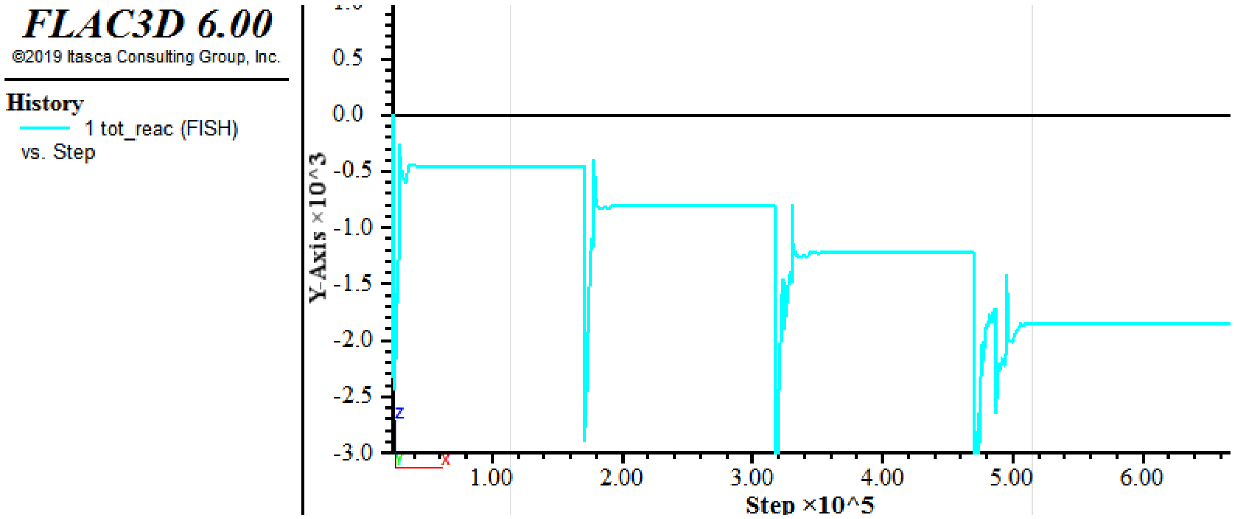

Figure 4-19 Total reaction History acting on the pile at 1, 2, 5 and 10cm Displacement applied

As we can see from the Figure 4-19, at the end of the state (10cm) the value of the total reaction acting on top of the pile is -1.75*10^3 kN/m^2. It is worth to note that sharp changes in the graph above is due to the numerical algorithms implied by explicit scheme used by FLAC3D.

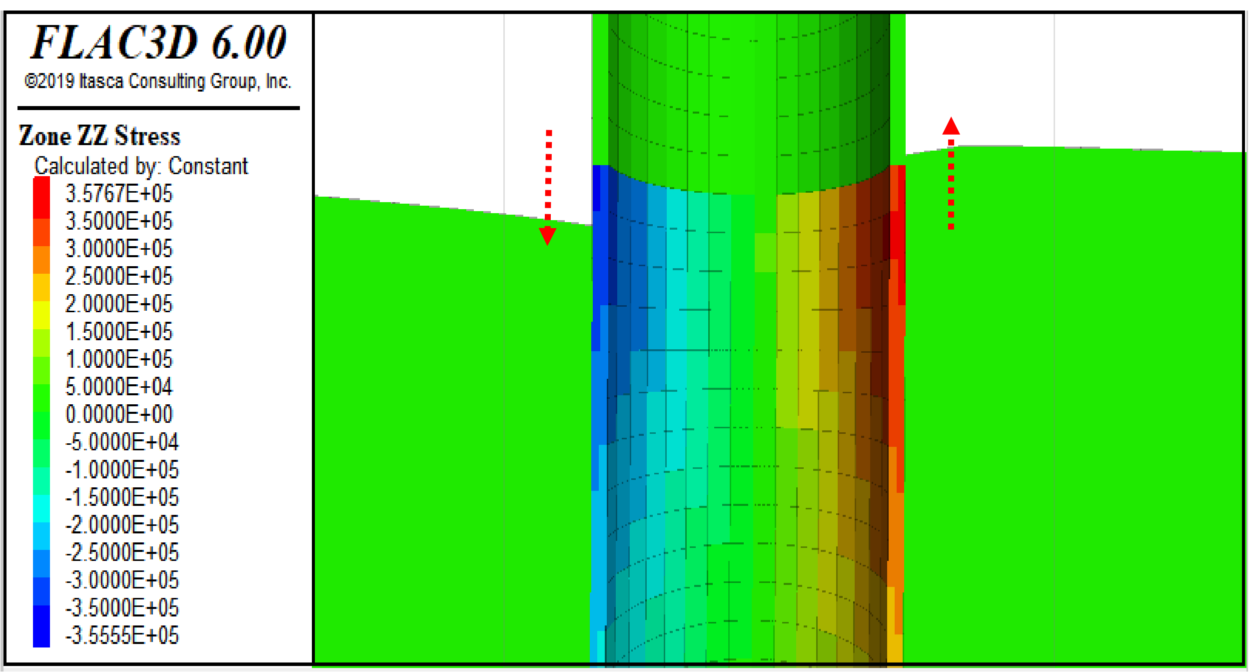

Figure 4-20 Large Strain on and the real effect of pushing Displacement (velocity)

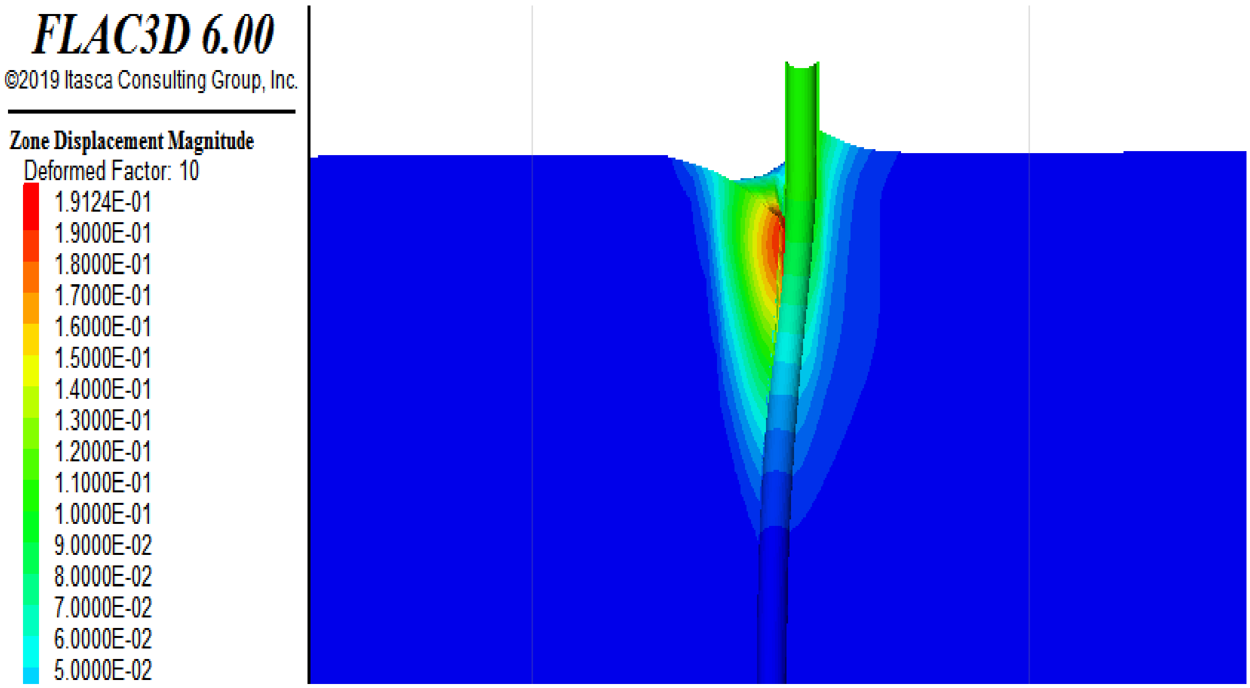

Figure 4-21 Deformed shape of the model at 10 cm displacement applied with amplification factor of 10

4.3.5 Moment diagrams and P-Y Curves:

~~I~~In order to obtain moment diagram from FLAC3D, following method used for extracting the moment values from the results of FLAC3D:

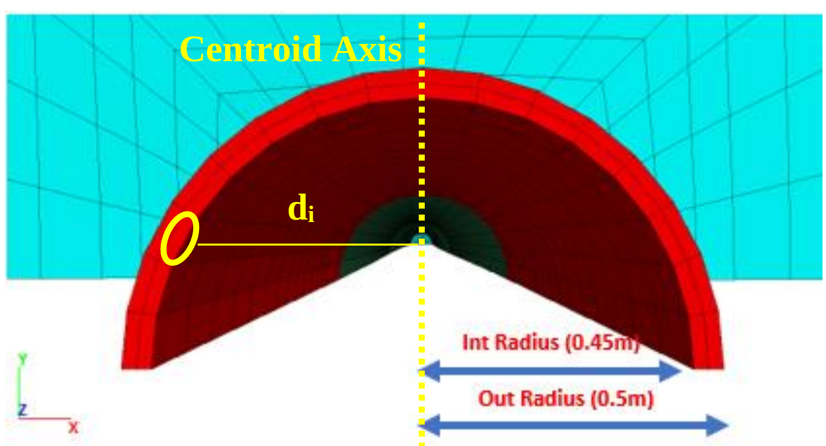

Figure 4-22 Section and element detail (32 element for section)

All elements considered separately for every section in different depth with respect to the element area (2*16) elements for every section called A_i using $\sigma_{zz,i}$ called from the Code at every step which is accessible from the FLAC3D results and with following formula through the Fish Coding language:

(1) $F_i = (\sigma_{zz,i}) * A_i$

(2) $F_i * d_i$

where d_i is distance from Centroid axis,

(3) $M_{tot} = \sum_i^n M_i$

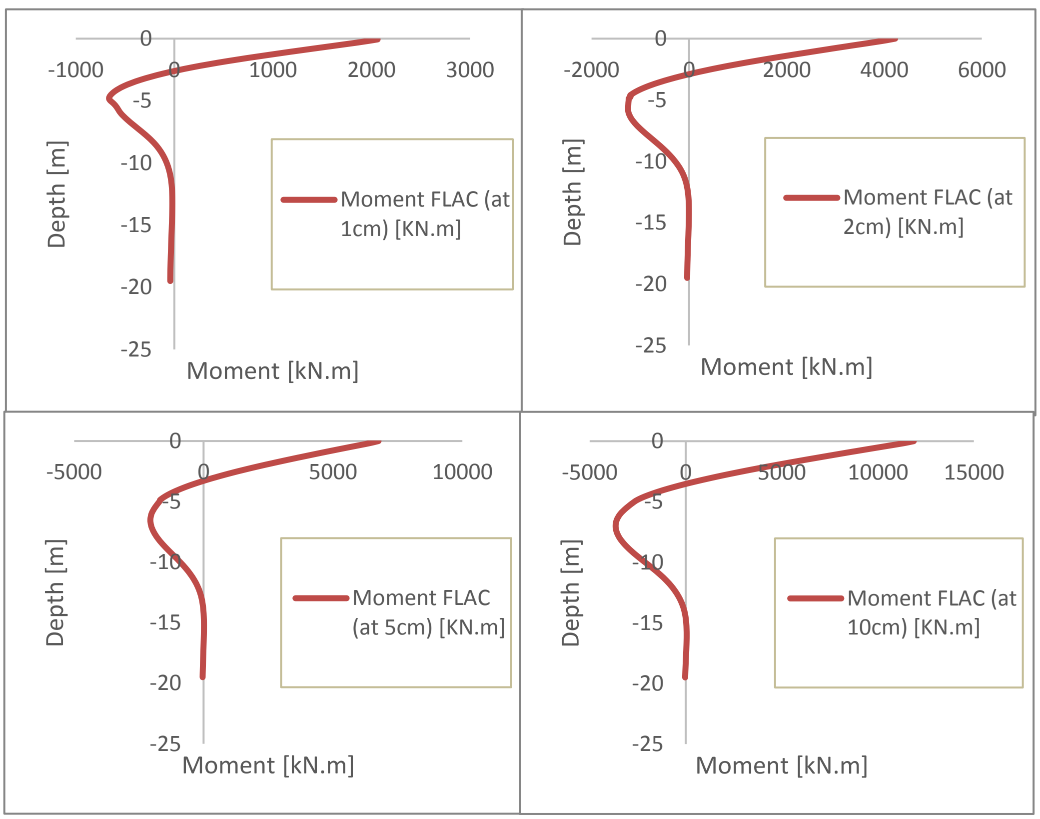

Figure 4-23 Elastic Moment Diagram of the pile at 1,2,5 and 10cm Displacement applied

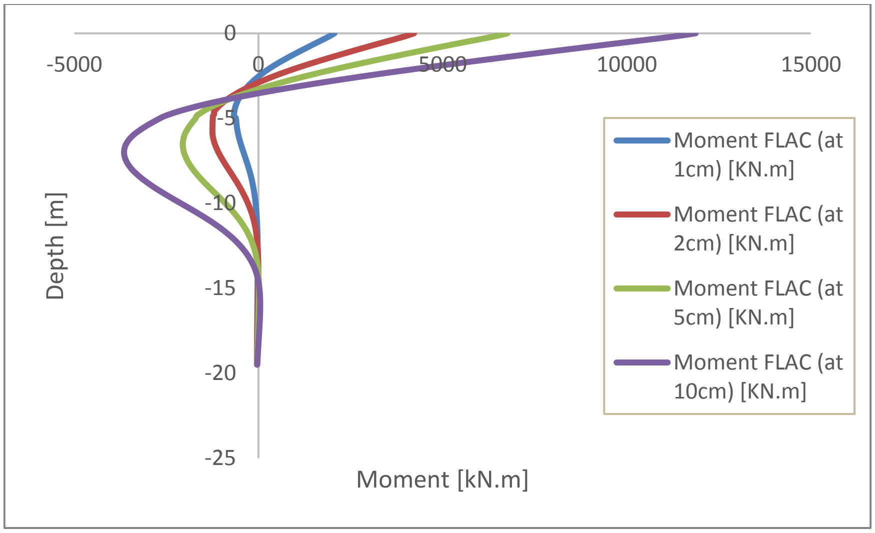

Figure 4-24 Elastic Moment Diagram of different steps of loading, obtained by FLAC3D

As we have applied displacement of 1, 2, 5 and 10 cm, by extracting total reaction values obtained by fish coding feature of the software, now it is possible to create P-Y curve of this case:

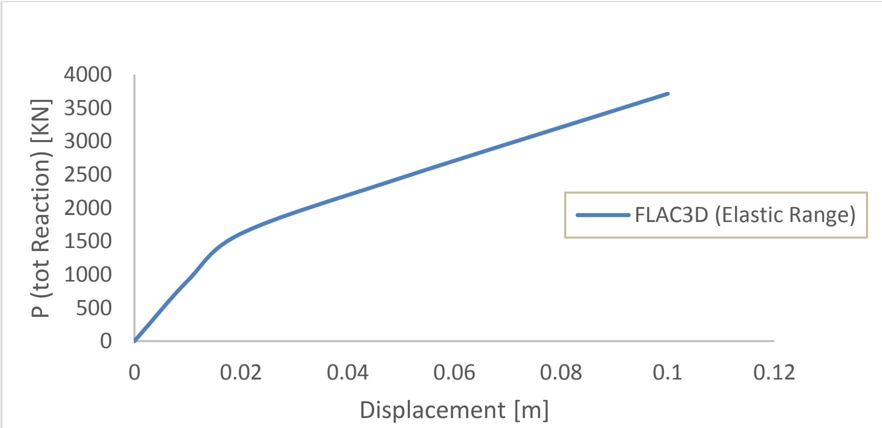

Figure 4-25 P-Y Curve obtained by FLAC3D for Elastic Pile

4.4 FLAC3D Sensitivity analysis for parameters E, G

As matter of numerical modeling and differences between results of FLAC3D and Seismostruct Sensitivity analysis is needed for both FLAC3D and Seismostruct model, in FLAC3D by changing Young modulus E and Shear Modulus G of the soil to the new value which is half of the previous ones in order to have less stiffness for the soil (Granular soil).

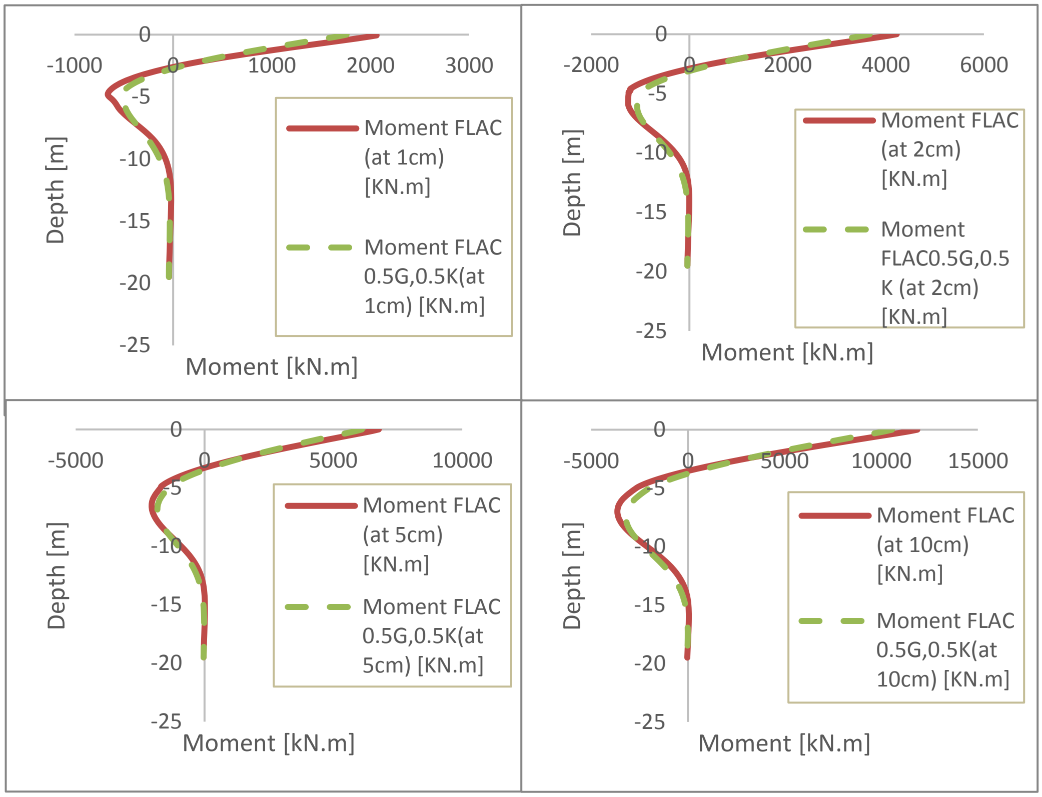

Figure 4-26 Elastic moment diagram for 0.5E,0.5G Vs E, G in FLAC3D at 1, 2, 5 and 10cm Displacement applied

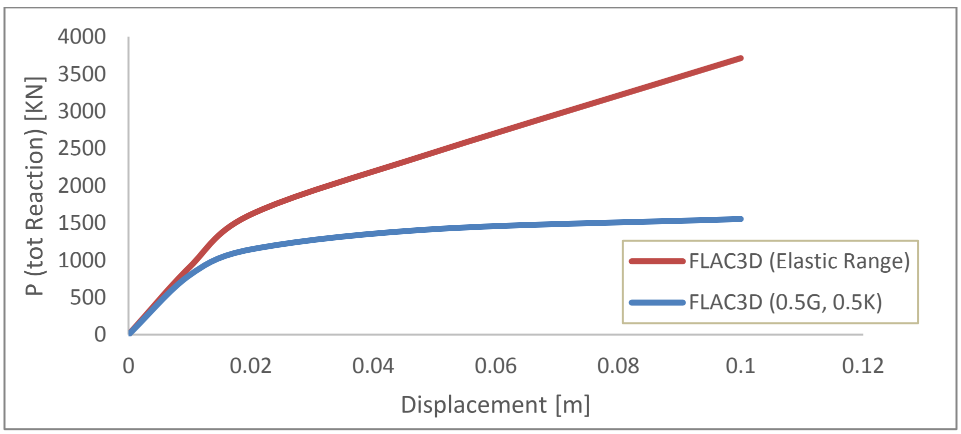

Figure 4-27 P-Y Curve for 0.5E,0.5G Vs E, G in FLAC3D

It is observed from Figure 4-32 that in softer soil model case, full plastic mechanism is formed at smaller horizontal displacement of the foundation, since the relative stiffness contrast of pile with respect to the surrounding zone is altered.

4.5 Single Pile Seismostruct Model:

As well as FLAC3D modeling we made the same model using Seismostruct in order to can verify our model. For this purpose, we modeled our problem in Seismostruct using Winkler and non-linear independent springs approach for subgrade reactions and modeling the soil behavior. Therefore, first the pile defined as 40 elements for every 0.5 meter and total length of the 20 meters with elastic material assignment for the sections and same section as in FLAC3D with circular hollow section with 1 meter out Diameter and 0.9-meter int diameter.

4.5.1 Hyperbolic Model for Non-linear Springs (ASCE):

Along the pile elements 40 springs defined with 3 different elastic modulus with respect to their depth in the soil considering ASCE Hyperbolic relationship (Stevens & Audibert., 1979), using Tri-Linear springs in Seismostruct, where they suggested the following formula for obtaining the elasticity modulus for non-linear springs. Hyperbolic law which is explained in the following has some challenging factors like N_{qh} or Y_u which are not exact, and, in this sense, sensitivity analysis would be required.

$$P = \frac{y}{A' + B'y}$$

Where:

$A' = 0.15 * y_U / P_U$

$B' = 0.85 * P_U$

$P_U = \bar{\gamma} * H * N_{qh} * D$

$$y_U = \begin{cases} 0.07 \text{ to } 0.1\ (H + D/2) \text{ for loose sand} \\ 0.03 \text{ to } 0.05\ (H + D/2) \text{ for medium sand} \\ 0.02 \text{ to } 0.03\ (H + D/2) \text{ for dense sand} \end{cases}$$

$\bar{\gamma}$ = effective unit weight of the soil

H = Depth of the element

N_{qh} = Horizontal bearing capacity factor (obtained from the Figure 3-44)

D = External-Diameter of the pile

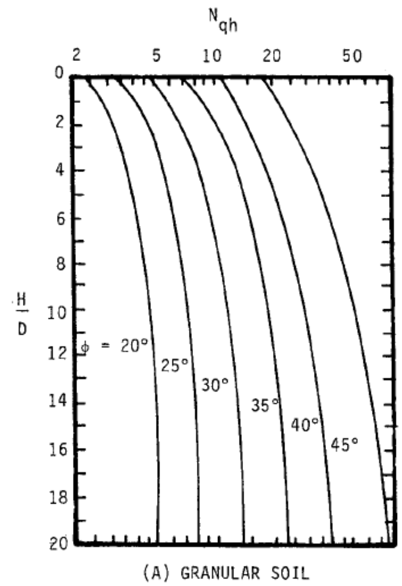

Figure 4-28 Horizontal Bearing capacity factor as a function of depth to diameter ratio (Adapted from Hansen., 1955)

By using a spreadsheet ,using above equations different elasticity modulus obtained to model the non-linearity of the soil (springs) with respect to displacement applied with steps of 0.005 meter or every 0.5 centimeter in order to obtain the p-y curves as well for every element in different depths, and then connecting every defined springs to the pile elements in order to model the Soil-Pile behavior. An elastic pile with 40 elements (every 0.5 meter) with length 20m modeled as well (Figure 3-26). Therefore, static pushover analysis method applied to this model with steps of 0.005m or 0.5cm and by extracting the shear force diagram values for every spring with respect to the displacement applied, p-y curves obtained for this model as well as moment diagram for the purpose of the comparison with FLAC3D, shown in the following figures.

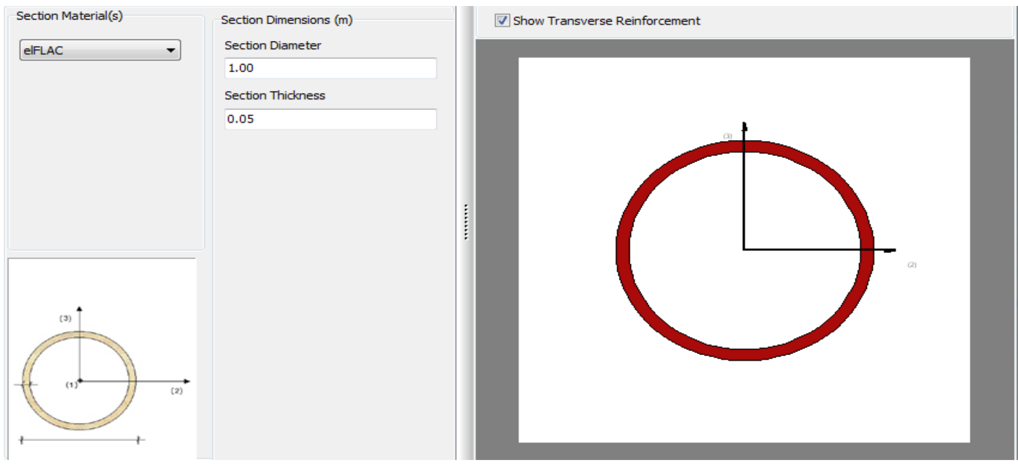

Figure 4-29 Hollow circular cross section Defined in Seismostruct

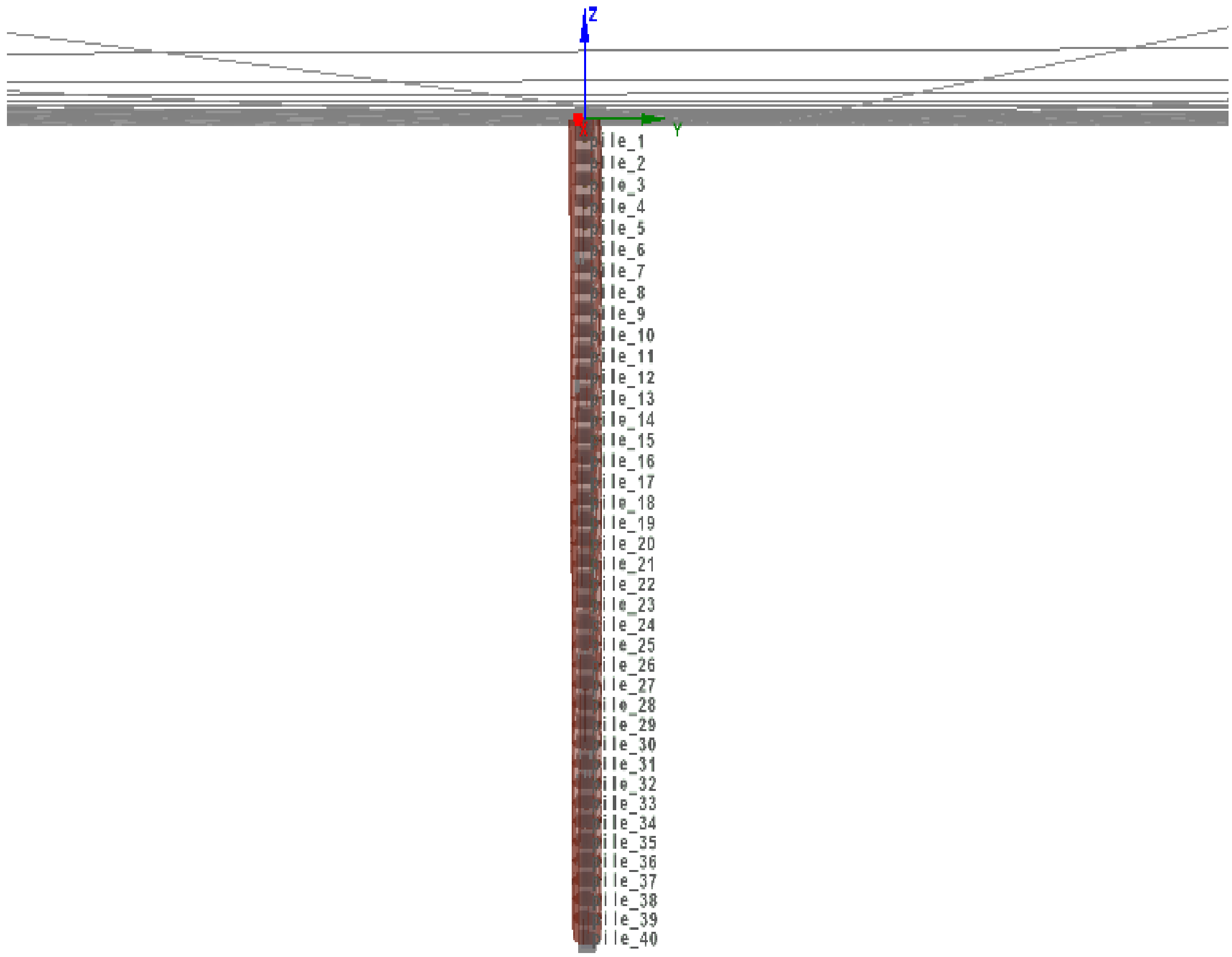

Figure 4-30 Seismostruct Model Illustration

It is worth to mention that the code is fiber-based, thus, the cross-sectional response is determined by uniaxial stress-strain response of the fibers present inside the section. In linear pile case, the model of fibers is elastic with young’s modulus constant defined in FLAC3D.

4.5.2 Seismostruct Results (Elastic Pile Material):

After running static pushover analysis with total 10 cm horizontal displacement (X-Axis) applied results below obtained

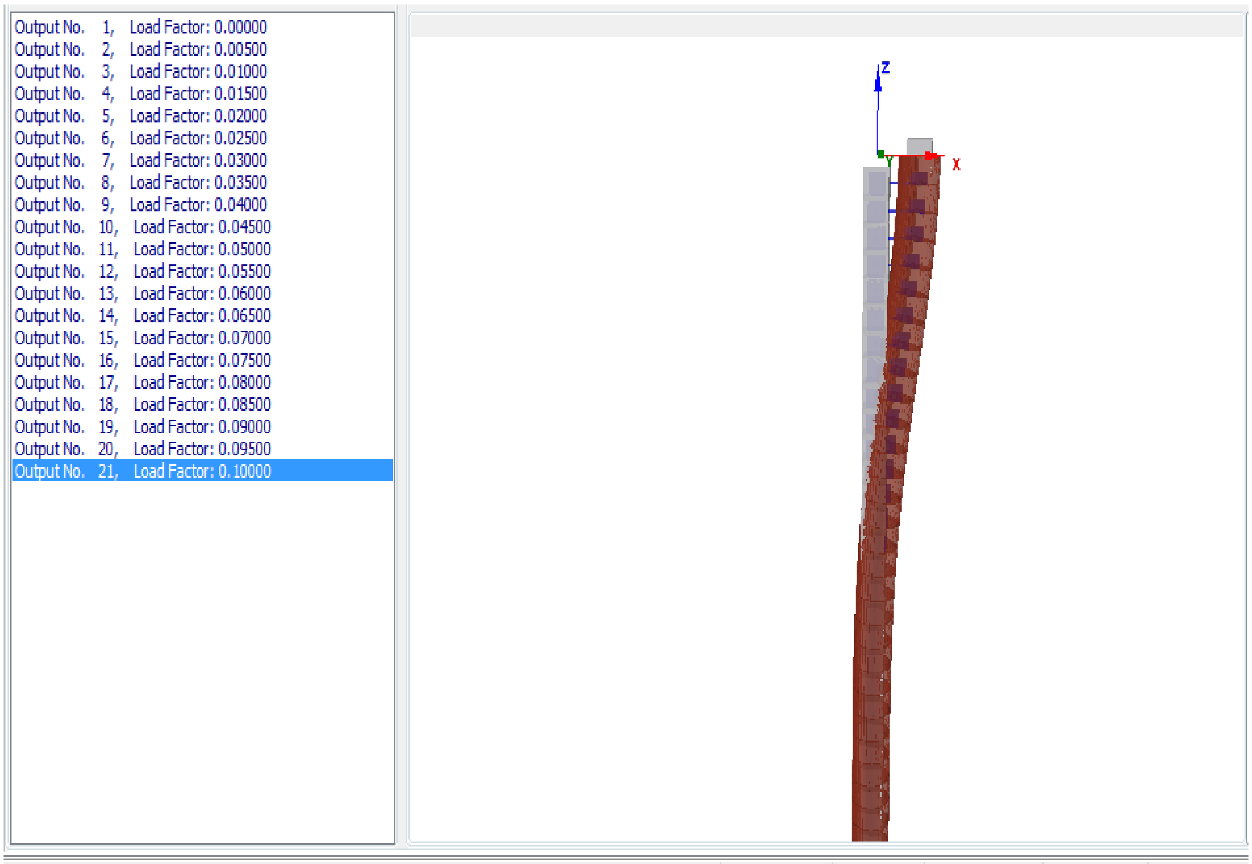

Figure 4-31 Deformed Shape of the Seismostruct after 10 cm displacement pushed

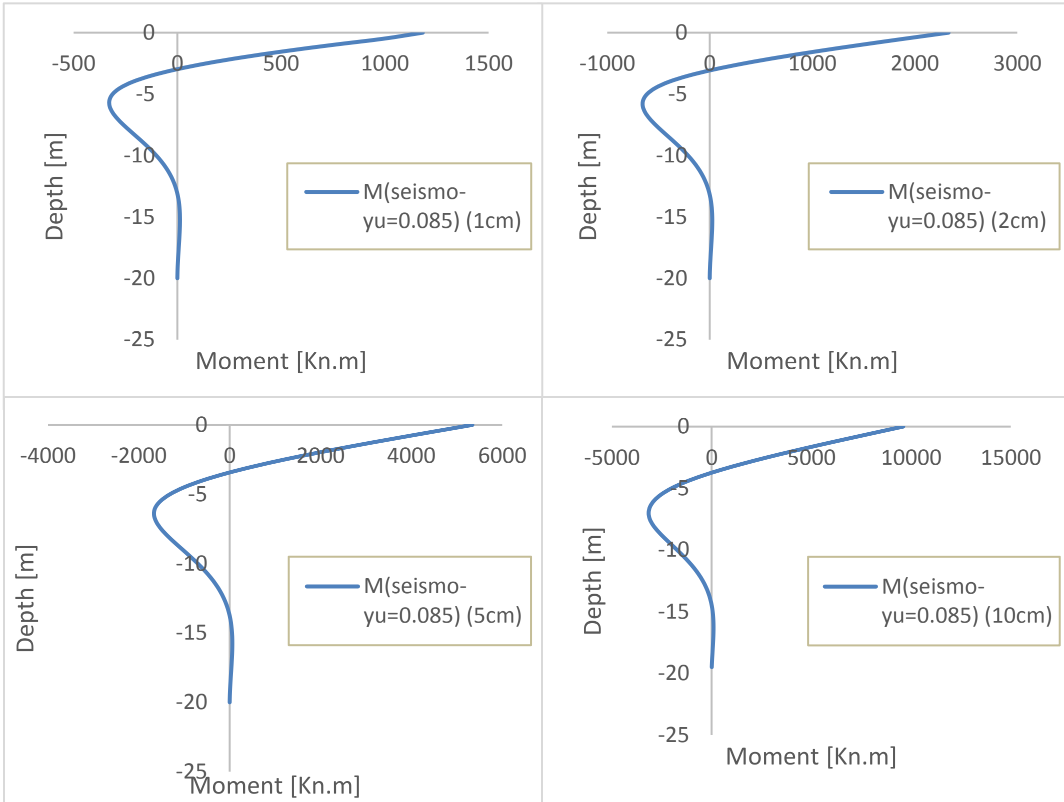

Figure 4-32 Elastic Moment Diagram of different steps of loading, obtained by Seismostruct

By extracting shear forces acting on the pile we can easily obtain p-y curve for different displacement pushed to the pile:

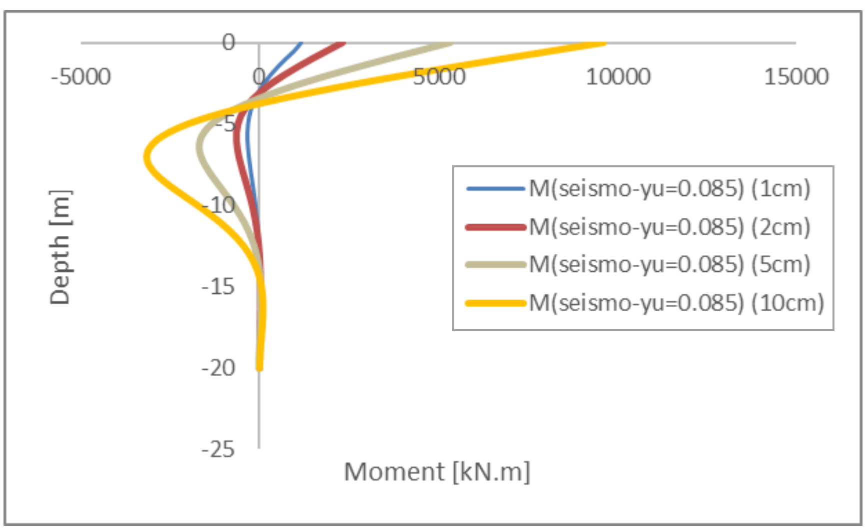

Figure 4-33 Moment Diagram obtained by Seismostruct at 1, 2,5 and 10cm applied displacement (Yu=0.085)

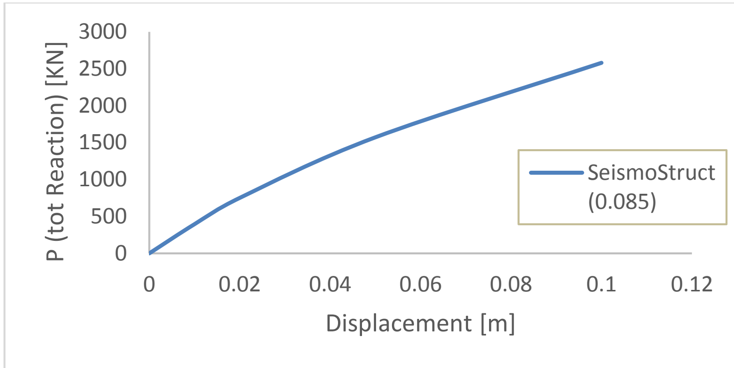

Figure 4-34 P-Y Curve obtained by Seismostruct

4.6 Seismostruct Sensitivity Analysis for parameter y_u:

Values for y_u used and calculations repeated with constant value of 0.04 and variable value from 0.02 to 0.085 with respect to depth in order to have better distribution of the depth's coefficient which previously was constant value of 0.085.

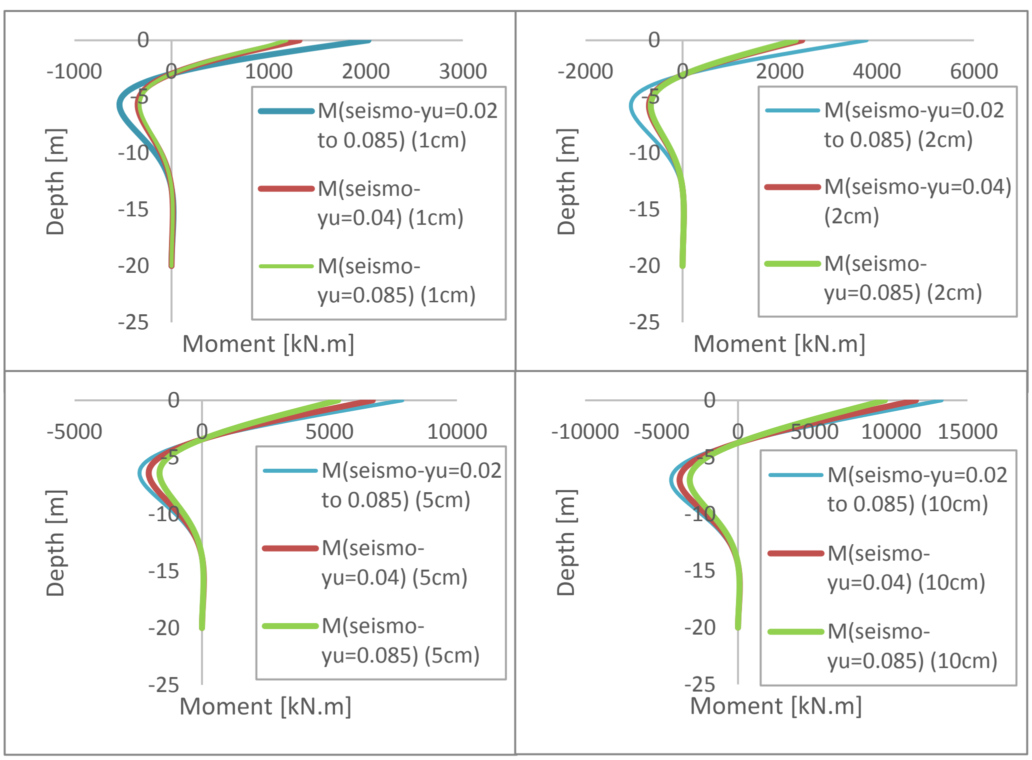

Figure 4-35 moment diagram for Y_u 0.04, 0.02 Vs y_u 0.085 in Seismostruct at 1, 2, 5 and 10cm Displacement applied

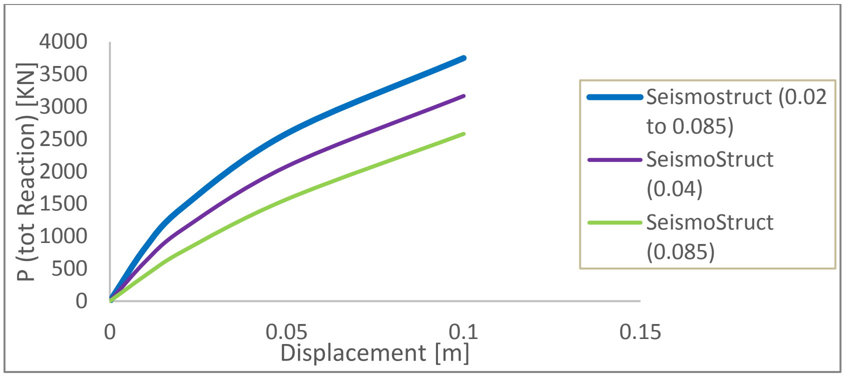

Figure 4-36 P-Y Curve for 0.085, 0.4, 0.02 in Seismostruct

Strong dependencies of moment diagrams and total horizontal force capacity (P) are noted as a function of the spring elasticity constants (i.e. yu parameter controlling these constants)

4.7 Finding best match of the results obtained from FLAC3D and Seismostruct:

In order to find the best match from the results obtained by both software we need to plot all in one graph and compare the results as following:

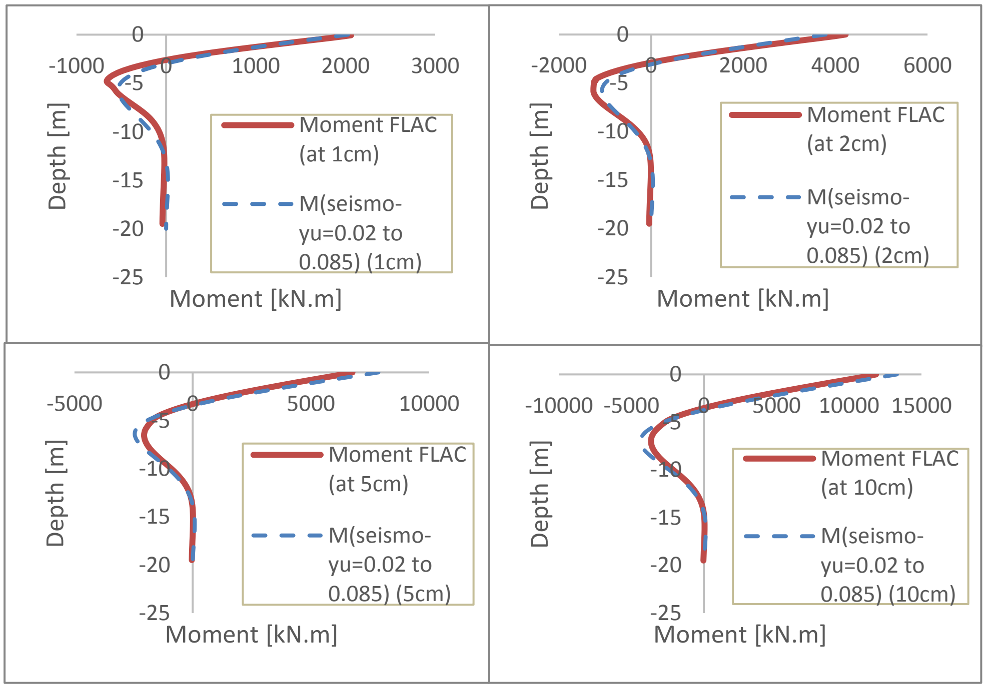

Figure 4-37 Best Elastic moment diagram's match among the results at 1, 2, 5 and10cm displacement applied

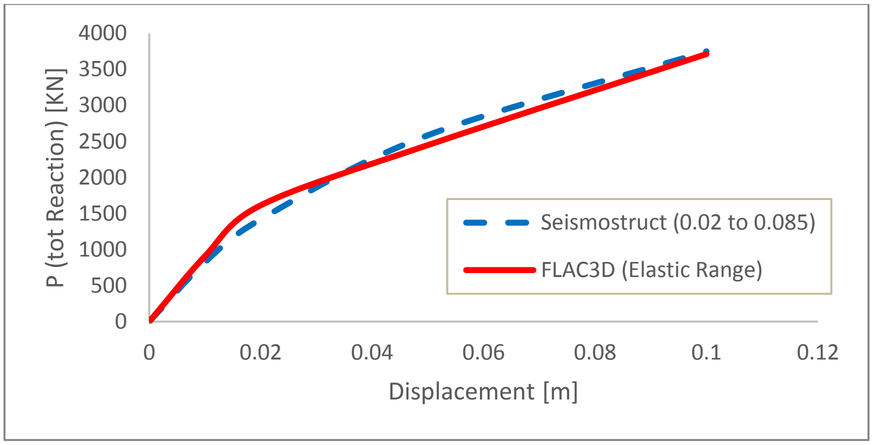

Figure 4-38 Best Elastic P-Y curve's match among the results

According to the stiffness ratio present in the model, p-y approach is able to predict the distribution of the moment diagram and global force-displacement relation with a reasonable accuracy.

4.8 FLAC3D & Seismostruct Results (Plastic Pile Material):

After getting good match between the results of FLAC3D and Seismostruct, now we can Model and consider Plastic behavior of the piles which is so-called Non-Linear behavior of the material, by inserting the Von-Mises model to the pile zones with corresponding cohesion. Then with help of a fish script (discussed earlier), we easily obtained the M_{pl} acting on sections in every different depth with the same mesh we used previously, considering average weighted moment for every different element of on section with respect to its distance from the centroidal axis of the section.

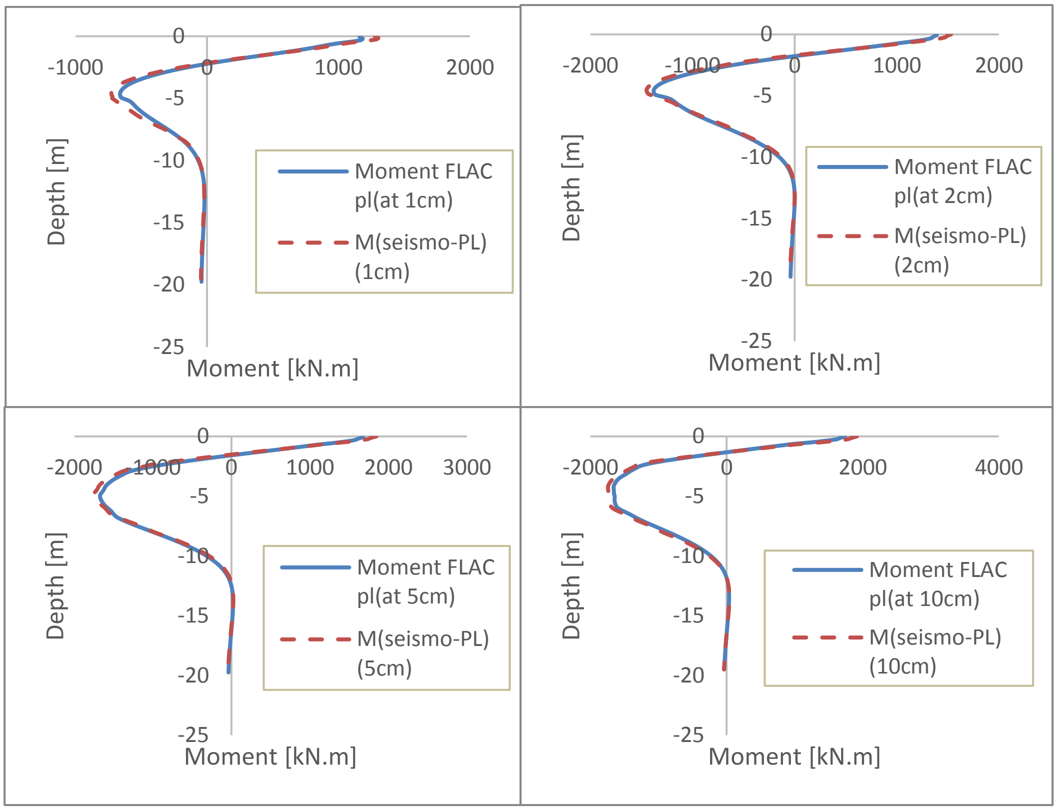

Figure 4-39 Comparison of the Plastic moments obtained by FLAC3D and Seismostructof different displacement applied

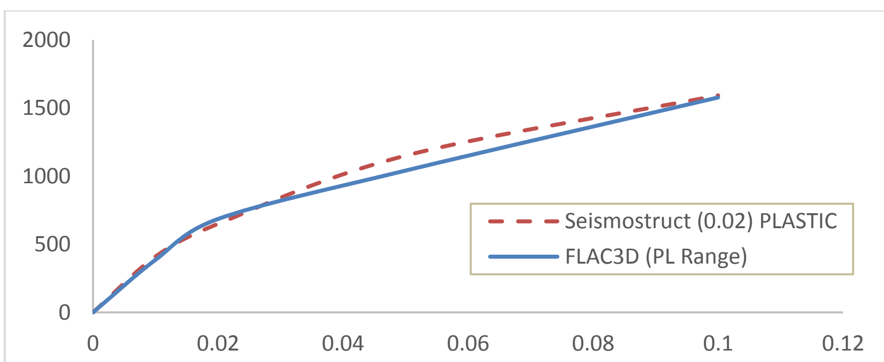

Figure 4-40 Comparison of the Plastic P-Y curve obtained by FLAC3D and Seismostruct

On the model of SeismoStruct, on the other hand, simply the constitutive relation of the fibers is changed to symmetric elasto-plastic with uniaxial strength equals to 2 times the cohesion value (adopting the concept of Mohr's Circles). The corresponding match between two approaches are found reasonably close.

CHAPTER 5
NUMERICAL CASE STUDY OF A 3x3 PILE GROUP UNDER LINEAR AND NON-LINEAR PILE RESPONSE

The continuum model of the pile group, built in FLAC3D (ITASCA 2009), is validated in this section by simulating a specific pile group problem as well as modeling this problem by Seismostruct software by means of modeling the pile group using set of subgrade set of non-linear springs playing the rule of soil reaction to the piles, where in both modeling pile considered both as elastic and plastic materials. Pushover analysis applied in both software in order to compare the results and calculating the group reduction factor and group efficiency.

5.1 FLAC3D Model:

In FLAC3D software a pile group of 3x3 with spacing of 3 times diameter center to center of the piles considered where because of the symmetry of the problem just half of the case modeled and then the results multiplied by 2. Pile diameters are same as before (1m) and 25 meters of the soil modeled around the piles to have all the effected part of the soil. 3 different case considered as pile groups with elastic material, pile groups with plastic material and pile groups with plastic material considering surcharge applied on the surface of the soil.

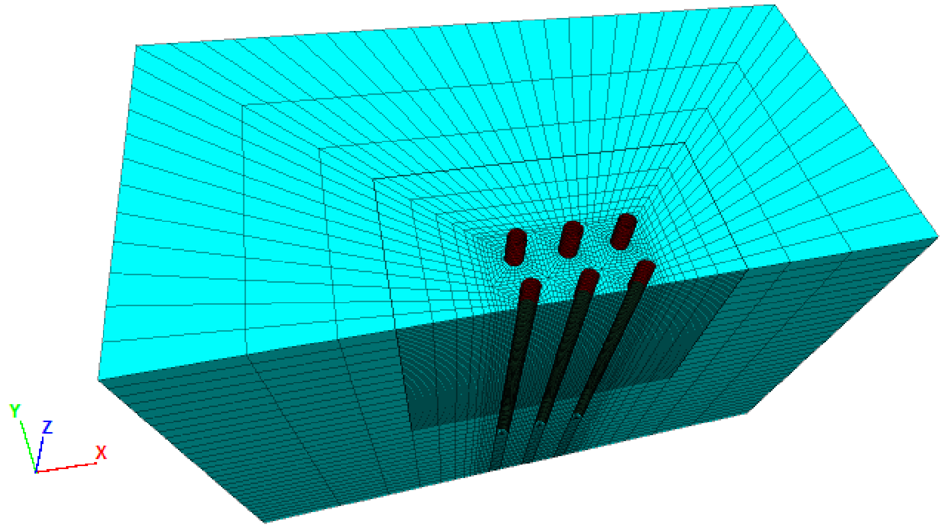

Figure 5-1 Model and meshing of 3x3 pile group (Half of the model)

5.2 Application of the load:

For applying the load, a pushover method used by means of pseudo-velocity (=target displacement / number of cycles) in FLAC3D which can be considered as displacement in static case and the steps of applying the load is the same as used in the previous section (1, 2, 5 and 10 cm) to the top of the piles, where a group of stem defined and the loads applied to them in x-direction. For the sake of checking if the mechanism changing by adding surcharge or not, 50 kPa distributed surficial pressure applied in another case in order to check the mechanism and effect.

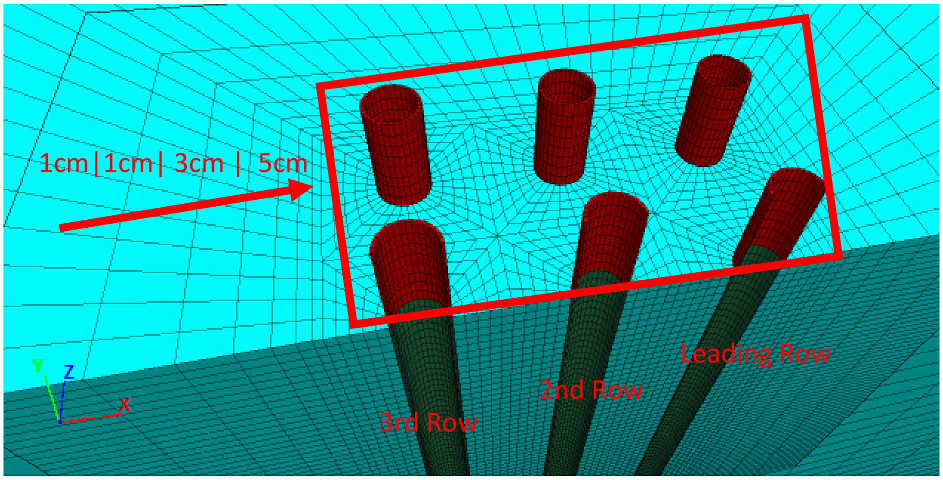

Figure 5-2 Application of the load

5.3 Material Properties:

As properties of the pile and soil following parameters used for this model:

Material	Zone Constitutive model	Shear Modolus G [kN/m2]	Elastic Modolus E [kN/m2]	Friction angle ϕ (º)	Cohesion c (º)
Pile	Elastic and Drucker-Pruger	$3.8 * 10^{7}$	$8.7 * 10^{7}$	0	$2.7 * 10^{6}$
Soil	Mohr-Coloumb	$3.8 * 10^{4}$	$1.75 * 10^{5}$	30	0

Table 5-1 Model Properties used in FLAC3D Modeling.

5.4 Results obtained from FLAC3D:

The results which obtained from FLAC3D are different for every pile in group with respect to the position they have, these values are close to each other if they are in the same row with respect to the displacement applied (loading direction) to the piles.

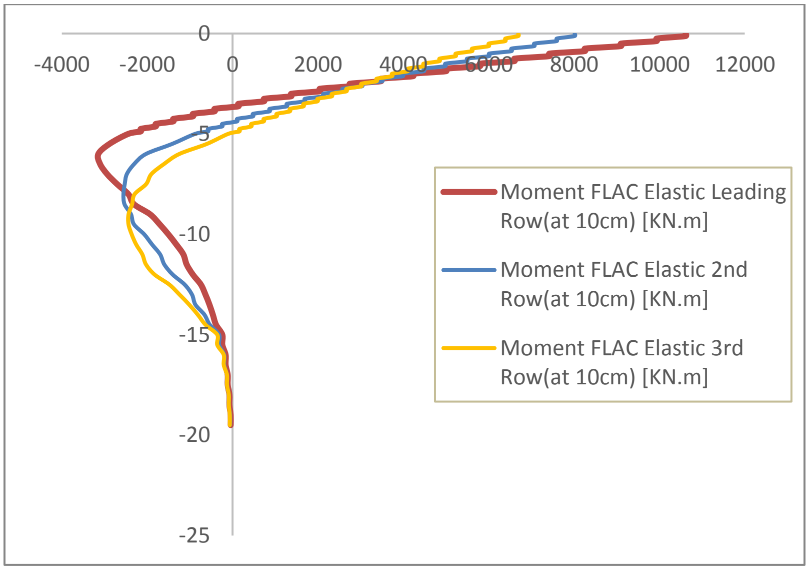

Figure 5-3 Moment diagram acting on the pile in different rows with respect to the loading direction with Elastic Material

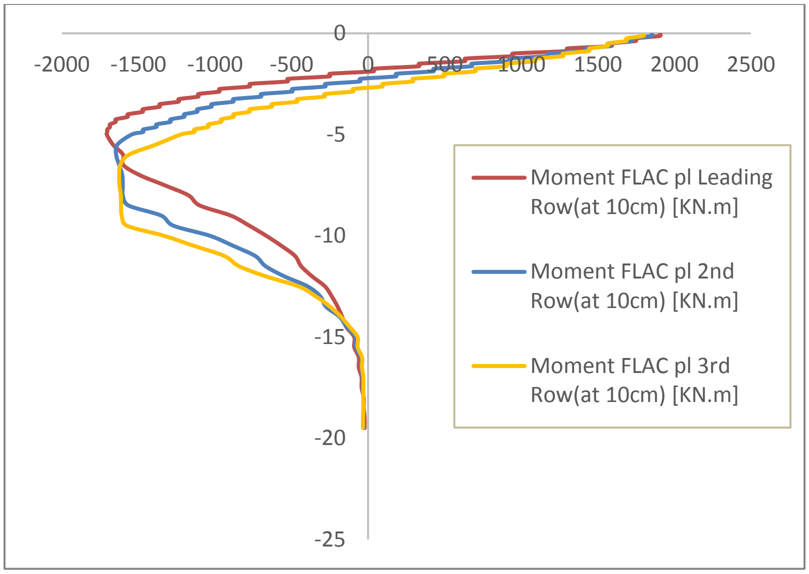

Figure 5-4 Moment diagram acting on the pile in different rows with respect to the loading direction with Plastic Material

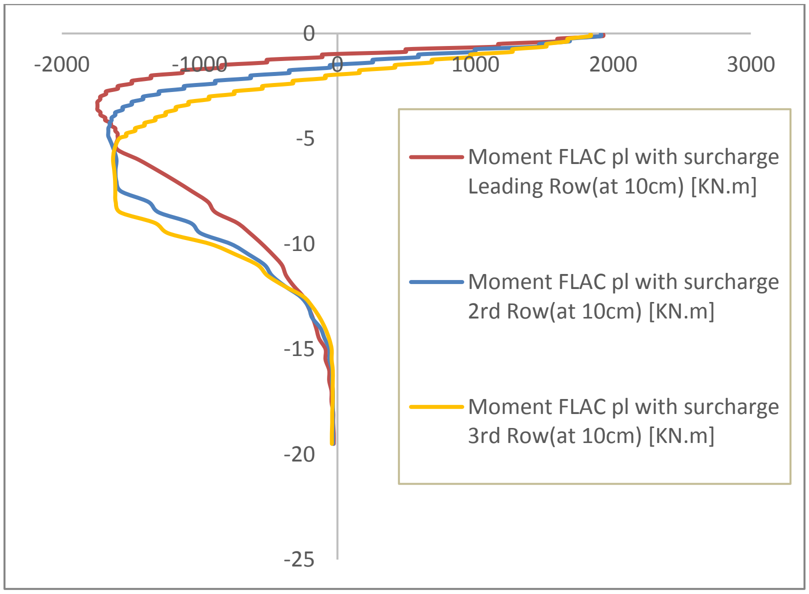

Figure 5-5 Moment diagram acting on the pile in different rows with Plastic Material with surcharge

The presence of surcharge shifted the moment diagrams to upper elevations due to increased passive resistance. A local increase on the plastic moment value in the leading row piles is noted. This is because of high confining passive-pressure exerted by the soil, especially in the case under the effect of surcharge.

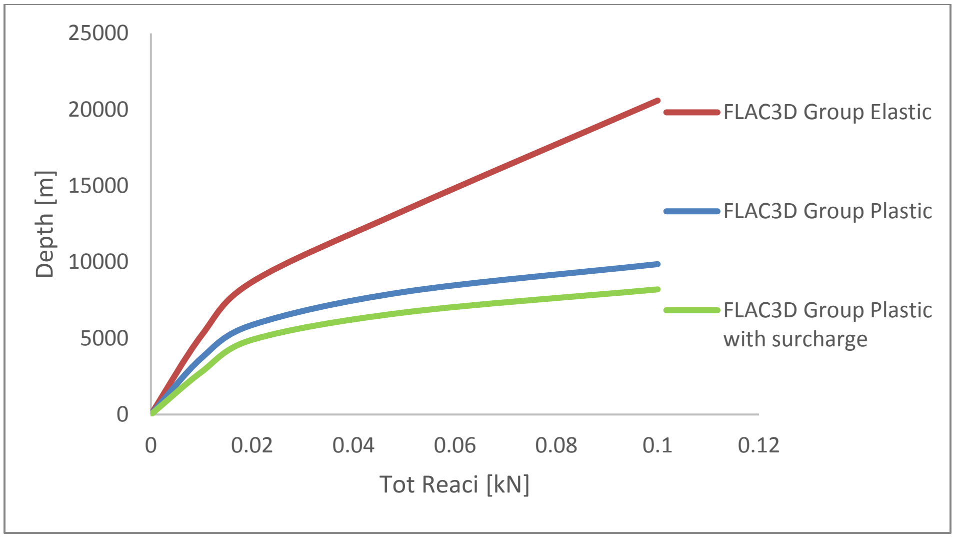

Figure 5-6 P-Y Curve for Elastic, Plastic pile group material and Plastic pile group material with surcharge (FLAC3D)

From the Figure 5-6, firstly it is visible that the capacity of the group with elastic material (increased value of the Drucker-Prager cohesion) has significant difference than the pile group with plastic material and behavior. Secondly in pile group with plastic material if a surcharge would be added to the surface of the soil, it decreases the pile group capacity, but this reduction is not significant in our case, and it doesn't affect the behavior of the group visibly.

5.5 Seismostruct Model:

A pile group (3x3) with 3 times diameter spacing of the center to center with 20 meters of length modeled. Pile diameters are 1 meter and soil modeled by means of set of non-linear springs with linear variable coefficient of the depth using hyperbolic law connected to every element of the pile with different value for the E values of the springs for depth for leading row with respect to the direction of the load and all these value were reduced by reduction factors for second row and third row (Suggested by Christensen, 2006). Row reduction factors directly used for E values of the non-linear springs in the software are 1, 0.7 and 0.65 for the leading row, 2nd row and 3rd row respectively. Modeled for elastic and plastic material for the piles. All piles were modeled with 40 elements in vertical direction (0.5-meter length for every element).

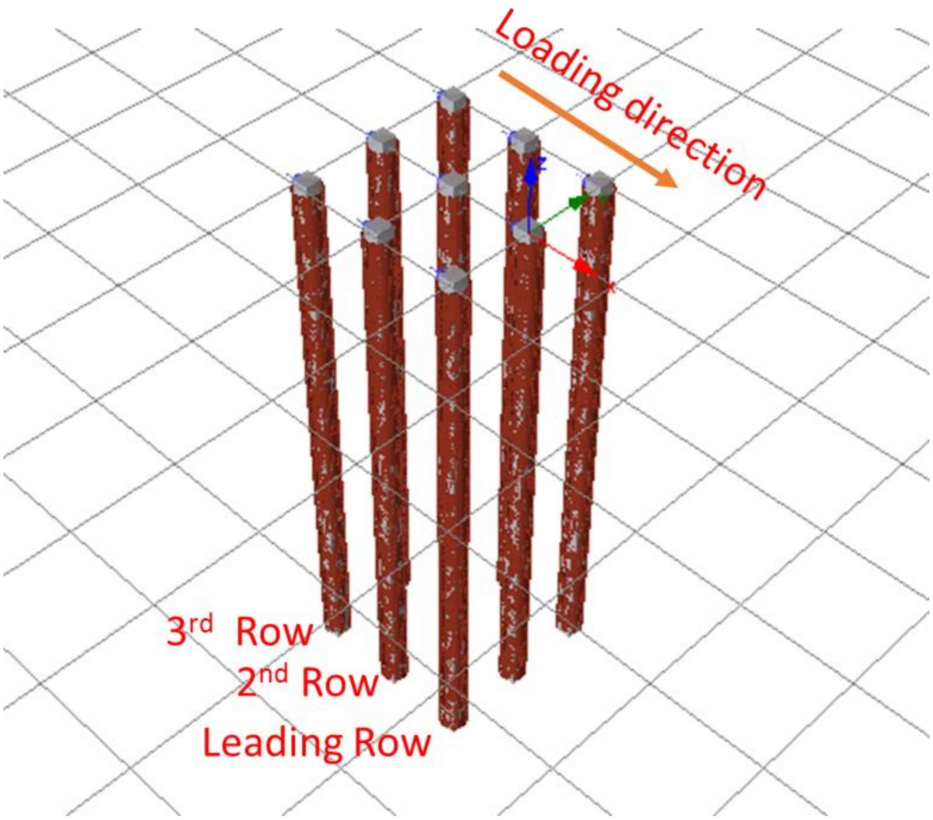

Figure 5-7 Seismostruct Model

5.6 Application of the Load:

For applying the load, a static pushover analysis method applied with steps of 0.05 meter in x-direction in order to extract results for the state of (1, 2, 5 and 10 cm).

5.7 Material Properties:

As properties of the pile elastic modulus E [kN/m2]: 87230000, different values of the young modulus for different depth and also different rows of the pile.

Material	Shear Modulus G [kN/m2]	Elastic Modulus E [kN/m2]	Friction Angle ϕ (º)	Cohesion c (º)
Pile	$3.8 * 10^7$	$8.7 * 10^7$	0	-

Table 5-2 Model Properties used in Seismostruct Modeling

5.8 Results obtained from Seismostruct:

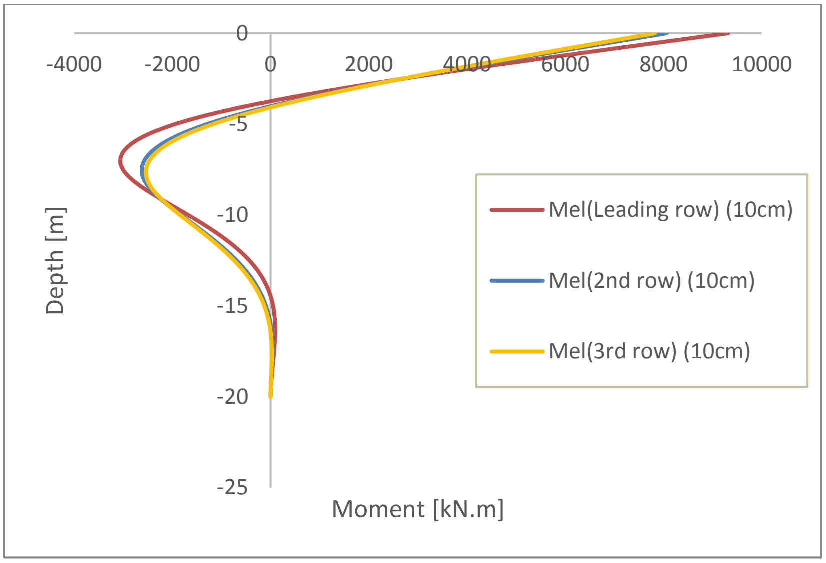

Figure 5-8 Moment diagram acting on the piles in different rows with Elastic Material (Seismostruct)

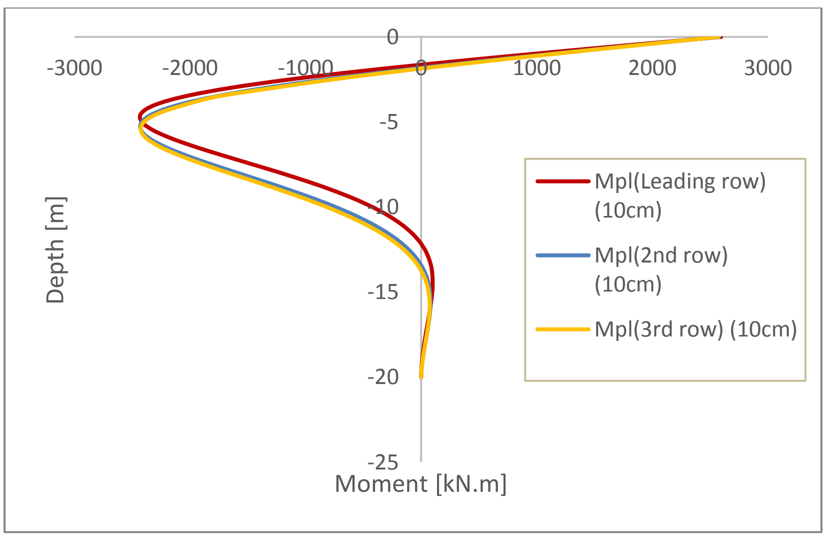

Figure 5-9 Moment diagram acting on the piles in different rows with Plastic Material (Seismostruct)

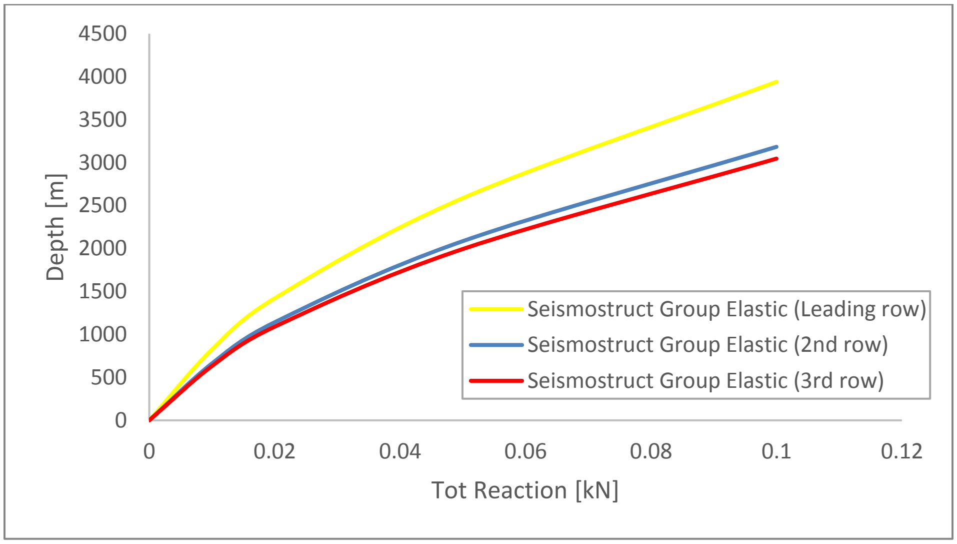

Figure 5-10 P-Y Curve for Elastic material pile group Leading row, 2^{nd} row and 3^{rd} row (Seismostruct)

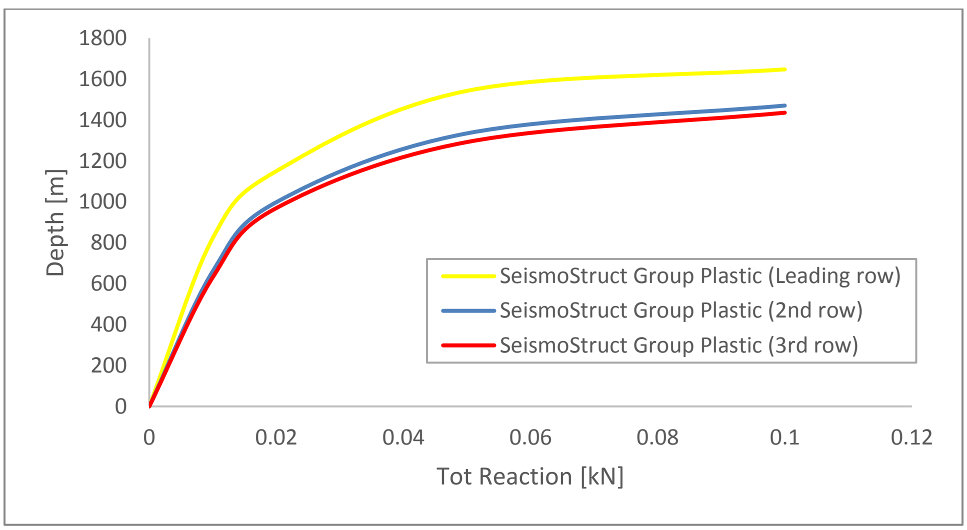

Figure 5-11 P-Y Curve for Plastic material pile group Leading row, 2^{nd} row and 3^{rd} row (Seismostruct)

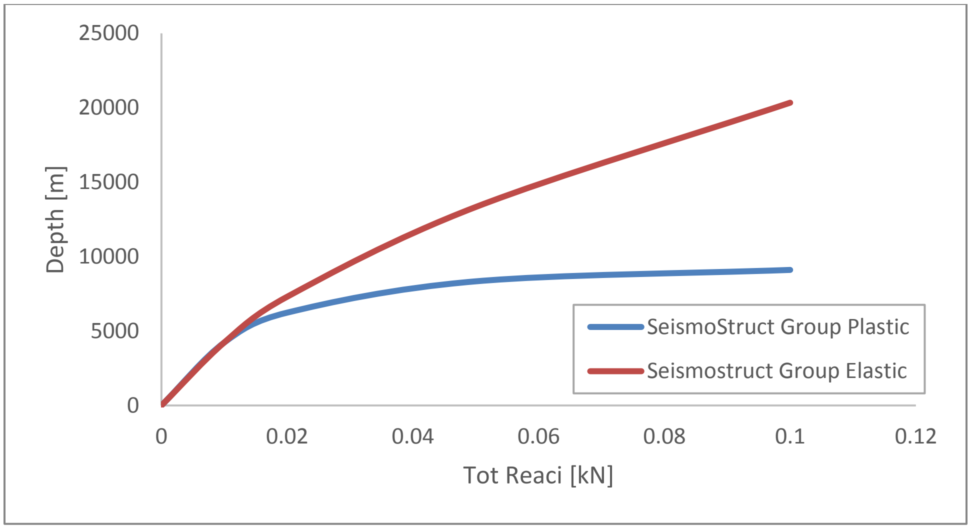

Figure 5-12 P-Y Curve Elastic and Plastic pile group (Seismostruct)

As we can see by moment diagrams and p-y curves from Figures 5-10, 5-11, 5-12 and 5-13 the capacity of the leading row is more than 2nd and 3rd row with a significant decrease of the capacity, where 2nd and 3rd row have almost the same capacity, this behavior is the same for both Pile material (Elastic and Plastic). Moreover, from Figure 5-14 we can see a particular decrease of the group effect for different pile material (Elastic and Plastic), where mobilization is visible in plastic pile material case but this state is not reach yet for elastic pile material.

5.9 Comparison of the results obtained by FLAC3D and Seismostruct:

A comparison is made with respect to the pile positions through the group as leading row, 2nd row and 3rd row. For example, piles positioned in the leading row have almost the same values of the moment and same the p-y curves. Therefore, we can take one pile results from each row to compare the results.

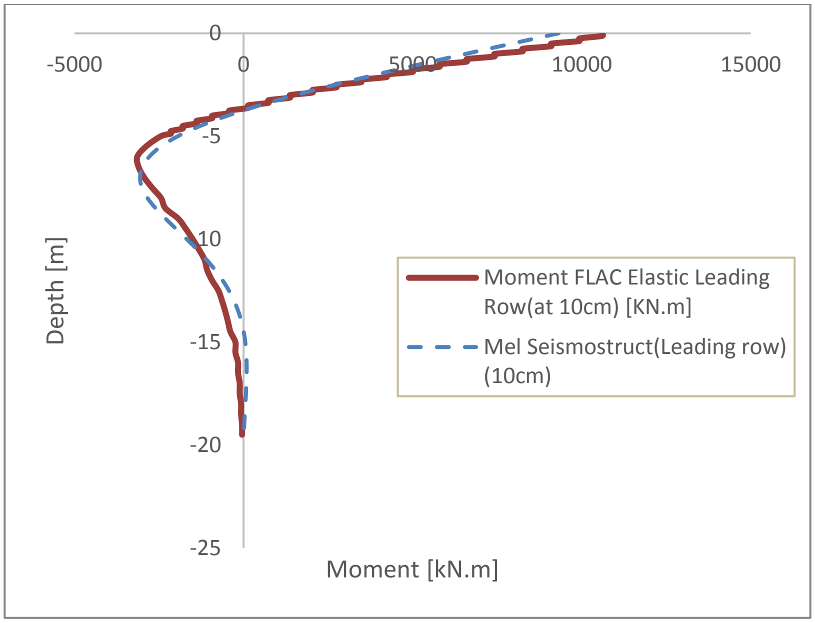

Figure 5-13 Elastic Moment Diagram acting on Leading row piles (FLAC3D vs Seismostruct)

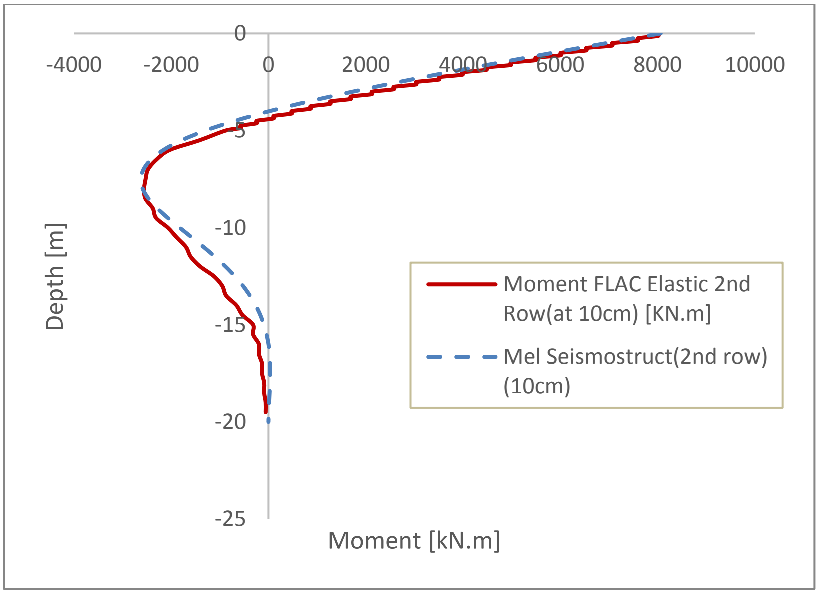

Figure 5-14 Elastic Moment Diagram acting on 2nd row piles (FLAC3D vs Seismostruct)

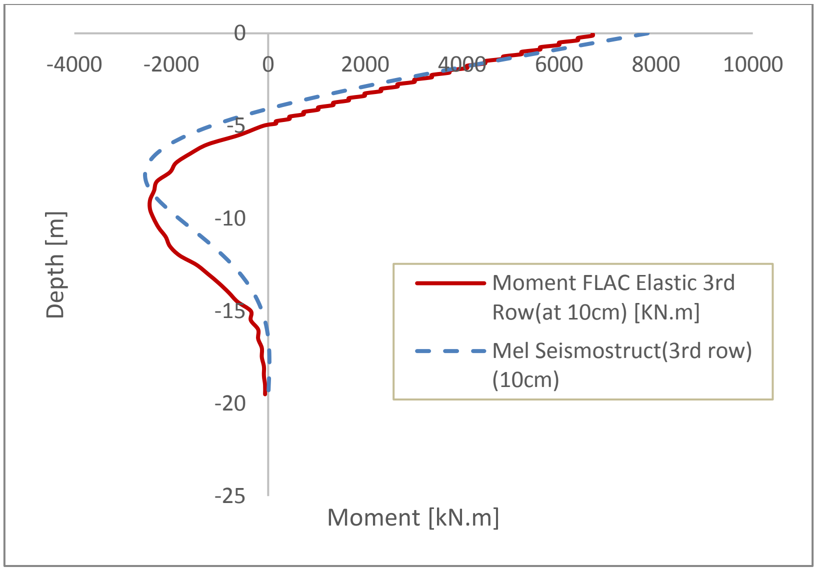

Figure 5-15 Elastic Moment Diagram acting on 3rd row piles (FLAC3D vs Seismostruct)

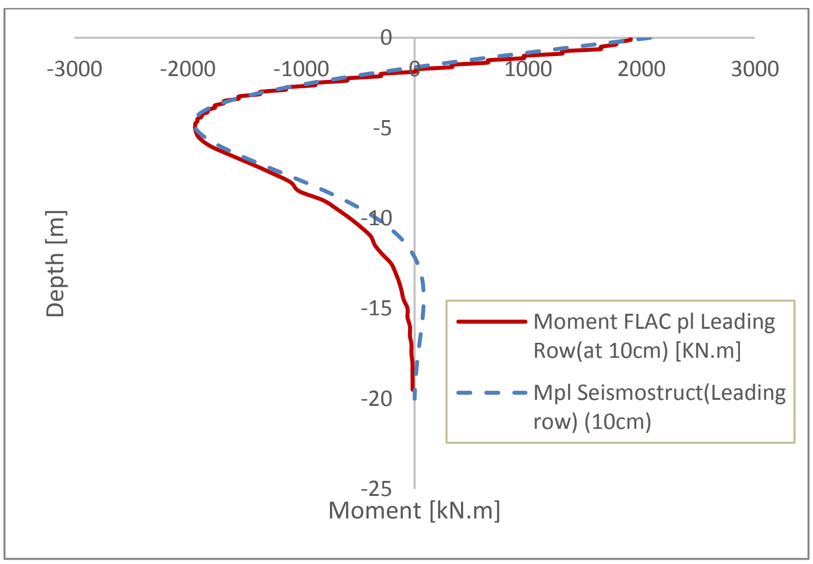

Figure 5-16 Plastic Moment Diagram acting on Leading row piles (FLAC3D vs Seismostruct)

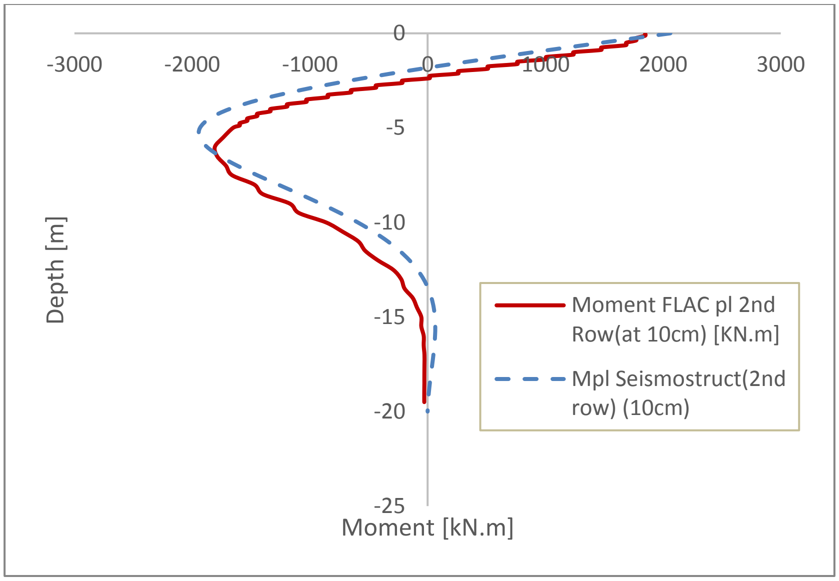

Figure 5-17 Plastic Moment Diagram acting on 2nd row piles (FLAC3D vs Seismostruct)

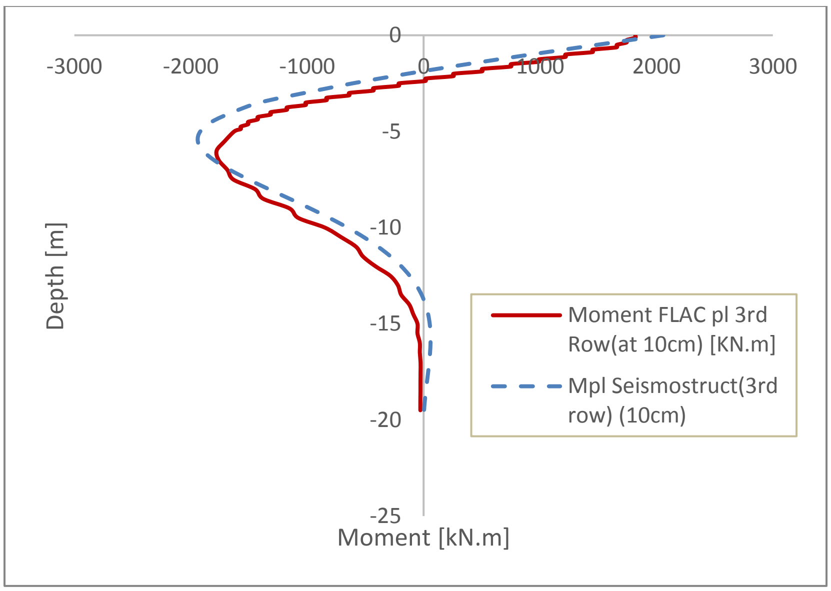

Figure 5-18 Plastic Moment Diagram acting on 3rd row piles (FLAC3D vs Seismostruct)

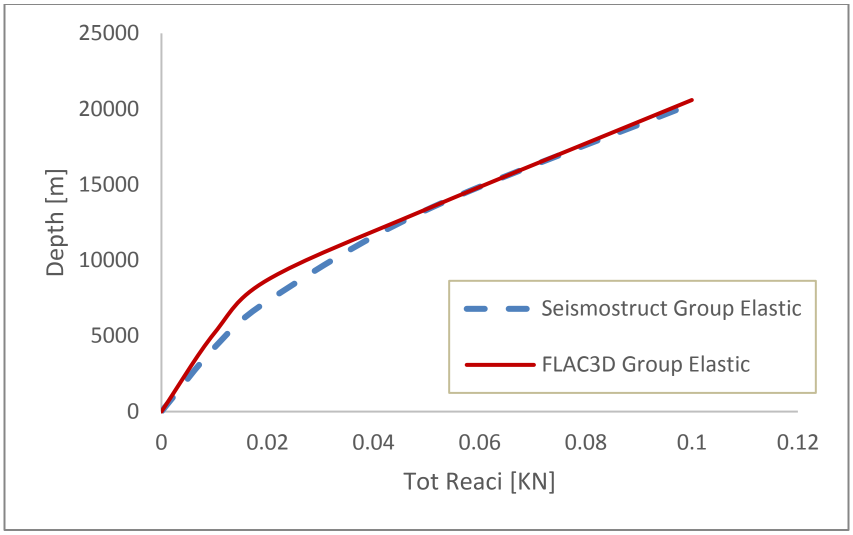

Figure 5-19 Comparison of the P-Y curves (ELASTIC) FLAC3D Vs Seismostruct

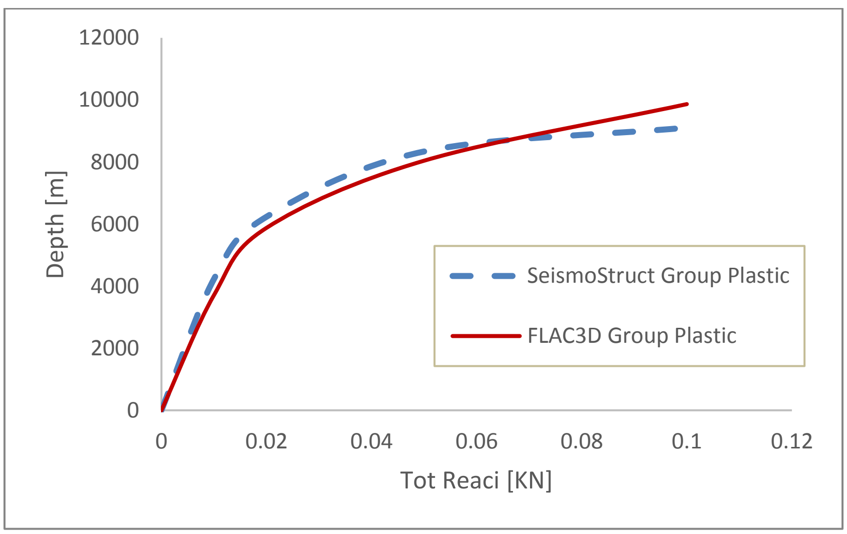

Figure 5-20 Comparison of the P-Y curves (PLASTIC) FLAC3D Vs Seismostruct

As we can see the results obtained by two software have good agreement to each other, where p-y response at foundation level is found satisfactory, In elastic pile case, 1st and 2nd row pile bending moment responses could be approached with p-y method, yet in the last row, maximum moment is observed at higher depths and in plastic pile case, from the p-y approach, it seems that maximum moment is slightly overestimated for 2nd and 3rd row of piles with an upwards shift on its position.

5.10 Calculation of the group efficiency factor using results of the single pile and group of pile obtained from FLAC3D:

By using the group effect factor formula as following we can easily now calculate the group effect factor for the cases, we simulated

$$\eta = \frac{Group\ reaction}{n_p.(reaction\ of\ one\ pile\ acting\ as\ single)}$$

Linear Group Effect			
	Flac3d Single Elastic	Flac3d Group Elastic	Group Effect
Tot Reaction at 1cm	968	5194.74	0.596
Tot Reaction at 2cm	1613.7	8704.22	0.599
Tot Reaction at 5cm	2449.16	13382.02	0.607
Tot Reaction at 10cm	3712.2	20592.86	0.616
Non-Linear Group Effect			
	Flac3d Single Plastic	Flac3d Group Plastic	Group Effect
Tot Reaction at 1cm	750	3600	0.533
Tot Reaction at 2cm	1080	5800	0.597
Tot Reaction at 5cm	1380	8060	0.649
Tot Reaction at 10cm	1560	10000	0.712
Non-Linear Group Effect (Surcharge)			
	Flac3d Single Plastic	Flac3d Group Plastic	Group Effect
Tot Reaction at 1cm	750	3712	0.550
Tot Reaction at 2cm	1122	5878	0.582
Tot Reaction at 5cm	1401.2	8042.6	0.638
Tot Reaction at 10cm	1577.685	9864	0.695

Table 5 3 Group Efficiency Factors for different case simulated by FLAC3D (Total reaction used)

As we see from the tables the value of the group efficiency of the group of 3*3 piles at 10 cm forced displacement with Elasto-Plastic material is 0.695 which is fairly in agreement with value suggested by (Taiebat., et al., 2014) where they used suggested values by (Christensen., 2006) as 0.783. the little difference is due to the soil and structural properties used in our model and maximum displacement we forced to the piles as well as loading paths.

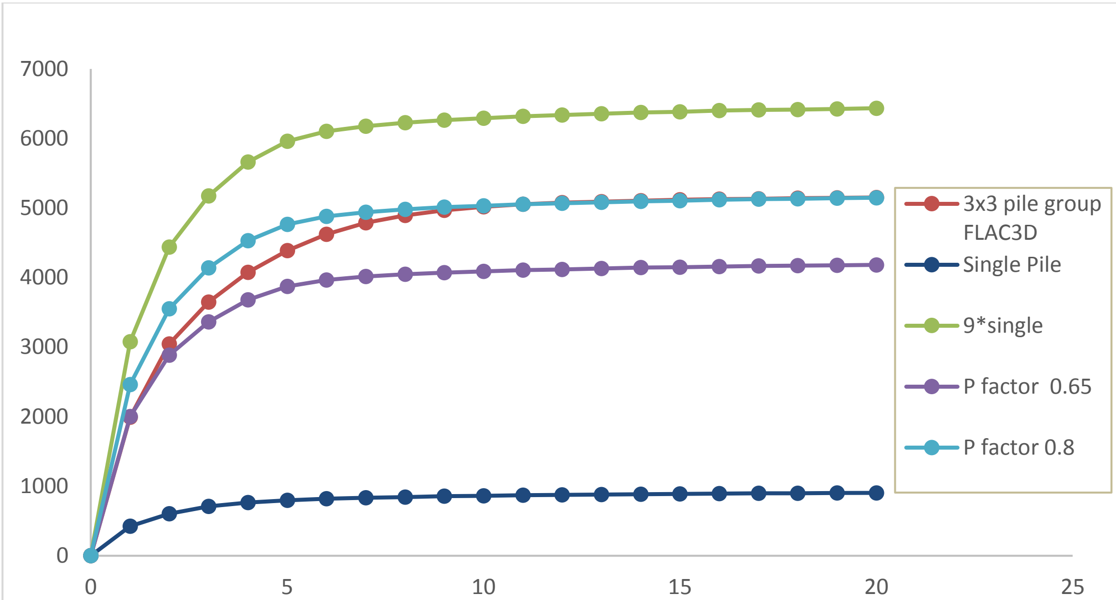

Figure 5-21 Comparison of the 3x3 pile group effect factor by means of P-Y Curve

As it is shown in the graph above, a comparison is done. Single pile reaction(Dark Blue), shown as well as single pile reaction multiplied by 9 (Green line), where we have data taken from FLAC3D for 3x3 pile group (Red Line), Lower bound reduction factor of 0.65 (Purple line) and upper bound reduction factor of 0.8 (Light Blue) used also in order to have a range, as we can see from the graph lower bound factor is matched for lower values of the displacement applied and upper bound value is matched for upper values of the displacement applied, FLAC3D Results are between Lower bound and Upper bound reduction Factors.

CHAPTER 6
AN EXTENSIVE NUMERICAL DATASET TOWARD THE DEFINITION OF A NEW GROUP EFFICIENCY PROPOSAL

This section is based on the extended work done by the author starting from a proposal by Becci et al. (2019). A review of existing literature on this topic reveals that available theoretical or experimental studies on ultimate lateral capacity of pile groups are quite limited mainly due to the intrinsic complexities of this problem which is governed by a tight interaction between geotechnical and structural aspects. Such difficulties also rest in the practical complexities in setting up full scale loads tests which are usually just conducted on single piles.

As for practical designs, group efficiency is often used. Such factor is normally defined as:

$$\eta = \frac{\text{Group reaction}}{n_p \cdot (\text{reaction of one pile acting as single})} \tag{1}$$

in which n_p is the number of piles in the group and the reaction is a pile (or group) force corresponding with a given top deflection.

Such parameter can be of course defined with respect to vertical or lateral response. In the first case, η is currently defined with respect to a quite low deformation level, thus giving a measure of group efficiency with respect to group stiffness. In contrast, such approach is rarely adopted in defining vertical capacity. As for lateral behavior, a different η factor is usually defined, to scale the so-called p-y curves that still very frequently adopted in modelling the interaction of piles with surrounding soil: in this respect, again, η should be considered as a matter of stiffness rather than of resistance. However, in such case the same (or very similar) η factor used to scale p-y curves is frequently also used to calculate group ultimate lateral capacity, based on the ultimate capacity of single piles. Such procedure, in our opinion, may be often inappropriate since group behavior at failure may differ significantly from the behavior of single piles. Moreover, by simply taking an efficiency factor into account without looking more in details in group behavior, unsafe design of crucial structural details may result. In the light of these simple observations stemming from current practice, a simple proposal is worked out in following, which may contribute to improve current design of laterally loaded pile groups.

6.1 A simple model for lateral group capacity assessment

Ultimate lateral capacity H_{ult} of single piles or pile groups intimately depends on both surrounding soil resistance and on structural bending capacity of pile cross sections. As for single pile capacity, such behavior at failure has been excellently explained by Broms, whose proposals (Broms (1964a, 1964b), still stand as a fundamental contribution widely used in the practice. As it will be shown in the following, Broms theory also produces results in a very close agreement with numerical models.

An attempt to extend Broms approach to a piling group with a regular geometrical pattern is presented in the following. We limit our attention to closely spaced pile group in a homogeneous granular soil, whose resistance is expressed by a friction angle ϕ. Following Fleming et al. (2009), or Patra & Pise (2001), we consider a block failure mechanism in which soil resistance is fully activated on the front side (passive resistance) (Figure 1) and along lateral sides.

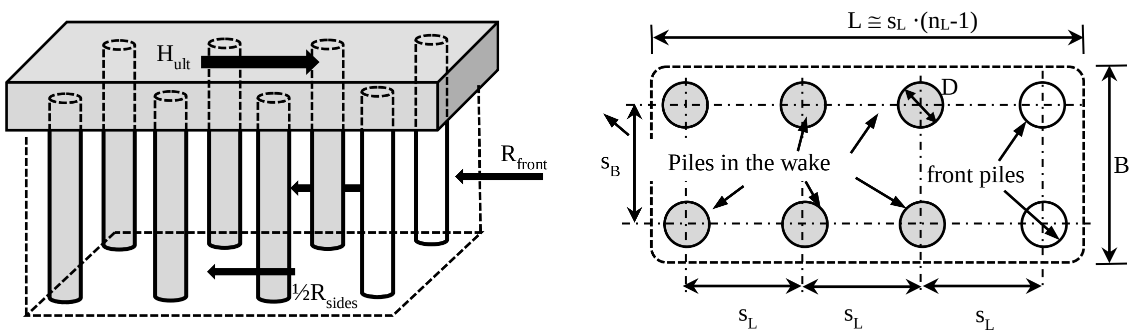

n_B = no. of piles in one row normal to load direction (n_B=2 in this figure)
n_L = no. of piles in one row parallel to load direction (n_L=4 in this figure)
$n_p = n_B \times n_L$

Figure 6-1. Pile group geometry and symbol definition

Driving active thrust at rear face is neglected, since it represents a small fraction of other components. As for n_B piles in the front row, passive soil resistance from pile top to depth x, acting on a front width B, is given by

$$R_{front}(x)=K_P \cdot B \cdot \left(q \cdot x+\frac{\bar{\gamma} \cdot x^2}{2}\right) \quad (2)$$

in which K_P is passive thrust coefficient depending on ϕ, q is uniform surcharge at soil surface (included as recommended by Cecconi et al. (2006) and $\bar{\gamma}$ is soil unit weight, which must be set equal to buoyancy weight for water table at pile top. B is given by

$$B=\min(3\cdot D\cdot n_B, D+(n_B-1)\cdot s_B) \tag{3}$$

In Equation 3, it is assumed that for quite distant piles, B is simply the sum of passive resistance pertaining single piles, which is set equal to 3·D according to Broms formulation. We now limit our analysis to long piles fully restrained at pile top, which represents the most common assumption occurring in the practice. Ultimate resistance for such piles is reached when two plastic hinge form, one at pile top and one at an unknown depth x_1. By observing that at such depth, the shear forces in yielding piles is null, corresponding with a maximum M_y in bending moment distribution, we can compute x_1 by simply imposing moment equilibrium for piles above that depth:

$$2\cdot n_B\cdot M_y-K_P\cdot B\cdot\left(q\cdot\frac{x_1^2}{2}+\frac{\bar{\gamma}\cdot x_1^3}{3}\right)=0 \tag{4}$$

This equation is easily solved by an iterative procedure and then the contribution of front piles to overall resistance is obtained by substituting x_1 in Equation 2. It should be noted that setting q=0, n_B=1 and setting K_P to Rankine value, classical Broms (1994a) formulation is reproduced.
We now consider all the piles behind the front ones, in other words $n_B\cdot(n_L-1)$ piles in the wake of the leading ones. We will assume that all of them equally contribute to the resistance provided by soil resistance at the sides. This contribution is assumed to be:

$$R_{sides}(x)=2\cdot K_{LAT}\cdot\tan(\phi)\cdot L\cdot\left(q\cdot x+\frac{\bar{\gamma}\cdot x^2}{2}\right) \tag{5}$$

L is defined in Figure 1. K_{LAT} is a lateral earth pressure coefficient, for which Fleming et al. (2009) recommend considering a value ranging between at rest coefficient K_0 and 1. As a matter of fact we found that K_{LAT} plays an important role in the calculation of H_{ult}, so much more attention to it will be given in following section. Like front piles, we will assume that all the piles in the wake, equally loaded by same fraction of R_{sides}, will form a plastic hinge at pile top and a second one at the same depth x_2. As before, we compute x_2 by solving

$$2\cdot n_B(n_L-1)\cdot M_y-K_{LAT}\cdot\tan(\phi)\cdot L\cdot\left(q\cdot\frac{x_2^2}{2}+\frac{\bar{\gamma}\cdot x_2^3}{3}\right)=0 \tag{6}$$

Finally, overall pile group capacity is

$$H_{ult} = R_{front}(x_1) + R_{sides}(x_2) \tag{7}$$

It is worth noting that, by including the same bending capacity M_y for all the piles, different values for x_1 and x_2 are obtained, being usually $x_2 > x_1$. This means that lower plastic hinges form at different depth, depending on pile position in the group. Assigning same moment capacity is really a very crude assumption since bending capacity is affected by axial forces in piles. However, this assumption greatly simplifies the formulation and we also believe that including a safely assessed average value in the light of applied loads may provide a reasonable estimate of ultimate capacity as well. Implementing equations 1 to 7 in a spreadsheet, a very quick estimate of group capacity for various group patterns can be obtained. A most valuable result is also group efficiency η with respect to ultimate conditions, by dividing H_{ult} by the number of piles and by the single pile capacity (Broms value). For example, taking ϕ=33°, K_P= 3.39, q=0, $\overline{\gamma}$=18 kN/m³, D=1 m, M_y=1500 kN·m, s/D = 3, in both direction, we obtain ultimate capacities and group efficiencies summarized in Table 1 for various pile patterns.

Case	n_B	n_L	K_{LAT}	R_{front} [kN]	x_1 [m]	R_{sides} [kN]	x_2 [m]	H_{ult} [kN]	η
0	1	1	n.a.	1229	3.66	n.a.	--	1229	n.a.
1	2	2	0.7	2457	3.66	1384	6.50	3841	0.781
2	2	2	1.0	2457	3.66	1559	5.77	4016	0.817
3	2	4	0.7	2457	3.66	3907	6.91	6365	0.648
4	4	2	0.7	4915	3.66	2197	8.19	7122	0.724
5	2	4	1.0	2457	3.66	4401	6.16	6858	0.698
6	4	2	1.0	4915	3.66	2427	7.27	7389	0.752

Table 6-1 some results using Equations 1 to 7

Beyond ultimate capacity values, a relevant result provided by this procedure is an increased depth of lower plastic hinge in shadowed piles, as compared with front piles. This observation suggests to carefully increase pile reinforcement fairly below the depth that would have been requested by single pile solution. R_{sides}, x_2 and η are significantly affected by K_{LAT}. In this respect, an attempt to better assess such parameter deserves additional attention.

6.2 A NUMERICAL STUDY

6.2.1 Approach description

To attempt a rational selection of governing parameters of the proposed procedure, in particular K_{LAT} factor governing block side resistance, a set of benchmark results would be necessary. However, in our best knowledge, it is quite hard to access enough experimental data covering relevant conditions for practical applications. Therefore, we considered performing some advanced numerical simulations of typical groups using the commercial code FLAC3D (Itasca (2018)). Such models include following main components:

- a uniform soil layer to which Mohr-Coulomb constitutive model is assigned;
- piles (o single pile) which are modelled as elastic perfectly plastic pipes, in such a way to model reinforced concrete shafts with a known bending capacity;
- a slip interface between pile and soil, whose resistance is assigned through a friction angle δ.

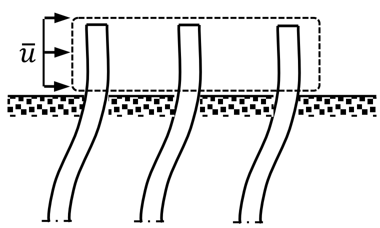

Figure 6-2. prescribed boundary condition at pile top

At the top of the piles, fixed head support condition is modelled by prescribing same lateral movement $\bar{u}$ to all the grid points of a portion of piles projecting above soil surface (Figure 2). For each pile pattern, including single pile conditions, a FLAC 3D analysis has been performed, according with following sequence:

a) set up of initial at rest condition by assigning an initial K_0 stress field
b) insertion of piles (and their interface)
c) progressive increase of top displacement $\bar{u}$, with 20 increments of 1 cm each, up to a final displacement of 20 cm.

Such procedure is accomplished by means of the nonlinear explicit pseudo-dynamic integration scheme offered by FLAC3D, by simply applying prescribed velocities for a suitable number of steps. Between each displacement increment, additional cycles with null velocities are performed, until overall top reaction (i.e. the resultant of all the lateral reactions where lateral displacement is assigned) is stabilized. In this study, only 1000 mm dia., 20 m long concrete piles are considered, in a granular dry soil. Pile spacing s/D =3 is kept constant in all the analyses, as such value corresponds with the most frequent spacing adopted in the practice. Additional parameters are soil modulus E=100 MPa, ν=0.30, dilatancy ψ=0°, $\bar{\gamma}$=18 kN/m³, K_0=0.5, E_{pile}=25 GPa.

Several models have been analyzed, by varying pile pattern (including single pile models to allow a comparison with Broms predictions), ϕ, δ and M_y. For all such models a top load-displacement curve is computed. In Figure 3, typical FLAC3D model is shown: one half of the group is modelled due to geometry and load symmetry. The model is extended, far from loaded zone, about 20 m in front and behind external piles in load direction as well as far from outer piles in lateral direction. A 10 m thick soil layer is considered under pile toe. Horizontal displacements normal to each boundary plane are fixed. In Table 5-2, a summary of performed analysis is included, corresponding with a total amount of 40 analyses.

pattern				ϕ	δ/ϕ	M_y
	n_B	n_L				[kN·m]
single	1	1		30°	0.5	1050
2 × 2	2	2	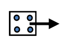	36°	1	2100
3 × 3	3	3	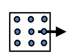			
3 × 5	3	5	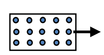			
5 × 3	5	3	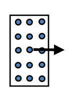			

Table 6-2. summary of parameter variations

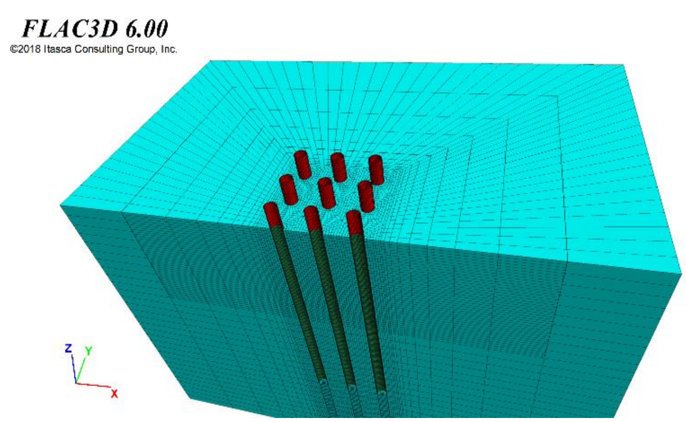

Figure 6-3. Typical FLAC 3D model: in this case a model with nB=5 and nL=3 is shown.

6.2.2 Result summary

Below Some typical results are shown. A Contour map of displacement can highlight a block failure mechanism encompassing all the piles, combined with a more complex deformation field between single pile rows parallel to load direction.

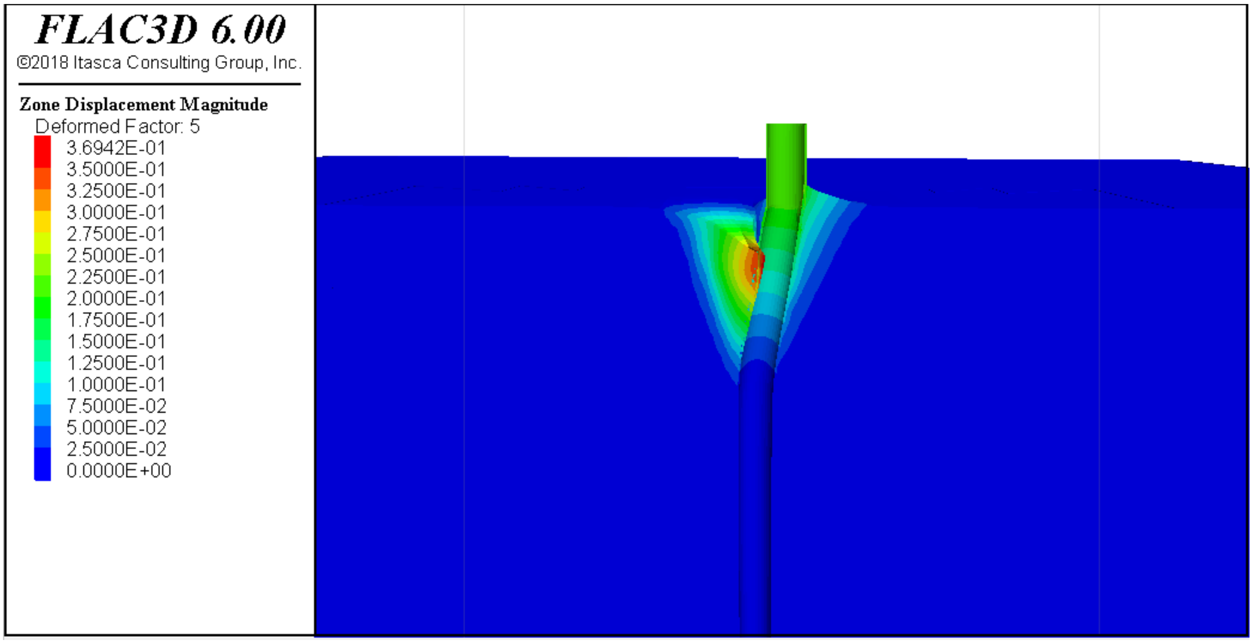

Figure 6-4 Zone Displacement and Deformed Shape at 20 Cm Displacement applied (Single Pile)

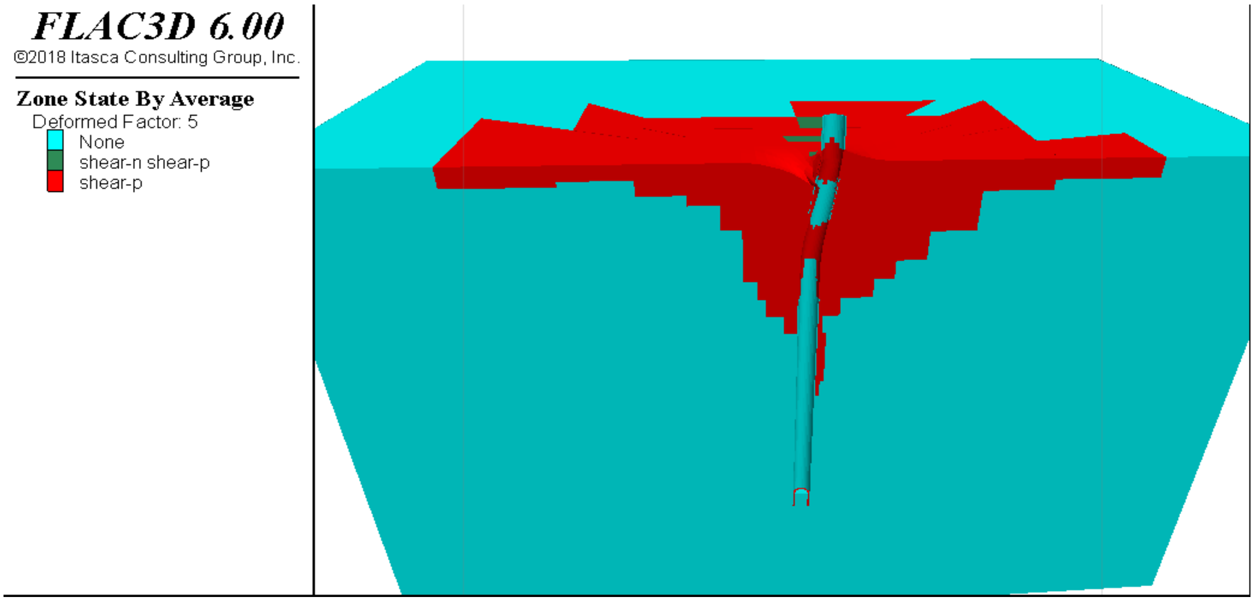

Figure 6-5 Zone State (Mobilization of the soil and pile) at 20 cm Displacement applied (Single Pile)

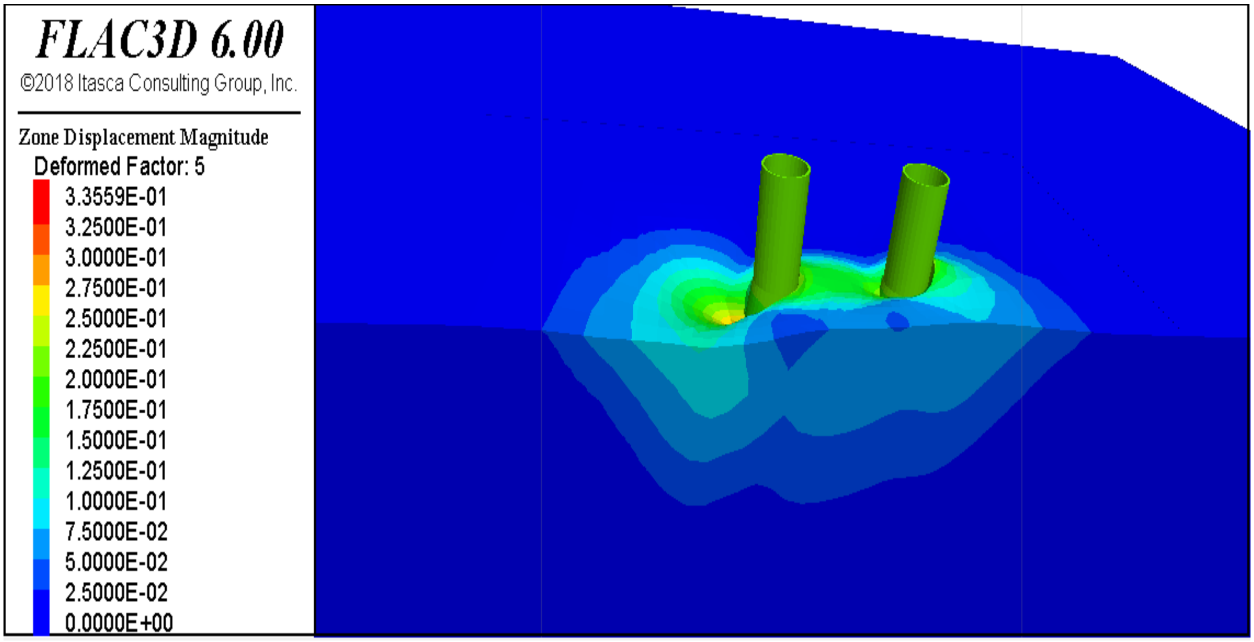

Figure 6-6 Zone Displacement and Deformed Shape at 20 Cm Displacement applied (2x2 Pile)

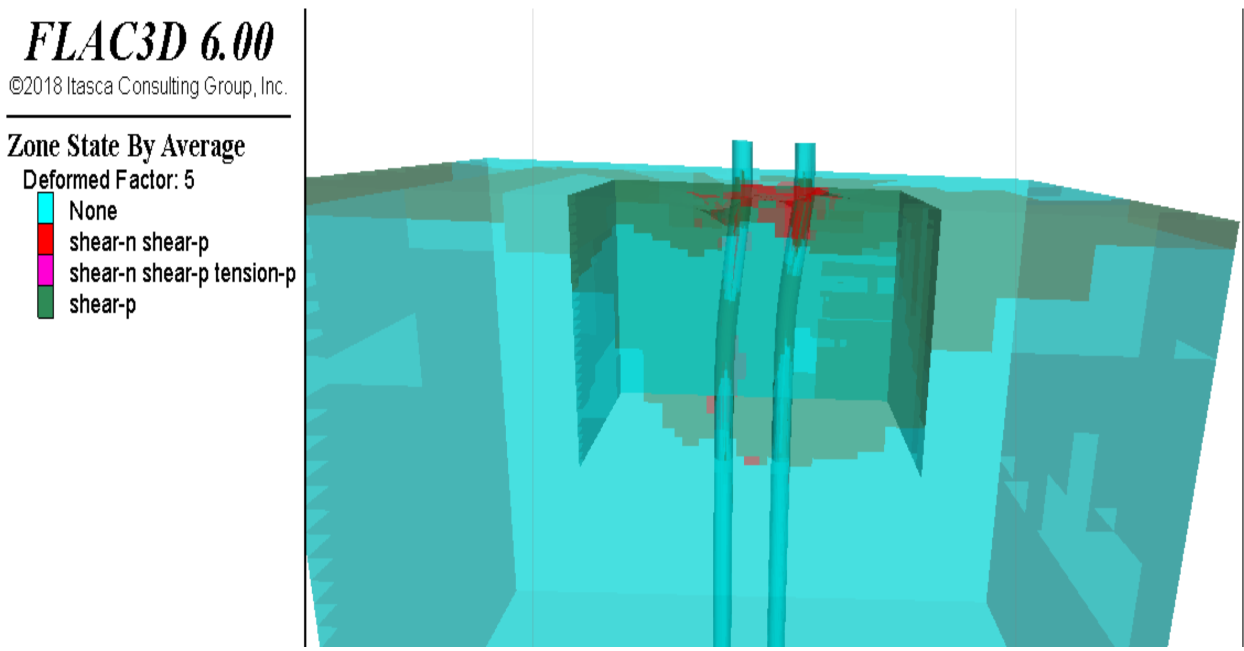

Figure 6-7 Transparence view of Zone State (Mobilization of the soil and pile) at 20 cm Displacement applied (2x2 Pile)

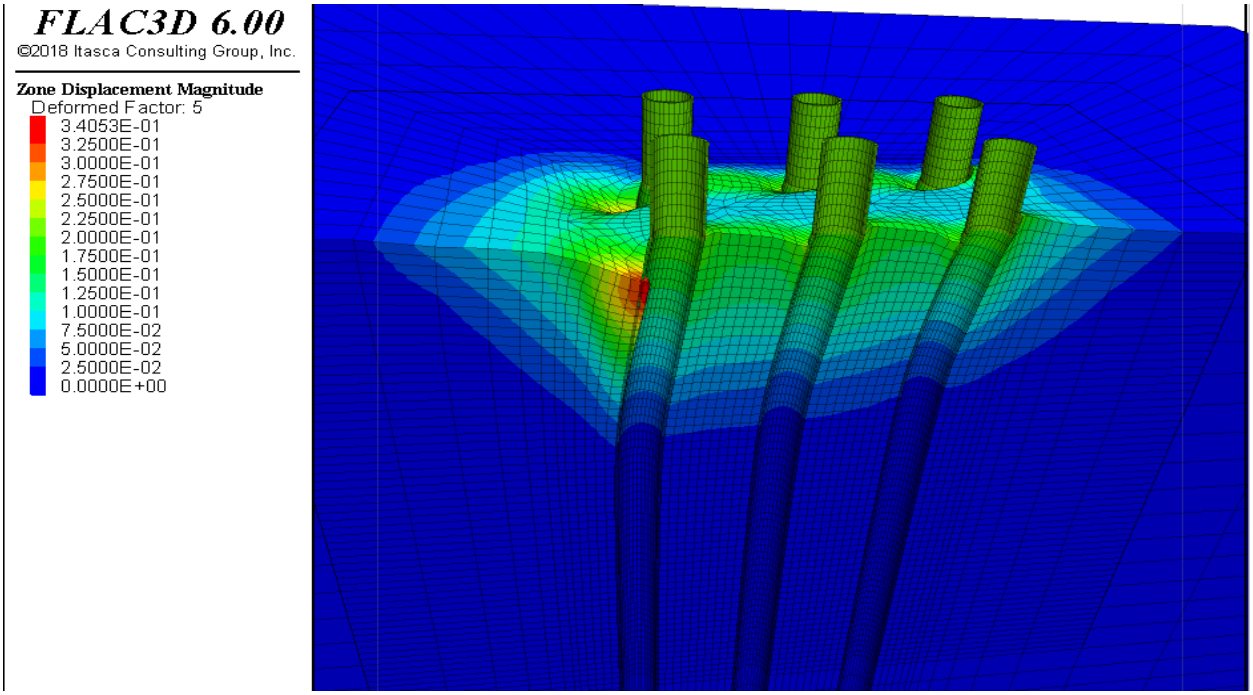

Figure 6-8 Zone Displacement and Deformed Shape at 20 Cm Displacement applied (3x3 Pile)

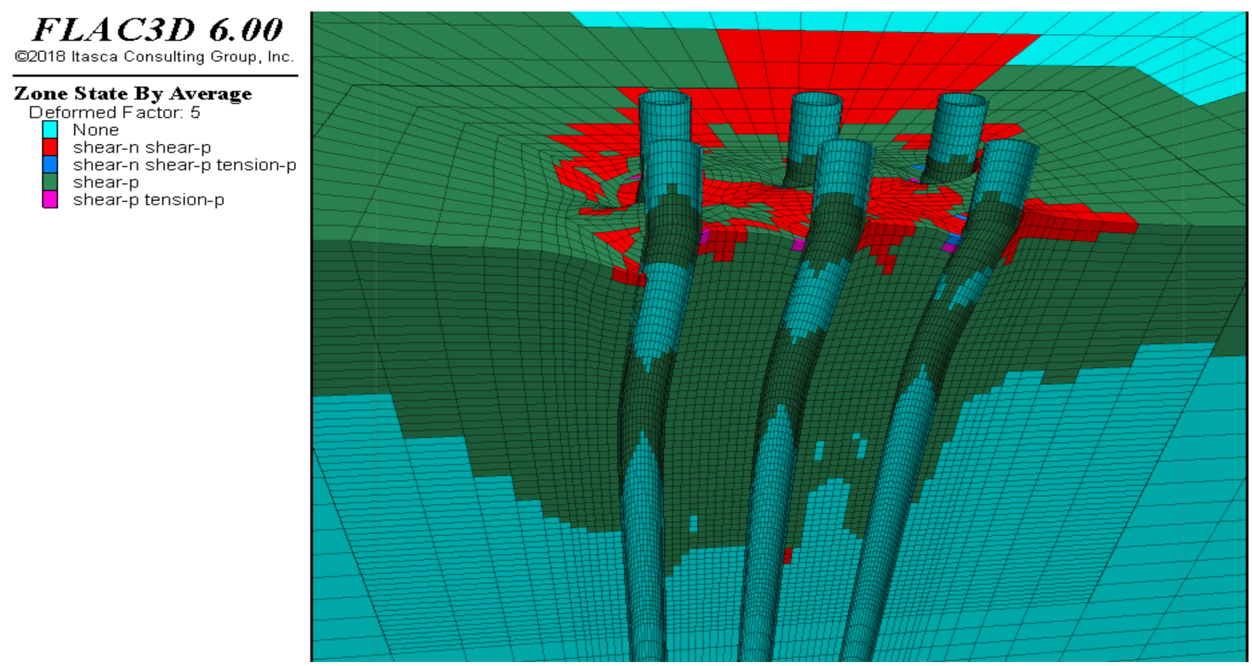

Figure 6-9 Zone State (Mobilization of the soil and pile) at 20 cm Displacement applied (3x3 Pile)

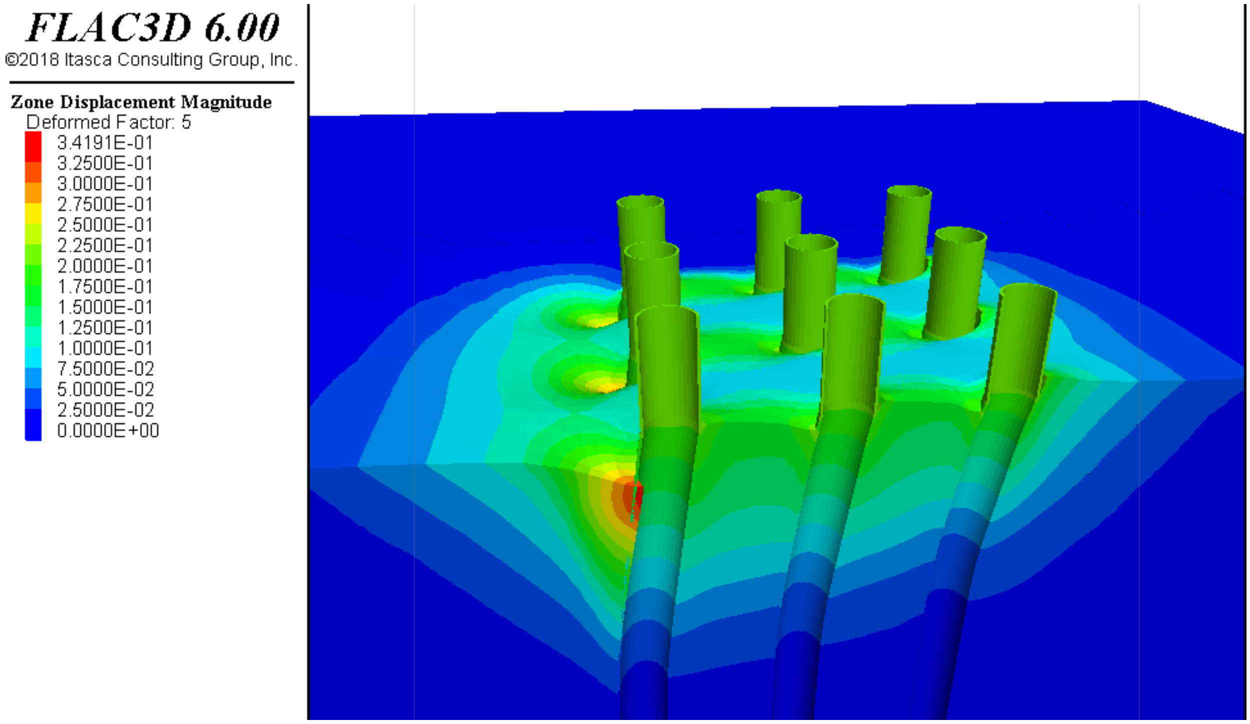

Figure 6-10 Zone Displacement and Deformed Shape at 20 Cm Displacement applied (3x5 Pile)

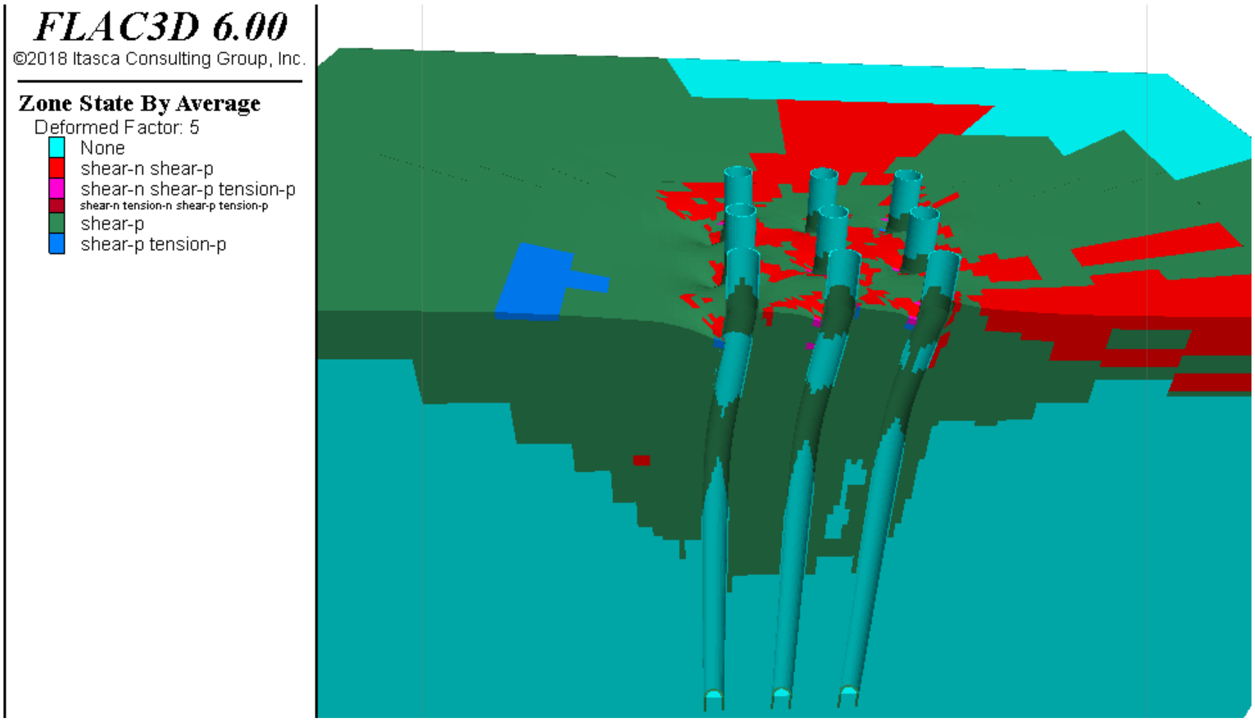

Figure 6-11 Zone State (Mobilization of the soil and pile) at 20 cm Displacement applied (3x5 Pile)

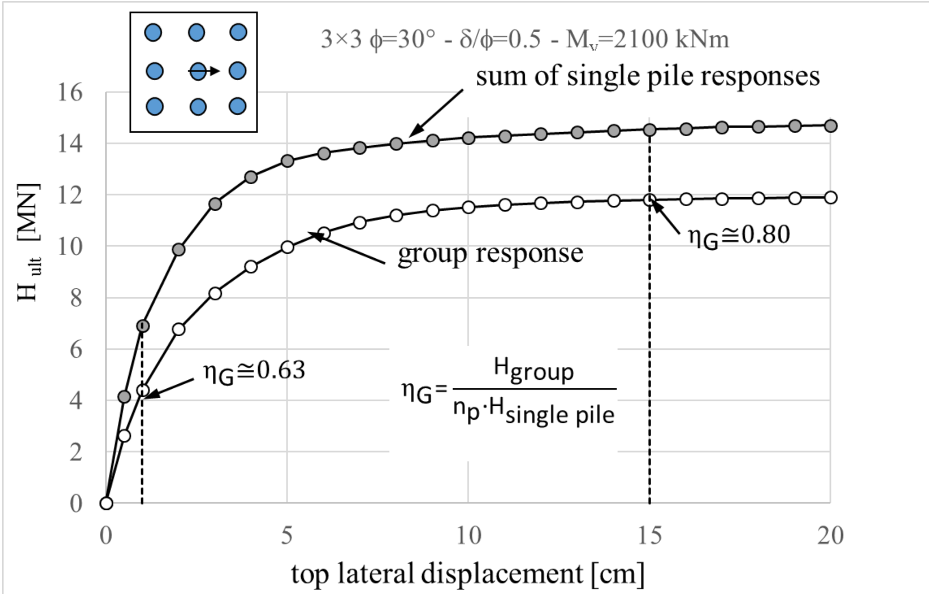

Figure 6-12 Group Response computed by FLAC3D

In Figures 6-5. 6-7, 6-9 and 6-11 we can appreciate different plastic zone development in piles, depending on pile position. As anticipated in previous section, lower plastic zone (plastic hinge) is deeper for piles in the wake of the front ones. In figure 6-12, nonlinear overall behavior is shown at early deformation stages, while ultimate load is almost reached at a top displacement of about 10%D. Such behavior is the same for all the investigated cases. Moreover, it is noticed that group efficiency increases with top displacement. Such results may be explained by the fact that at low deformation, elastic interaction between piles prevails, thus reducing overall stiffness; when limit state is almost reached, yielding in soil somehow reduces the coupling between adjacent piles thus reducing group reduction with respect to the sum of single pile responses. Such finding, however, is in contrast with other studies (e.g. Fayyazi et al. (2014), Rollins et al. (2005)) and suggests further research to be clarified. However, an important conclusion from this study is that group efficiency is strictly related to the level of mobilization at which is computed.

An overview of the performed analyses is included in Table 6-3, left part.

		FLAC3D				Proposed formulation with $K_{LAT}=K_P$			
		ϕ=30°				ϕ=30°			
	$\delta/\phi \rightarrow$	0.5		1		0.5		1	
pattern	My $\rightarrow$	1050	2100	1050	2100	1050	2100	1050	2100
single	H_{ult} (*)	1004	1634	1093	1808	1047	1662	1104	1753
2 × 2	H_{ult}	3641	5808	4042	6327	4014	6372	4233	6719
	□G	0.91	0.89	0.92	0.87	0.96	0.96	0.96	0.96
3 × 3	H_{ult}	7476	11908	8184	13092	7954	12626	8387	13313
	□G	0.83	0.81	0.83	0.80	0.84	0.84	0.84	0.84
3 × 5	H_{ult}	11592	18206	12668	19917	12531	19892	13213	20974
	□G	0.77	0.74	0.77	0.73	0.80	0.80	0.80	0.80
5 × 3	H_{ult}	12342	19840	13518	21758	12000	19050	12645	20086
	□G	0.82	0.81	0.82	0.80	0.76	0.76	0.76	0.76
		ϕ=36°				ϕ=36°			
	$\delta/\phi \rightarrow$	0.5		1		0.5		1	
pattern	My $\rightarrow$	1050	2100	1050	2100	1050	2100	1050	2100
single	H_{ult}	1153	1937	1202	2101	1190	1889	1281	2033
2 × 2	H_{ult}	4227	6739	4673	7490	4735	7516	5097	8091
	□G	0.92	0.87	0.97	0.89	0.99	0.99	0.99	0.99
3 × 3	H_{ult}	8641	13854	9619	15273	9472	15036	10198	16188
	□G	0.83	0.79	0.89	0.81	0.88	0.88	0.88	0.88
3 × 5	H_{ult}	13413	21178	14910	23299	15087	23949	16242	25782
	□G	0.78	0.73	0.83	0.74	0.85	0.85	0.85	0.85
5 × 3	H_{ult}	14298	22908	15936	25372	14247	22616	15338	24347
	□G	0.83	0.79	0.88	0.80	0.80	0.80	0.80	0.80

(*) H_{ult} in [kN]

Table 6-3. FLAC3D Analysis summary and comparison with proposed formulation

In the right part of Table 6-3, for each analysis, group capacity is computed by means of the proposed approach in section 2. To obtain a close agreement with FLAC3D results, two important aspects had to be included, namely 1) a K_P value depending also on δ/ϕ by adopting the passive thrust coefficients suggested by Lancellotta (2006) and 2) a quite high K_{LAT} value set equal to K_P as well, a value much higher than those recommended by previously cited authors, but, as theoretically expected, closely related just to soil resistance. By comparing the deformed shapes and plastic zones in piles in FLAC3D with computed plastic hinge depth with simplified approach, a quite satisfactory agreement is also observed. Efficiency coefficients computed by current study both by FLAC3D and by simplified approach, are in general higher than those frequently adopted in the practice (for example, Callisto & Rampello (2013), Fayyazi et al.

(2014), Viggiani et al. (2012)). As already discussed, such relevant discrepancy rests in the fact that previous values have been estimated corresponding with low deformations and/or different top restraint conditions. This observation, however, suggests that using traditional group factors tuned for group stiffness, also for group capacity is a conservative assumption.

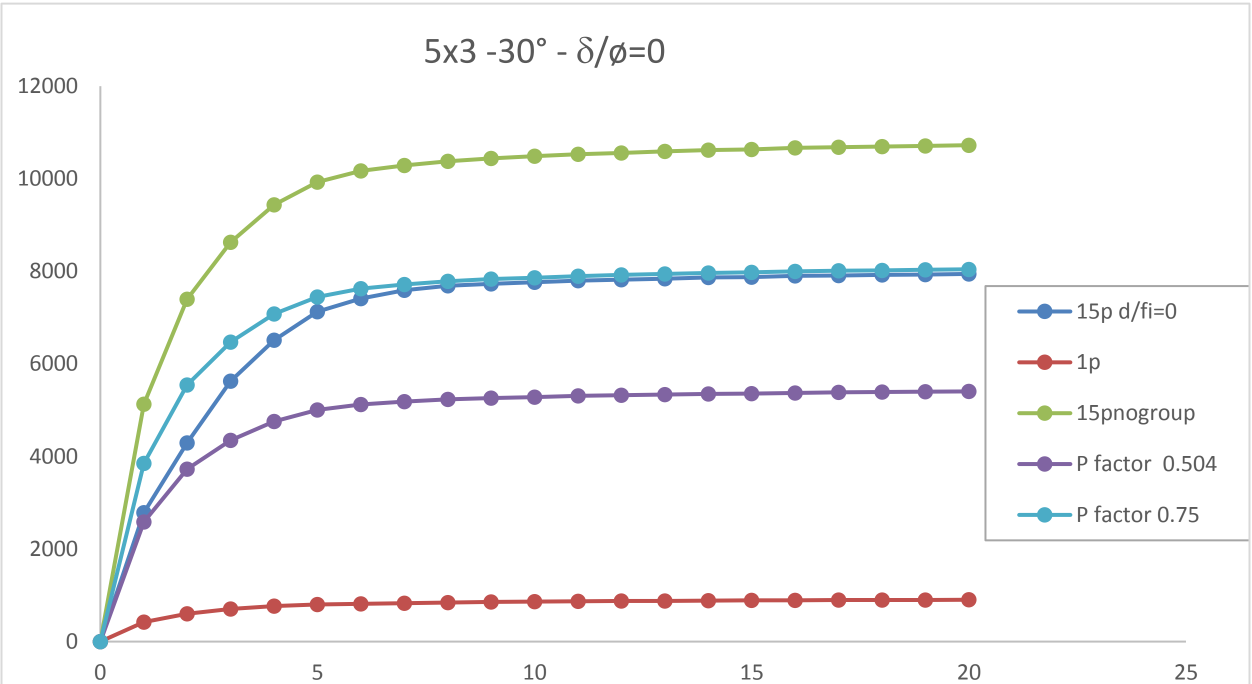

Figure 6-13 Comparison of the Group Efficiency factors by means of P-Y Curves and Group reduction factors

CHAPTER 7
A PROPOSAL FOR CLOSED FORM ASSESSMENT OF GROUP EFFECT

In Figure 7-1, left, predicted capacities obtained by proposed equations are compared with FLAC3D analysis results. Aiming at providing a safe formulation in which all result points fall below the dotted line, proposed equation results have been multiplied by reduction factor 0.90: doing so all the results point are brought into safe region (Fig. 7-1, right). In general, the agreement is better for almost square patterns (n_B=n_L). For unsymmetrical case 5×3, simplified approach seems to be very conservative: this may be explained in the light of a more complex actual failure mechanism dissipating more plastic work than what is assumed by simple block scheme. In such case, a more complex scheme, as proposed by Ashour et al. (2004) may provide better agreement.

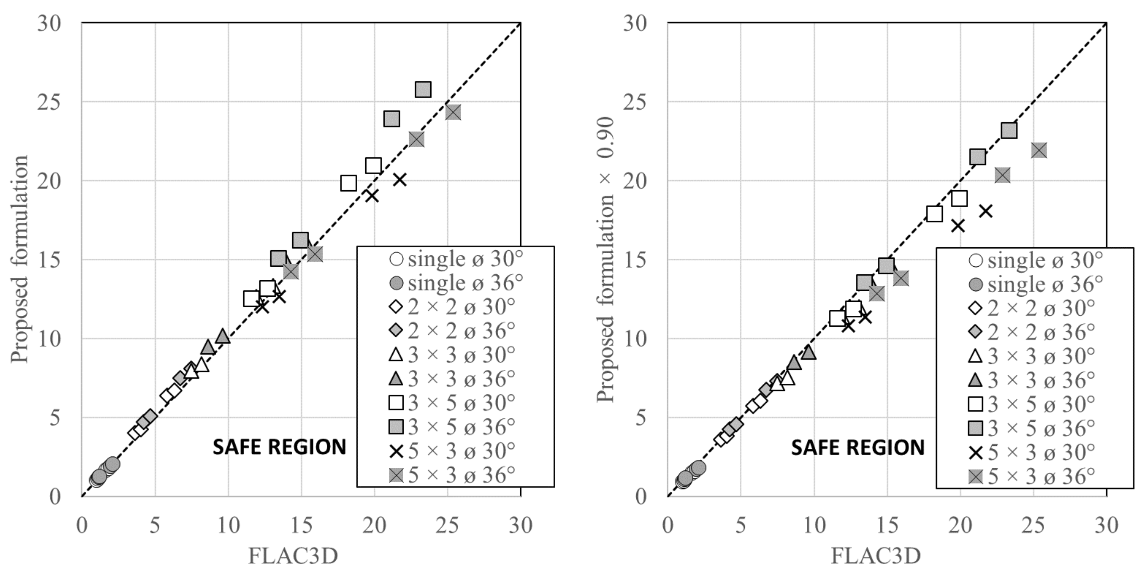

Figure 7-1. Predicted vs computed pile group capacity [MN]. Left: uncorrected values. Right: reduced values using 0.90 factor in proposed formulation

.

7.1 Group Efficiency Factor:

By inspecting FLAC3D results, a simple equation for efficiency factor can also be obtained, which has the ability to account for both overall number of piles in a group and their configuration with respect to applied loads. We define a group efficiency with respect to ultimate capacity, which can be computed by the following equation (considering the equations 1 to 7 of the chapter 6, this equation would be 8^{th}):

$$\eta_{G,ult}=0.9\cdot(n_B)^{-0.025}\cdot(n_L)^{-0.15} \tag{8}$$

Ultimate capacity of single pile can be computed by either Broms formulation or equivalent equations in section 2, including improved K_P coefficients accounting for appropriate δ/ϕ parameter. Group capacity is computed by using efficiency as per Equation 8 which already includes a reduction factor 0.90. Finally, the depth of reinforcement cage to be provided to ensure the validity of the assumed formulation can be assessed by the following iterative procedure:

a) calculate $\eta_{G,ult}$ using Eqn. 8;
b) iteratively calculate group capacity using equations 1 to 7 (from chapter 6), by progressively reducing K_{LAT} (starting with $K_{LAT}=K_P$) until same $\eta_{G,ult}$ is obtained.
c) record lowest hinge depth corresponding with the last reduced K_{LAT} factor;
d) provide adequate pile reinforcement down to such depth plus at least 3 pile diameters, to all piles in the group.

Of course, an appropriate design of piles subjected to lateral forces is not only affected by calculation approach, but also by a good selection of construction detailing. What is required to ensure overall lateral capacity must be compared with ordinary pile analysis via p-y curves and the most stringent values must be adopted in design.

7.2 A worked example of proposed method:

As an example of proposed procedure, we consider the following rail-way bridge embedment, whose plan view is shown in the figure below. All the piles are 1.5-meter diameter bored shafts in granular soil with characteristic friction angle equal to 38^o and k_p can be taken as 4.204 (ignoring the friction between piles and soil $k_p = k_{LAT}$). The water table is assumed at the pile top: this is included by considering a sub-merged unit weight of 11 kN/m^3. An average moment capacity of the pile is 3694 kN.m for all piles where the reinforcement needed is 29φ30 calculated by the procedure mentioned above. According to equation 8 above, the group factor should be $\eta_{G,ult}=0.9\cdot(4)^{-0.025}\cdot(3)^{-0.15} = 0.737$. Now lateral capacity of the single pile without group effect can be calculated through Brom's theory and then by following formula H_{ult} of single pile is:

$\frac{H}{k_P \gamma d^3} = \sqrt[3]{(3676\frac{M_y}{k_P \gamma d^4})^2}$ therefore H_{ult} = 2338 kN

Therefore, the group resistance is 2338*12*0.737 = 20677 kN. Now by iteratively changing k_{LAT} in Equation 5 and 6 we find a value of k_{LAT} = 2.21 corresponding with a reduction factor equal to 0.527 applied to k_p. According to this final value the following plastic hinges are computed: Lower plastic hinge depth is 7.63m and recommended reinforcement cage depth is 7.63 + 3*D which is equal to 12.13m. it worth to mention that the computed plastic hinge corresponds with maximum depth between front and back piles. Of course, in this example as well as in all this work, no safety factor aspects have been addressed. We are aware that in practical design safety factors must be carefully included according to applicable design codes.

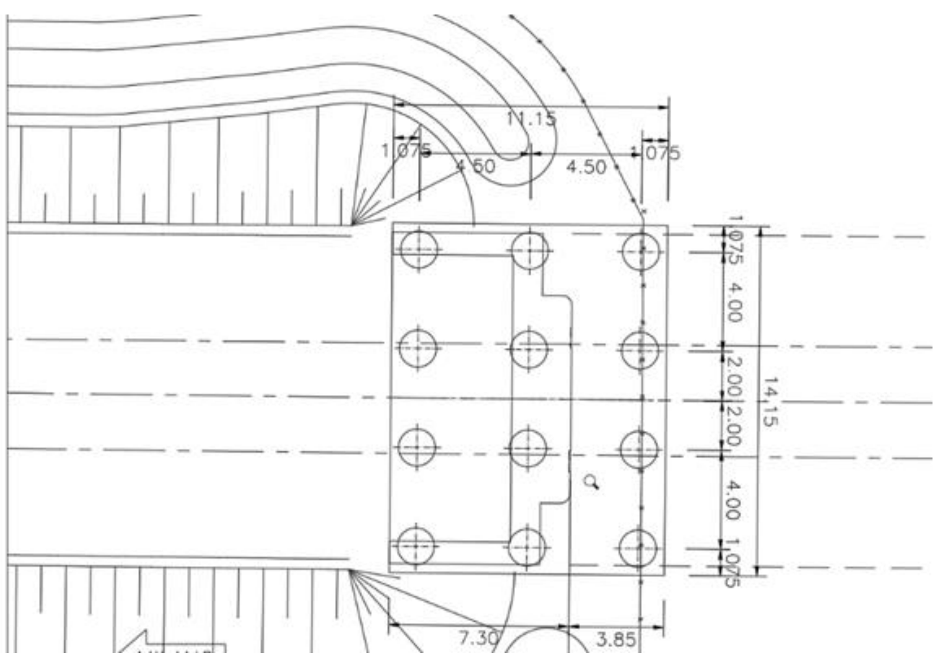

Figure 7-2 Autocad Plan view of the Group of pile under the bridge

LATERAL PILE GROUP RESISTANCE (GRANULAR SOIL) Becci - 2018											
JOB	example										
ϕ_k	38	°	γ_ϕ	1		D	1.5	m			
δ	0	°									
γ	11	kN/m³	for submerged soil, use γ'			M_y	3694	kN·m			
K_{lat} perc	0.527	(this parameter will be modified by the command below)									
q	0	kPa	surcharge			n_B	4		s_B	4	m
k_h	0	g				n_L	3		s_L	4.5	m
k_v	0	kh				no. of piles	12		s	0	m
ξ_3	1		γ_R	1							
ϕ_d	38	°									
B	16.5	m									
L	10.5	m									
K_{PE}	4.204										
$K_{P,calc}$	4.204	$=K_P/\xi_3$									
$K_{lat,calc}$	2.215374	$=K_{lat}/\xi_3$									
x_1	4.88	m		10.005	m crit						
x_2	7.63	m	sl.crit	15.6354	m						
$x._{single}$	4.74	m	H_{single}	**2338**	kN						
			(Broms)	9.719	m (sl crit)						
R_{front}	9084	kN									
R_{sides}	11626	kN									
	20710	kN									
R_d	**20710 / 1. =**		**20710**	**kN**							
η_G	= 20710 / (2338 · 12)			**0.738**							
safe estimate (Eqn 8)				**0.737**	0.000942	compute Kp perc.					
used K_{LAT}/ξ_3				2.22							
				solution with 474 trials							
$R_{d,SAFE}$				**20683**	**kN**						
lower plastic hinge depth					**7.63**	m					
recommended reinforcement cage depth					**12.13**	m					

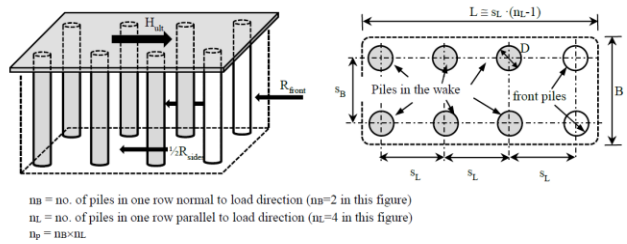

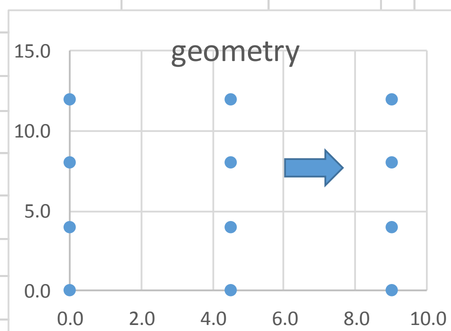

Figure 7-3 Spreadsheet and parameters used for formulating the problem

CHAPTER 8
Conclusions

By modeling single and group of piles in FLAC3D software by means of continuum model, and modeling with Seismostruct software by means of p-y curve approach, a verification was made, and p-y approach showed good agreement by results in comparison with continuum model used in FLAC3D both in linear (Elastic) and non-linear (Plastic) response of the piles. After verifications, forty FLAC3D numerical analyses of laterally loaded single piles and pile groups in uniform dry sands have been performed. Obtained results have been used as benchmarks to define a simple procedure to calculate ultimate capacity of pile groups with fixed head condition.

Numerical analyses of single piles revealed that established design equations such as Broms (1964a, b) formulation very well agree with numerical results. Moreover, it has been realized that interface friction δ between pile and soil provides a significant contribution to pile capacity. This can be incorporated in the Broms equations by simply using appropriate K_P values. As for pile groups, a block failure mechanism has been investigated, showing that such assumption well fits numerical results, provided side resistance of such block is related to K_P as well.

A simple procedure and a closed form equation for group efficiency limited to regular pile patterns and to s/D=3 is proposed. It should be emphasized that the proposed procedure is limited to the assessment to ultimate group capacity: in other words, it does not aim at offering a general procedure for elastoplastic analysis of groups including a reliable estimate of group deformation or force distribution among different piles. For general pile group analysis, reference can be made to abundant available literature (e.g. Russo 2016, Ashour et al. (2004), Stacul & Squeglia (2018)) or to available engineering software.

A merit of the proposed procedure, beyond its simplicity, is a clear emphasis to appropriate structural detailing required to ensure the real validity of the proposed design.

Further work is required to investigate the role of additional parameters such as surface surcharge and different pile spacings. An extended comparison with experimental data would also be very valuable, albeit, for the time being, relevant difficulties may be envisaged in the light of practical and economic implications in running realistic lateral loads tests for pile groups.

References

AASHTO. 2012. AASHTO LRFD bridge design specifications. 6th ed. American Association of State Highway and Transportation Officials (AASHTO), Washington, D.C.

American Petroleum Institute (API). (1987). "Recommended practice for planning, designing and constructing fixed offshore platfonns." APIRP2A, 17th Ed., Washington, D.C.

American Society of Civil Engineers (ASCE) (1984) Guidelines for the Seismic Design of Oil and Gas Pipeline Systems, Committee on Gas and Liquid Fuel Lifeline, ASCE, Reston.146 p

API. (1993). Recommended practice for planning, designing, and constructing fixed offshore platforms-working stress design (Vol. 21 edition). API RP2A-WSD, American Petroleum Institute, Washington D.C.

API. 2007. Recommended practice for planning, designing, and constructing fixed offshore platforms. API Recommended Practice 2A-WSD. 21st ed. American Petroleum Institute, Washington, D.C.

Ashour M., Pilling P. and Norris G. 2004. Lateral Behavior of Pile Groups in Layered Soils. J. *Geotech. Geoenviron. Eng*. ASCE, vol. 130: 580–592.

Baguelin, F. J., Frank. R. A., and Said, Y. (1977). "Theoretical study of lateral reaction mechanism of piles. "Ge6technique, London, England, 27(3), 405-434.

Becci B., Cardella N. and Carni M. 2019 A numerical study of ultimate lateral capacity of pile groups, submitted to 7ICEGE conference, Rome, Italy

Bowles, J.E. 1996. Foundation analysis and design. 5th ed. McGraw-Hill Education.

Bransby, M. F. (1995). "Piled foundations adjacent to surcharge loads," PhD thesis, Univ. of Cambridge, Cambridge, England.

Broms B.B. 1964a. Lateral resistance of piles in cohesionless soils. *ASCE J. Soil Mech. And Found. Div*., 90(SM3): 123–156.

Broms B.B. 1964b. Lateral resistance of piles in cohesive soils. *ASCE J. Soil Mech. and Found. Div*., 90(SM2): 27–63.

Brown, D. A., & Shie, C.-F. (1990). Three-Dimensional Finite Element Model of Laterally Loaded Piles. Computers and Geotechnics, 10(1), 59-79.

Brown, D., and Shie, C.-F. 1991. Modification of p-y curves to account for group effects on laterally loaded piles. In ASCE Geotechnical Special Publication 27. Geotechnical Engineering Congress. ASCE. Vol. 1, pp. 479–490.

Brown, D.A., Morrison, C., and Reese, L.C. 1988. Lateral load behavior of pile group in sand. Journal of Geotechnical Engineering, 114(11): 1261–1276. doi:10.1061/(ASCE)0733-9410(1988)114:11(1261).

Brown, D.A., ONeill, M.W., Hoit, M., McVay, M., El-Naggar, M.H., and Chakraborty, S. 2001. Static and dynamic lateral loading of pile groups. Technical Report NCHRP Report No.461. National Cooperative Highway Research Program, Washington, D.C.

Brown, D.A., Reese, L.C., and O'Neill, M. 1987. Cyclic lateral loading of a largescale pile group. Journal of Geotechnical Engineering, 113(11): 1326–1343. doi:10.1061/(ASCE)0733-9410(1987)113:11(1326).

Byrne, P. M., Anderson, D. L.. and Janzen, W. (1984). "Response of piles and casings to horizontal free-field soil displacements." Can. Geotech. J., Ottawa, Canada. 21. 720-725.

Callisto L. & Rampello S. 2013. Capacity Design of Retaining Structures and Bridge Abutments with Deep Foundations. *Journal of Geotechnical and Geoenvironmental Engineering*, ASCE, Vol. 139, No. 7: 1086-1095.

Cecconi M., Pane V., Isidori F. 2006. Un'estensione della Teoria di Broms nel calcolo dei pali sollecitati da forze orizzontali. *V Convegno Nazionale dei Ricercatori in Ingegneria Geotecnica*, Bari (Italy), 15-16 settembre 2006:295-311.

Chellis, R. D. Pile Foundations, Theory, Design, Practice. McGraw-Hill, New York, 1951.

Christensen, D.S. 2006. Full scale static lateral load test of a 9 pile group in sand. Master's thesis, Brigham Young University.

Clough, R.W., Chopra, A.K., [1966] "Earthquake stress analysis in earth dams", ASCE Journal of Engineering Mechanics Division, Vol. 92, pp. 197-211.

Cubrinovski, M., Ishihara, K., Poulos, H, [2009] "Pseudo-static analysis of piles subjected to lateral spreading", Bulletin of the New Zealand Society for Earthquake Engineering, Vol. 42, No. 1, pp. 28-38.

Cummings, A. E. Pile Foundations. Proc. Conf. on Soil Mechanics and Its Applications, Purdue Univ., Lafayette, Ind., Sept. 1940.

Dodds, A.M., and Martin, G.R. 2007. Modeling pile behavior in large pile groups under lateral loading. Technical Report MCEER-07-0004. The Multidisciplinary Center for Earthquake Engineering Research (MCEER), Buffalo, N.Y.

El Naggar MH, Bentley KJ (2000) Dynamic analysis for laterally loaded piles and dynamic p-y curves. Can Geotech J 37(6):1166-1183

Fayyazi M. S., Taiebat M. and Finn W.D. L. 2014. Group reduction factors for analysis of laterally loaded pile groups. Can. Geotech. J. 51: 758–769. www.nrcresearchpress.com/cgj on 13 March 2014

FEMA. 2012. Foundation analysis and design. FEMA P-751. In NEHRP recommended

Fleming W. G. K., Weltman A. J., Randolph M. F., Elson W. K. 2009. Piling Engineering. 2nd ed., Taylor & Francis, Inc.

Frank, R. A. (1981). "Design of piles subjected to lateral pressures in soft soils." Colloquy of Jablonna, Gdan§k, Poland.

Gabr, M. A., and Borden, R. (1988). "Analysis of load deflection response of lateralIy loaded piers using DMT." Penetration testing 1988. /SOPT-1. A. A. Balkema, Rotterdam, The Netherlands, 513-520.

Hannigan, P., Goble, G., Likins, G., and Rausche, F. 2006. Design and construction of driven pile foundations. Number FHWA-NHI-05-042. In Reference manual. Federal Highway Administration, U.S. Department of Transportation, Washington, D.C.

Hoit, M., Hays, C., and McVay, M. C. (1997). "The Florida Pier Analysis Program-methods and models for pier analysis and design." Design and analysis offoundations and sand liquefaction. TRB Rec. No. /569. Transp. Res. Board, Washington, D.C., 1-8.

Hoit, M., McVay, M. C., Hays, C. 0., and Andrade, P. W. (1996). "Nonlinear bridge pier analyses using FLPIER." J. Bridge Engrg., ASCE.

Huang, A., Hsueh, C., O'Neill, M.W., Chern, S., and Chen, C. 2001. Effects of construction on laterally loaded pile groups. Journal of Geotechnical and Geoenvironmental Engineering, 127(5): 385–397. doi:10.1061/(ASCE)1090-0241(2001)127:5(385)

Itasca Inc. 2018. FLAC3D. Version 6.0

Itasca. 2009. FLAC: Fast Lagrangian Analysis of Continua in 3 Dimensions. Version 4.0. Itasca Consulting Group, Inc., Minneapolis, Minn.

J. Brinch Hansen: Simpel beregning af fundamenters baereevne. Insenioren, 22-1-1955

Japan Society of Civil Engineers (JSCE) (2007) Standard Specifications for Concrete Structures (Design) JSCE Guidelines No. 15. 29 p.

Kodikara, J., Haque, A., & Lee, K. Y. (2010). Theeoretical p-y Curves for Laterally Loaded Single Pile in Undrained Clay Using Beizer Curves. Journal of Geotechnical & Geoenvironmental Engineering, 136(1), 265-268.

Kramer, S. L. (1988). Development of p-y curves fro analysis of laterally loaded piles in western Washington. Technical report, Washington State Department of Transportation, Washington.

Lancellotta R. 2007. Lower-bound approach for seismic passive earth resistance. Géotechnique. Vol. 57, No. 3: 319-321.

Larkela, A. 2008. Modeling of a pile group under static lateral loading. Master's thesis, Helsinki University of Technology.

Law, H.K., and Lam, I.P. 2001. Application of periodic boundary for large pile group. Journal of Geotechnical and Geoenvironmental Engineering, 127(10): 889–892. doi:10.1061/(ASCE)1090-0241(2001)127:10(889).

Leonards, G. A. Foundation Engineering. McGraw-Hill, New York, 1962.

Likos, W.J., Lu, N., [2004] "Hysteresis of capillary stress in unsaturated granular soil", Journal of Engineering Mechanics ASCE, Vol. 130, No. 6, pp. 646-655.

Luco J.E (1982) Linear Soil-Structure Interaction: A Review. Earthquake Ground Motions and Its Effects on Structures. Applied Mechanics Division, ASME 53: 41-57.

Mander, J.B., Priestley, M.J.N., Park, R. [1988] "Theoretical stress-strain model for confined concrete", Journal of Structural Engineering (ASCE), Vol. 114, No. 8, pp. 1804-1826.

Matlock, H. (1970). Correlation for Design of Laterally Loaded Piles in Soft Clays. Proceeding of the 2nd Annual OTC. Dallas, Texas.

McVay, M., Casper, R., and Shang, T. 1995. Lateral response of three-row groups in loose to dense sands at 3D and 5D pile spacing. Journal of Geotechnical Engineering, 121(5): 436–441. doi:10.1061/(ASCE)0733-9410(1995)121:5(436).

McVay, M., Zhang, L., Molnit, T., and Lai, P. 1998. Centrifuge testing of large laterally loaded pile groups in sands. Journal of Geotechnical and Geoenvironmental Engineering, 124(10): 1016–1026. doi:10.1061/(ASCE)1090-0241 (1998)124:10(1016).

Morrison, C., and Reese, L.C. 1988. Lateral-load test of a full-scale pile group in sand. Technical report. Geotechnical engineering report CR86-1. U.S. Army Engineer Waterway Experiment Station, Vicksburg, Miss.

O'Neill, M. W., & Gazioglu, S. M. (1984). An Evaluation of p-y Relationships in Clays. American Petoleum Institute Report PRAC 82-41-2.

O'Neill, N. W., and Murchison, J. M. (1983). "An evaluation of p-y relationships in sands." Res. Rep. No. GT-DF02-83. Dept. of Civ. Engrg., Univ. of Houston, Tex.

Patra N. R. and Pise P. J. 2001. Ultimate Lateral Resistance of Pile Groups in Sand. Journal of Geotechnical and Geoenviromental Engineering, ASCE, Vol.127, No. 6: 481-487.

Pedro F. Ruesta1 and Frank C. Townsend. (1997). "Evaluation of Laterally Loaded Pile Group at Roosevelt Bridge" J. Geotech. Geoenviron. Eng., 1997, 123(12): 1153-1161.

Pile Foundations and Pile Structures. In Manual of Engineering Practices, ASCE, No. 27, 1946.

Pile Foundations. In Design Manual Navdocks DM-7, Bureau of Yards and Docks, U.S. Department of the Navy, Washington, D. C, 1963, Ch. 13.

Poulos, H. G. (1971). "Behavior of laterally loaded piles: I-single piles, and II-pile groups." JSMFD, ASCE. 97(5). 711-731, 733-751.

Poulos, H. G. (1973). "Analysis of piles in soil undergoing lateral movement." JSMFD, ASCE. 99(5), 391-405.

provisions: design examples. Federal Emergency Management. Agency. National Institute of Building Sciences, Building Seismic Safety Council, Washington, D.C., chapter 5.

Rahmani, A., Taiebat, M., and Finn, W.D.L. 2014. Nonlinear dynamic analysis of meloland road overpass using three-dimensional continuum modeling approach. Soil Dynamics and Earthquake Engineering, 57: 121–132. doi:10.1016/ j.soildyn.2013.11.004.

Randolph, M. F. (1981). "The response of flexible piles to lateral loads: • Glotechnique, 31(2), 247 -259.

Randolph, M., & Susan, G. (2011). Offshore Geotechnical Engineering. 2 Park Square, Milton Park, Abhingdon, Oxon OX14 4RN: Spon Press.

Reese, L. C., Cox, W. R., & Koop, F. D. (1974). Analysis of Laterally Loaded Piles in Sand. Proceeding of Fifth Annual Offfshore Technical Conference, Paper No. OTC 2080. Houstaon Texas.

Reese, L., & Welch, R. C. (1975). Lateral Loading of Deep Foundations in Stiff Clay. Proceeding, ASCE, Vol 101, No. GT7, pp. 633-649.

Reese, L.C., and van Impe, W.F. 2010. Single piles and pile groups under lateral loading. 2nd ed. CRC Press.

Reese, L.C., Wang, S.T., Arrellaga, J.A., and Hendrix, J. 1996. Computer program GROUP for Windows. Version 4.0. User’s manual. Ensoft Inc., Austin, Tex.

Reese, L.C., Wang, S.T., Arrellaga, J.A., Hendrix, J., and Vasquez, L. 2010. Computer program GROUP. Version 8.0. A program for analysis of group of piles subjected to vertical and lateral loading. User's manual. Ensoft Inc., Austin, Texas.

Richart, F.E., Jr., Hall, J.R., Jr., and Woods, R.D. 1970. Vibrations of soils and foundations (Prentice-Hall International Series in Theoretical and Applied Mechanics). Prentice-Hall, Englewood Cliffs, N.J.

Rollins K.M., Lane J.D., Gerber T.M. 2005. Measured and computed lateral response of a pile group in sand. Journal of Geotechnical and Geoenvironmental Engineering, ASCE, 131 (1): 103 – 114.

Rollins, K.M., and Sparks, A. 2002. Lateral resistance of full-scale pile cap with gravel backfill. Journal of Geotechnical and Geoenvironmental Engineering, 128(9): 711–723. doi:10.1061/(ASCE)1090-0241(2002)128:9(711).

Rollins, K.M., Lane, J.D., and Gerber, T.M. 2005. Measured and computed lateral response of a pile group in sand. Journal of Geotechnical and Geoenvironmental Engineering, 131(1): 103–114. doi:10.1061/(ASCE)1090-0241(2005)131:1(103).

Rollins, K.M., Olsen, K.G., Jensen, D.H., Garrett, B.H., Olsen, R.J., and Egbert, J.J. 2006. Pile spacing effects on lateral pile group behavior: analysis. Journal of Geotechnical and Geoenvironmental Engineering, 132(10): 1272–1283. doi:10.1061/(ASCE)1090-0241(2006)132:10(1272).

Rollins, K.M., Peterson, K.T., and Weaver, T.J. 1998. Lateral load behavior of full-scale pile group in clay. Journal of Geotechnical and Geoenvironmental Engineering, 124(6): 468–478. doi:10.1061/(ASCE)1090-0241(1998)124:6(468).

Ruesta, P., and Townsend, F. 1997. Evaluation of laterally loaded pile group at Roosevelt Bridge. Journal of Geotechnical and Geoenvironmental Engineering, 123(12): 1153–1161. doi:10.1061/(ASCE)1090-0241(1997)123:12(1153).

Russo G. 2016. A method to compute the non-linear behavior of piles under horizontal loading. Soils and Foundations. 56(1): 33–43.

Seed H, Lysmer J (1977) Soil-Structure Interaction Analysis by Finite Element Method. State of the Art. Transactions of the International Conference on Structural Mechanics in Reactor Technology (SMiRT-4). San Francisco. Vol.K. K2/1.

Snyder, J.L. 2004. Full-scale lateral load tests of a 3 × 5 pile group in soft clays and silts. Master's thesis, Brigham Young University.

Springman, S. M. (1989). "Lateral loading on piles due to simulated embankment construction, PhD thesis, Univ. of Cambridge, Cambridge. England.

Stacul S. and Squeglia N. 2018. Analysis Method for Laterally Loaded Pile Groups Using an Advanced Modeling of Reinforced Concrete Sections. Materials,11, 300

Stevens, J. B., & Audibert, J. (1979). Re-examination of P-Y curve formulations. Proceeding of the 11th Annual OTC, Paper No. OTC 3402, pp. 397-403. Houston Texas.

Stewart. D. P., Jewell, R. J., and Randolph, M. F. (1994). "Design of piled bridge abutments on soft clay for loading from lateral soil movements." Glotechnique, 44(2), 277 - 296.

Sullivan, W. R., Reese, L. C., & Fenske, C. W. (1980). Unified Method for Analysis of Laterally Loaded Piles in Clay. Numerical Methods in Offshore Piling, ICE, London.

Viggiani C., Mandolini A., Russo G. 2012. Piles and Pile Foundations. Spon Press.

Viggiani, C. [1981] "Ultimate lateral load on piles used to stabilize landslides", 10th International Conference on Soil Mechanics and Foundation Engineering, Stockholm, Sweden, Balkema, Rotterdam, the Netherlands, Vol. 3, pp. 555-560.

Appendix

A.1 Numerical modeling with FLAC3D:

For the purpose of verification of the numerical and analytical results first a single pile without surrounded soil is modeled in order to compare the Maximum moment of the bottom of the pile subjected to horizontal load at top to the same analytical Maximum moment of one side of the beam, fixed at both ends subjected to horizontal load at the other side.

A pile with Geometry of 20 meters length and 1 meter Diameter modeled and The Meshing of the model on the length is every 0.5 meter which is 41 nodes and 40 couples of nodes (elements) for 20 meter length (vertically) and 360° of the circle divided to 16 parts which every semicircle has $22.5^{\circ}$and every semicircle divided to 6 equal zones from center of the circle, therefore we have 3840 total zones.

Elastic Constitutive Model assigned to the Zone, With zone properties as:

Bulk Modulus: $1.67*10^7$ kN/m^2

Shear Modulus: $1.25*10^7$ kN/m^2

and Density: 2.5 Ton/m^3

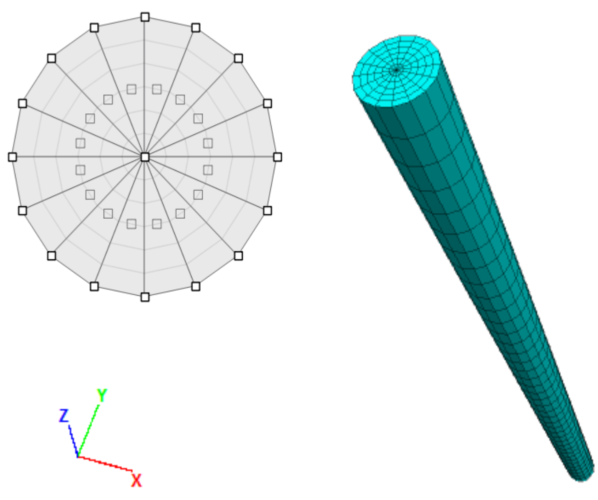

Figure A-1 Model geometry and mesh

In order to Apply Boundary conditions of the model, Boundary surfaces were modeled and Top (Elevation 0 surface) And Bottom (Elevation -20 surface) of the Pile was fixed in all directions x-, y-, z-Axis. As well as Rotation.

In order to Extract the Moment and Forces in different Surfaces of the mesh in different elevation and collecting the results easily, a beam element structed with low stiffness in order to not to affect our results and located at the center of the Pile and meshed in 40 zones every 0.5 meter same as Pile meshing to be matched with intended nodes. Assigned Values to the Pile are as Following:

Young modulus = $3*10^5$ kN/m^2

Poisson Ratio = 0.2

Cross-Sectional-Area = 0.785^e m^2

Moment of inertia-y = 0.0491 m^4 (for circular cross section r =0.5)

Moment of inertia-z = 0.0491 m^4 (for circular cross section r =0.5)

Moment of inertia-Polar = 0

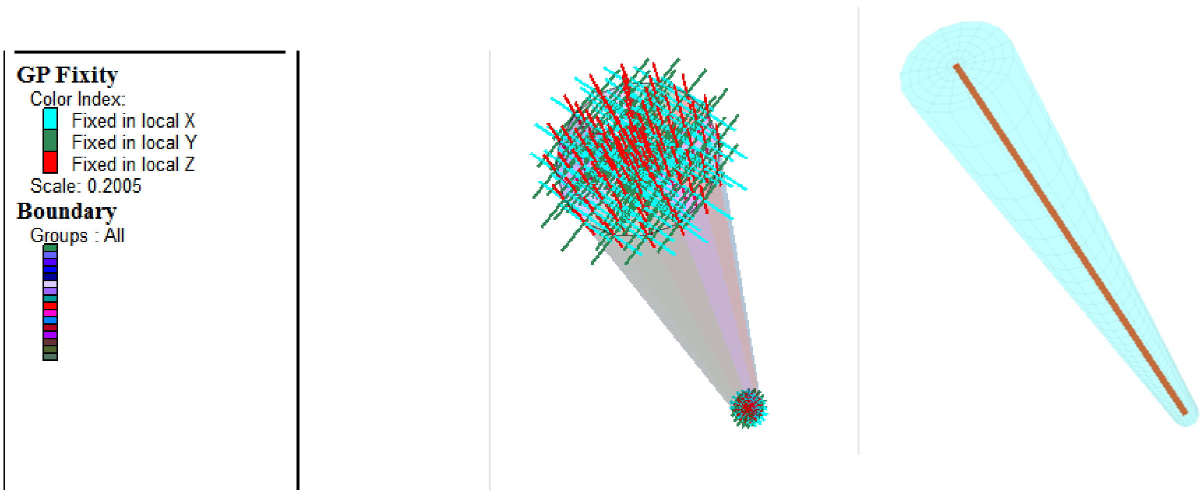

Figure A-2 Boundary conditions and Elastic Beam element inside the pile

A.2 Application of the load:

For Verifying our Analysis Different Loads with different Path of loading (Different Forced displacement as Fixed-Velocities with different number of steps) considering the Final Value of Displacement as u= n_{steps} * (Velocity segment) applied to the top surface of the pile (position (0,0,0)) and the following graphs of Moment History obtained, Finally Velocity forced to be 0 in order to have more clear Maximum Moment from the graph. However, after a sensitivity analysis as much as our slope of the loading pattern would be smaller (smoother loading) the result would be more resultant.

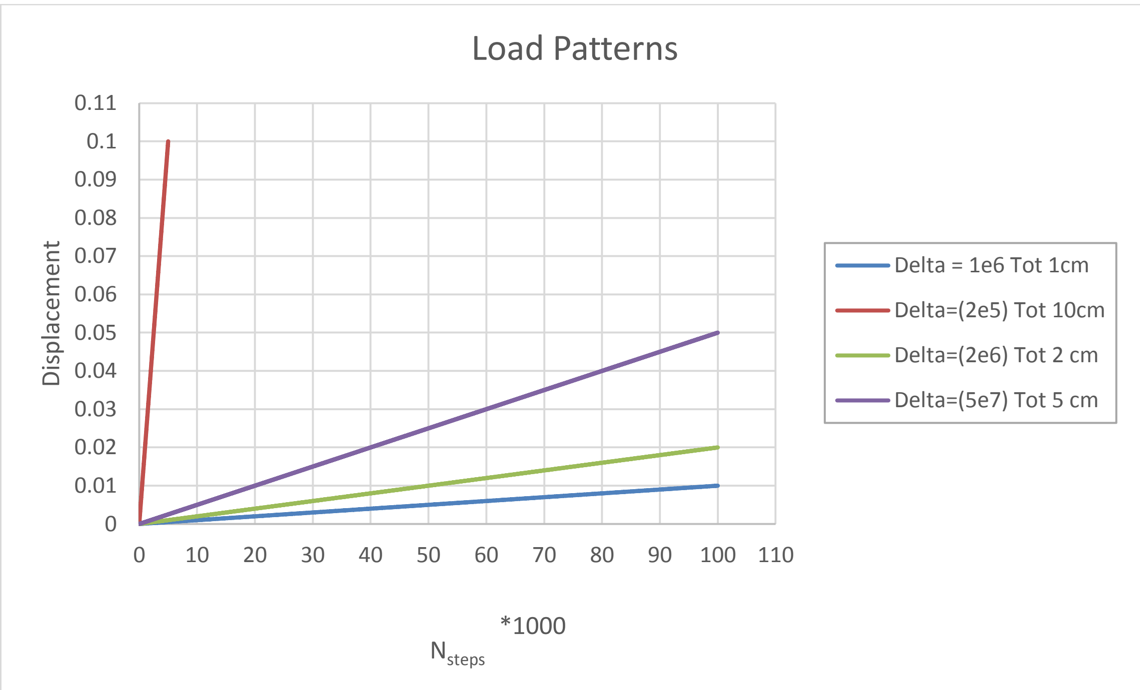

Figure A-3 Different Load Patterns

The Red path loading Delta=(2e5) Tot 10cm which is kind of instant loading pattern, was applied in order to have the most instability and can check the results.

For reading the results, as in FLAC3D Scripts and formulations elements are defined as end 1 and end 2 and end 2 of one element has the same position as end 1 of the next element, in order to verify the results, we checked whether the Values are the same in this order or not for some couple of nodes and different loadings. Therefore, moment History extracted in order to check for couple of nodes where we have more moment (z = -19.5 & z = -18.5). in the graphs My1b correspond to the Moment history of the End 2 of the element 1 and My2a for End 1 of the element 2 and so on.

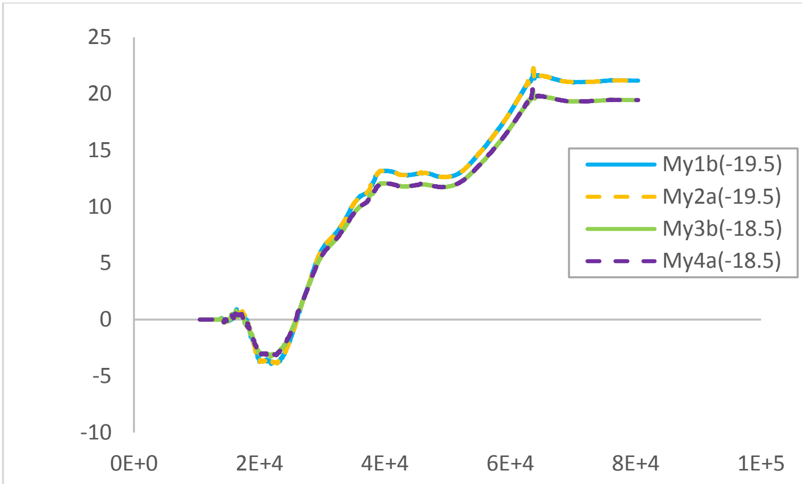

Figure A-4 Results of moment history at End2 of one Element with End1 of the next Element For 10CM displacement

As we can see from the graphs, the results are matched, and the values corresponds to the end of one element are the same as values for the beginning of the next element. This convergency is mandatory in any FEM methods and shows the continuous modeling. From the graphs above Maximum moment can be obtained where there is convergency:

Put all data on the same table

Load (m/1s)	**0.01**	**0.02**	**0.05**	**0.1**
M_{max} Numerical [kN.m]	2.19512	4.39151	11.00245	21.89125

Table A-1 Moment Values at different stages of applied displacement

A.3 Analytical solution:

Analytically Maximum Displacement of the Beam fixed at both ends with concentrated load at one end is:

$\Delta_{max} = \frac{M_{max} L^2}{6EI}$ where M_{max} is max moment (reaction) which is caused by applied force, L is the arm of the load (20m) E young’s modulus of the beam ($3*10^5$ N/m^2) and I moment of inertia of the cross section (0.0491 m^4).

$$M_{max} = \frac{\Delta_{max} 6EI}{L^2} \text{ which is:}$$

Δ_{max}	0.01	0.02	0.05	0.1
M_{max} Numerical [kN.m]	2.19512	4.39151	11.00245	21.89125
M_{max} Analytical [kN.m]	2.2	4.4	11	22

Table A-2 Moment Values for different displacement

Finally, we can compare the results obtained by numerical calculation of FLAC3d with Analytical solutions to check whether they are convergence or not. As we can see from tables 3 and 4 the results are very close which proves that the calculation is correct and the negligible difference between the results is due to boundary condition and the way how FLac3d considers fixity.

A.4 Scripts used in FLAC3D:

A.4.1 Geometry modeling

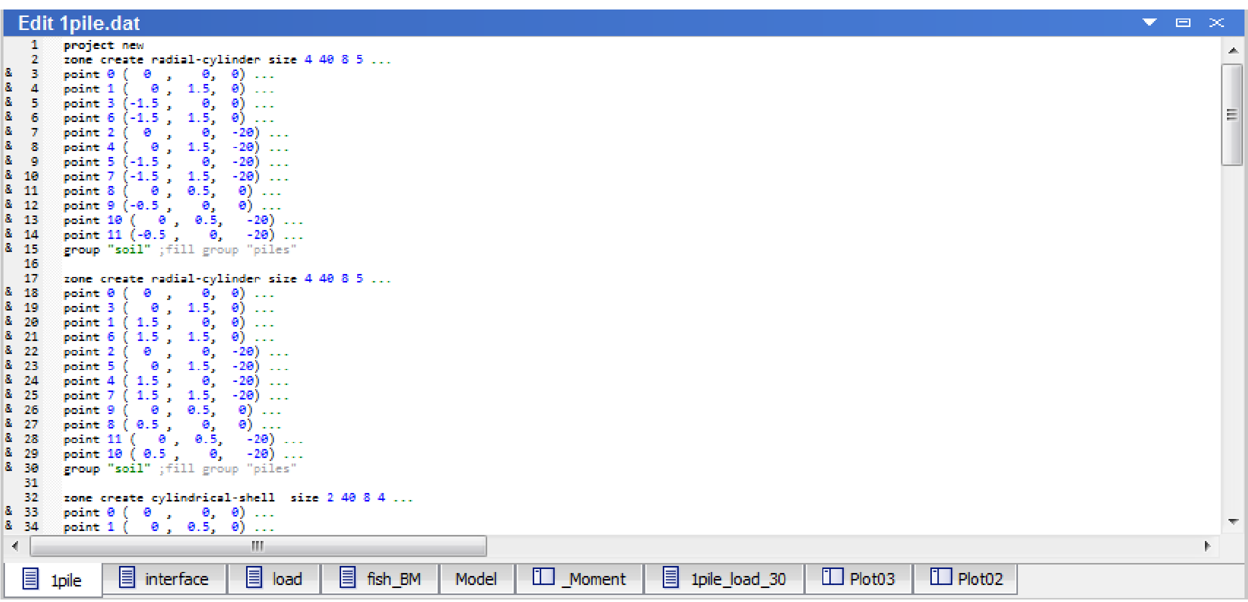
Edit 1pile.dat

```
project new
zone create radial-cylinder size 4 40 8 5 ...
point 0 (  0  ,    0,  0) ...
point 1 (    0 ,  1.5,  0) ...
point 3 (-1.5 ,    0,  0) ...
point 6 (-1.5 ,  1.5,  0) ...
point 2 (  0  ,    0,  -20) ...
point 4 (    0 ,  1.5,  -20) ...
point 5 (-1.5 ,    0,  -20) ...
point 7 (-1.5 ,  1.5,  -20) ...
point 8 (    0 ,  0.5,   0) ...
point 9 (-0.5 ,    0,   0) ...
point 10 (    0 ,  0.5,   -20) ...
point 11 (-0.5 ,    0,   -20) ...
group "soil" ;fill group "piles"

zone create radial-cylinder size 4 40 8 5 ...
point 0 (  0  ,    0,  0) ...
point 3 (    0 ,  1.5,  0) ...
point 1 ( 1.5 ,    0,  0) ...
point 6 ( 1.5 ,  1.5,  0) ...
point 2 (  0  ,    0,  -20) ...
point 5 (    0 ,  1.5,  -20) ...
point 4 ( 1.5 ,    0,  -20) ...
point 7 ( 1.5 ,  1.5,  -20) ...
point 9 (    0 ,  0.5,   0) ...
point 8 ( 0.5 ,    0,   0) ...
point 11 (    0 ,  0.5,   -20) ...
point 10 ( 0.5 ,    0,   -20) ...
group "soil" ;fill group "piles"

zone create cylindrical-shell  size 2 40 8 4 ...
point 0 (  0  ,    0,  0) ...
point 1 (    0 ,  0.5,  0) ...
```


Figure A-5 Geometry Script in FLAC3D (a)

```
point 3 (-0.5 ,    0,  0) ...
point 2 (  0  ,    0,  -20) ...
point 4 (   0 ,  0.5,  -20) ...
point 5 (-0.5 ,    0,  -20) ...
point 8 (   0 ,  0.45,   0) ...
point 9 (-0.45 ,    0,   0) ...
point 10 (   0 ,  0.45,   -20) ...
point 11 (-0.45 ,    0,   -20) ...
group "piles" fill group "soil_int"

zone create cylindrical-shell  size 2 40 8 4 ...
point 0 (  0  ,    0,  0) ...
point 3 (   0 ,  0.5,  0) ...
point 1 ( 0.5 ,    0,  0) ...
point 2 (  0  ,    0,  -20) ...
point 5 (   0 ,  0.5,  -20) ...
point 4 ( 0.5 ,    0,  -20) ...
point 9 (   0 ,  0.45,   0) ...
point 8 ( 0.45 ,    0,   0) ...
point 11 (   0 ,  0.45,   -20) ...
point 10 ( 0.45 ,    0,   -20) ...
group "piles" fill group "soil_int"

;ccccccccccccccccccccccccccccccccccczone copy (3,0 0) range position (-1.50, 0,-20) (1.50,1.50,0)
;ccccccccccccccccccccccccccccccccccczone copy (-3,0 0) range position (-1.50, 0,-20) (1.50,1.50,0)

;cccccccccccccccccccccczone reflect normal (0,1,0) origin (0,1.5,0) range position (-4.50, 0,-20) (4.50,1.50,0)
;ccccccccccccccccccccccccccccccccczone reflect normal (0,1,0) origin (0,3,0)   range position (-4.50, 1.5,-20) (4.50,3,0)

zone copy (0,0 2) range group "piles" position (-4.50, 0,-2) (4.5,4.50,0)
zone group "stem" range position (-4.50, 0,0) (4.5,4.50,99)
zone densify local segments 1,4,1 range group "stem"

zone create radial-tunnel size 4 40 4 10 ...
```

1pile | interface | load | fish_BM | Model | _Moment | 1pile_load_30 | Plot03 | Plot02

Figure A-6 Geometry Script in FLAC3D (b)

Edit 1pile.dat

```
point 0 (   0  ,    0,  0) ...
point 1 (   0 ,   25,  0) ...
point 3 (-25 ,    0,  0) ...
point 6 (-25 ,  25,  0) ...
point 2 (  0  ,    0,  -20) ...
point 4 (   0 ,  25,  -20) ...
point 5 (-25 ,    0,  -20) ...
point 7 (-25 ,  25,  -20) ...
point 8 (   0 ,  1.5,   0) ...
point 9 (-1.5 ,    0,   0) ...
point 10 (   0 ,  1.5,   -20) ...
point 11 (-1.5 ,    0,   -20) ...
point 12 (-1.5 ,  1.5,     0)...
point 13 (-1.5 ,  1.5,   -20)...
group "soil" ratio 1 1 1 1.5


zone create radial-tunnel size 4 40 4 10 ...
point 0 (   0  ,    0,  0) ...
point 3 (   0 ,   25,  0) ...
point 1 (25 ,    0,  0) ...
point 6 (25 ,  25,  0) ...
point 2 (  0  ,    0,  -20) ...
point 5 (   0 ,  25,  -20) ...
point 4 (25 ,    0,  -20) ...
point 7 (25 ,  25,  -20) ...
point 9 (   0 ,  1.5,   0) ...
point 8 (1.5 ,    0,   0) ...
point 11 (   0 ,  1.5,   -20) ...
point 10 (1.5 ,    0,   -20) ...
point 12 (1.5 ,  1.5,     0)...
point 13 (1.5 ,  1.5,   -20)...
group "soil" ratio 1 1 1 1.5
```

1pile | interface | load | fish_BM | Model | _Moment | 1pile_load_30 | Plot03 | Plot02

Figure A-7 Geometry Script in FLAC3D (c)

Edit 1pile.dat

```
zone gridpoint fix velocity-y range position-y 0
zone gridpoint fix velocity-y range position-y 25

zone gridpoint fix velocity-x range position-x -25
zone gridpoint fix velocity-x range position-x 25

zone gridpoint fix velocity-z range position-z -30
;cccccccccccccccccccccccccccreturn


;
; ccccccccccccccccccccccccccccccccInitialize gravity, pore-pressures, density, and stres state
model gravity 9.81
;cccccccccccccccccccccccccccccccccc water table information
;zone water density 1
;zone water plane origin (0,0,-99) normal (0,0,-1)
zone initialize density 1.80
zone initialize density  0.001 range group  'stem'
;
zone cmodel assign mohr-coulomb
zone property bulk 8.333e4  shear 3.846e4  cohesion 0 fric 36
;1st case bulk and shear   /2
;second case with actual values but large strain off
;3rd with 00 deleted from druccker cohesion in intgerface
zone cmodel assign elastic   range group 'pile' or 'stem'
zone property bulk 8.333e4  shear 3.846e4 range group 'pile' or 'stem'
zone initialize-stress ratio 0.50


;cccccccccccccccccccccccccccccccccccSolve to initial equilibrium
zone ratio local
model solve ratio 1e-4
model save 'initial'

```

1pile | interface | load | fish_BM | Model | _Moment | 1pile_load_30 | Plot03 | Plot02

Figure A-8 Geometry Script in FLAC3D (d)

A.4.2 Interface

Edit interface.f3dat

```
model new
model restore "initial"
zone property cohesion 0 fric 30  range group 'soil'

;azzero gli spostamenti
;
zone gridpoint initialize displacement 0.0,0.0,0.0
zone gridpoint initialize velocity 0.0,0.0,0.0
fish define tot_reac
    local total = 0.0
    loop foreach local bb gp.list
        local level = gp.pos.z(bb)
        if level >=0.0 then
            total = total + gp.force.unbal.x(bb)
        end_if
    end_loop
    tot_reac = total
end
;@tot_reac

model history name "unbalanced" mechanical unbalanced-maximum
fish history  @tot_reac
zone history name "top" displacement-x position (-0.5,0,2)
;
; zone property young 8.723e7 poisson 0.15 tension 1200000 cohesion-drucker 26846 ...
zone cmodel assign drucker-prager   range group 'piles' or 'stem'
zone property young 8.723e7 poisson 0.15 tension 1200000 cohesion-drucker 2684600 ...
            friction-drucker 0 ...
            range group 'piles' or 'stem'
;
zone cmodel assign null range group "soil_int"

zone select true  group "Default=stem" only by zone
```

1pile | interface | load | fish_BM | Model | _Moment | 1pile_load_30 | Plot03 | Plot02

Figure A-9 Interface Modeling in FLAC3D (a)

Edit interface.f3dat

```
zone select true  group "Default=stem" only by zone
zone hide range selected
zone select off
zone select true  group "Default=piles" only by zone
zone hide range selected
zone select off
zone face select  skin begin (1.23333,-13.2546,10.1002) direction (-0.0665874,0.772918,-0.631002) break-angle 45
zone face group "laterale" slot "Default" internal range selected
zone face select off internal use-hidden-zones
;zone face select  skin begin (0.585392,-6.58378,-4.83295) direction (-0.0362288,0.406374,-0.912988) break-angle
;zone face group "fondo" slot "Default" internal range selected
;zone face select off internal use-hidden-zones
zone hide off range use-hidden

zone interface "lat" create by-face separate range group "laterale"
;zone interface "bottom" create by-face separate range group "fondo"

; k = coef * (K + 4/3 G) / d_z
;   K   8.33E+04
;   G   3.85E+04
;   d_z 0.25
;   coef    5
;   kn = ks      2.69E+06

zone interface "lat" node property stiffness-normal 5e6 stiffness-shear 5e6 tension 0 cohesion 0 friction 21
;zone interface "bottom" node property stiffness-normal 1e9 stiffness-shear 1e9 tension 0 cohesion 1 friction 25

zone interface "lat" node initialize-stresses


model solve
model save "interface"
```

1pile | interface | load | fish_BM | Model | _Moment | 1pile_load_30 | Plot03 | Plot02

Figure A-10 Interface Modeling in FLAC3D (b)

A.4.3 Application of the load

Edit load.f3dat

```
model new
model restore "interface"

zone gridpoint fix vel-x 0 range group 'stem'
zone gridpoint fix vel-y 0 range group 'stem'
zone gridpoint fix vel-z 0 range group 'stem'

zone history name 'disp' displacement-x position (-0.5,0,0)
model largestrain off

zone gridpoint fix velocity-x 2e-6 range group 'stem'
cycle 5000
zone gridpoint fix velocity-x 0 range group 'stem'
solve ratio-local 1e-3
model save '1pile_1cm.f3sav'

zone gridpoint fix velocity-x 2e-6 range group 'stem'
cycle 7500
zone gridpoint fix velocity-x 0 range group 'stem'
solve ratio-local 1e-3
model save '1pile_2p5cm.f3sav'

zone gridpoint fix velocity-x 2e-6 range group 'stem'
cycle 12500
zone gridpoint fix velocity-x 0 range group 'stem'
solve ratio-local 1e-3
model save '1pile_5cm.f3sav'

zone gridpoint fix velocity-x 2e-6 range group 'stem'
cycle 25000
zone gridpoint fix velocity-x 0 range group 'stem'
solve ratio-local 1e-3
model save '1pile_10cm.f3sav'
```

1pile | interface | load | fish_BM | Model | _Moment | 1pile_load_30 | Plot03 | Plot02

Figure A-11 Application of the load in FLAC3D

A.4.4 Fish Coding for extraction of the results:

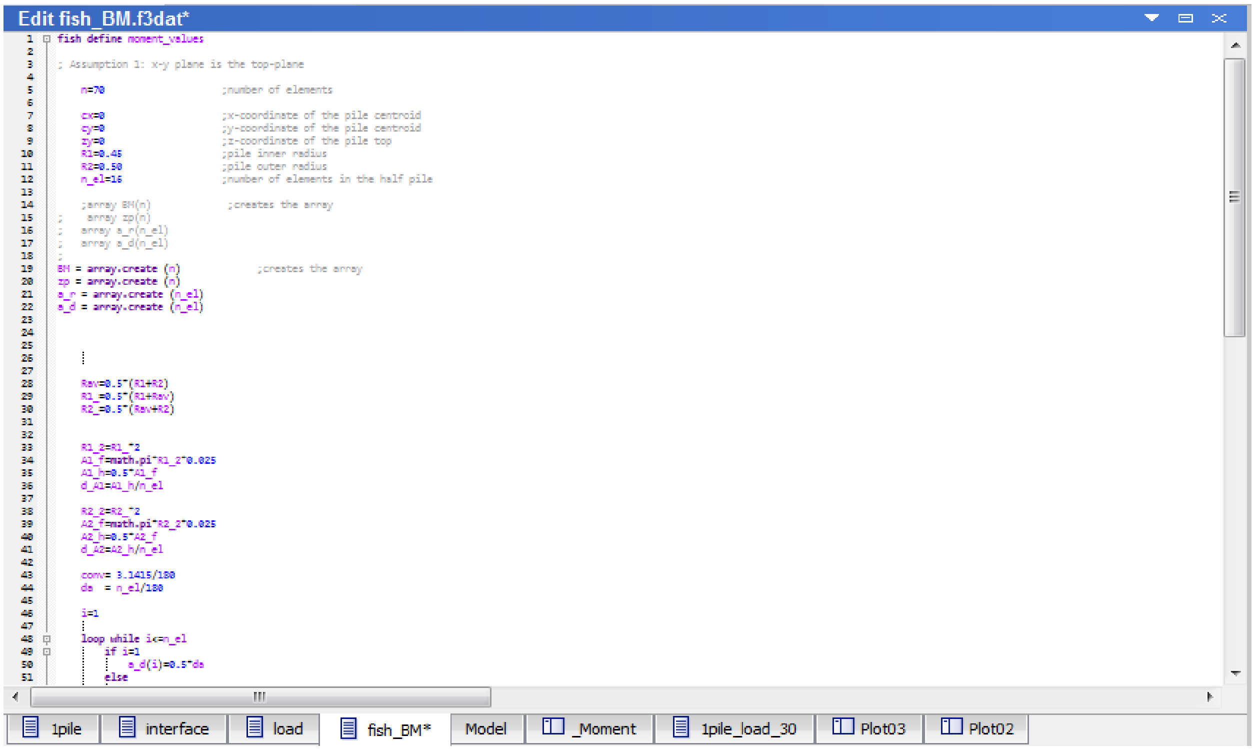


```
fish define moment_values

; Assumption 1: x-y plane is the top-plane

    n=70                    ;number of elements

    cx=0                    ;x-coordinate of the pile centroid
    cy=0                    ;y-coordinate of the pile centroid
    zy=0                    ;z-coordinate of the pile top
    R1=0.45                 ;pile inner radius
    R2=0.50                 ;pile outer radius
    n_el=16                 ;number of elements in the half pile

    ;array BM(n)             ;creates the array
;     array zp(n)
;    array a_r(n_el)
;    array a_d(n_el)
;
BM = array.create (n)            ;creates the array
zp = array.create (n)
a_r = array.create (n_el)
a_d = array.create (n_el)




    Rav=0.5*(R1+R2)
    R1_=0.5*(R1+Rav)
    R2_=0.5*(Rav+R2)


    R1_2=R1_^2
    A1_f=math.pi*R1_2*0.025
    A1_h=0.5*A1_f
    d_A1=A1_h/n_el

    R2_2=R2_^2
    A2_f=math.pi*R2_2*0.025
    A2_h=0.5*A2_f
    d_A2=A2_h/n_el

    conv= 3.1415/180
    da  = n_el/180

    i=1

    loop while i<=n_el
        if i=1
            a_d(i)=0.5*da
        else
```

Figure A-12 Fish Coding in FLAC3D (a)

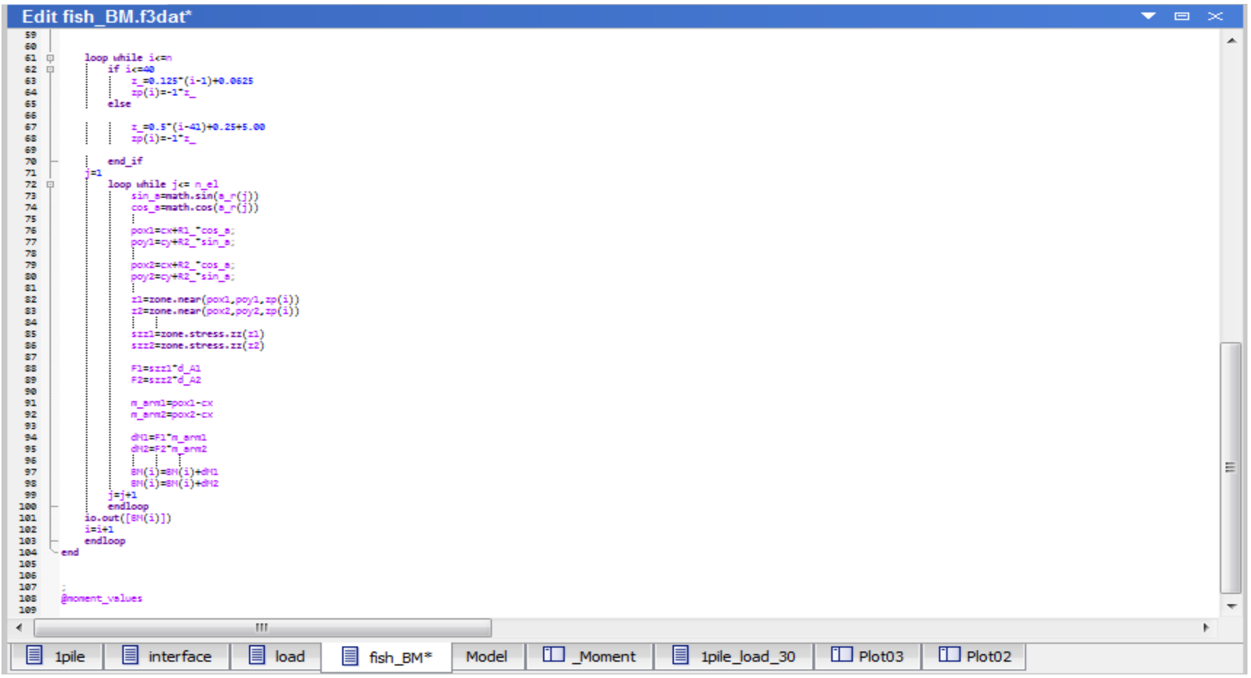


```


    loop while i<=n
        if i<=40
            z_=0.125*(i-1)+0.0625
            zp(i)=-1*z_
        else

            z_=0.5*(i-41)+0.25+5.00
            zp(i)=-1*z_

        end_if
    j=1
        loop while j<= n_el
            sin_a=math.sin(a_r(j))
            cos_a=math.cos(a_r(j))

            pox1=cx+R1_*cos_a;
            poy1=cy+R2_*sin_a;

            pox2=cx+R2_*cos_a;
            poy2=cy+R2_*sin_a;

            z1=zone.near(pox1,poy1,zp(i))
            z2=zone.near(pox2,poy2,zp(i))

            szz1=zone.stress.zz(z1)
            szz2=zone.stress.zz(z2)

            F1=szz1*d_A1
            F2=szz2*d_A2

            m_arm1=pox1-cx
            m_arm2=pox2-cx

            dM1=F1*m_arm1
            dM2=F2*m_arm2

            BM(i)=BM(i)+dM1
            BM(i)=BM(i)+dM2
        j=j+1
        endloop
    io.out([BM(i)])
    i=i+1
    endloop
end


;
@moment_values

```

Figure A-13 Fish Coding in FLAC3D (b)

A.5 Some Screenshots from Seismostruct Modeling:

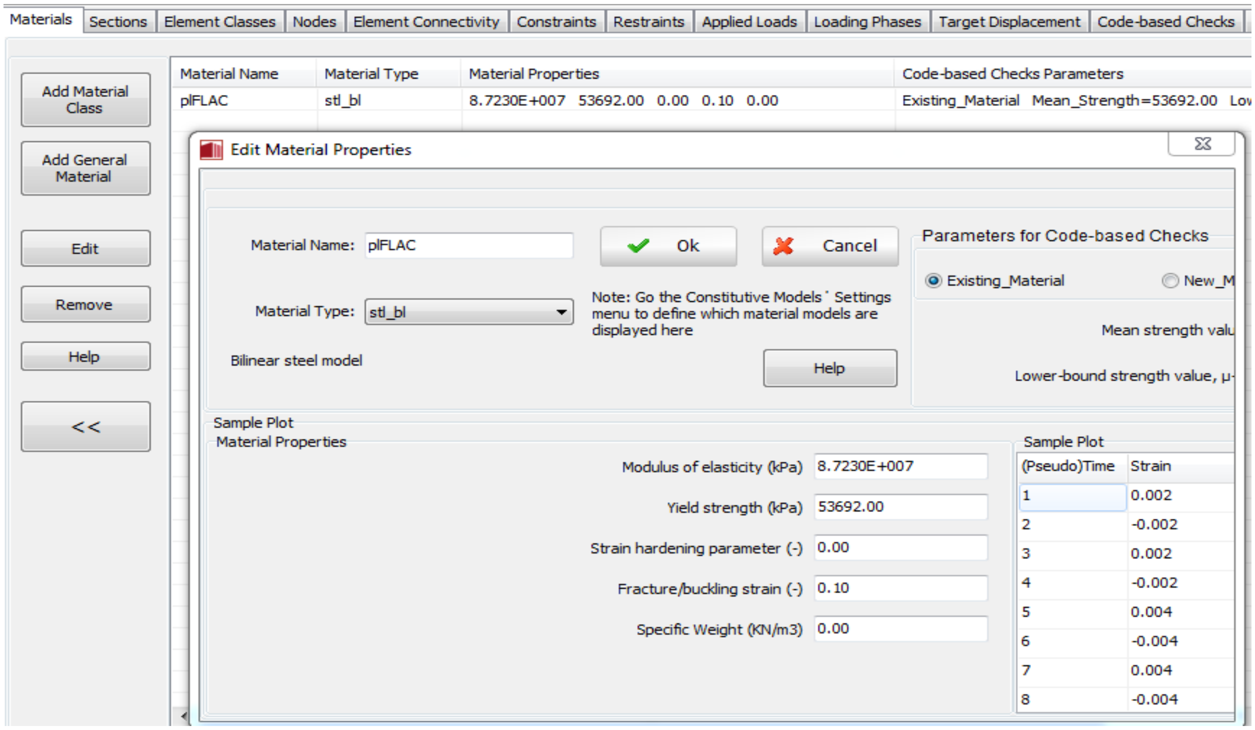

Figure A-14 Material Defining In Seismostruct

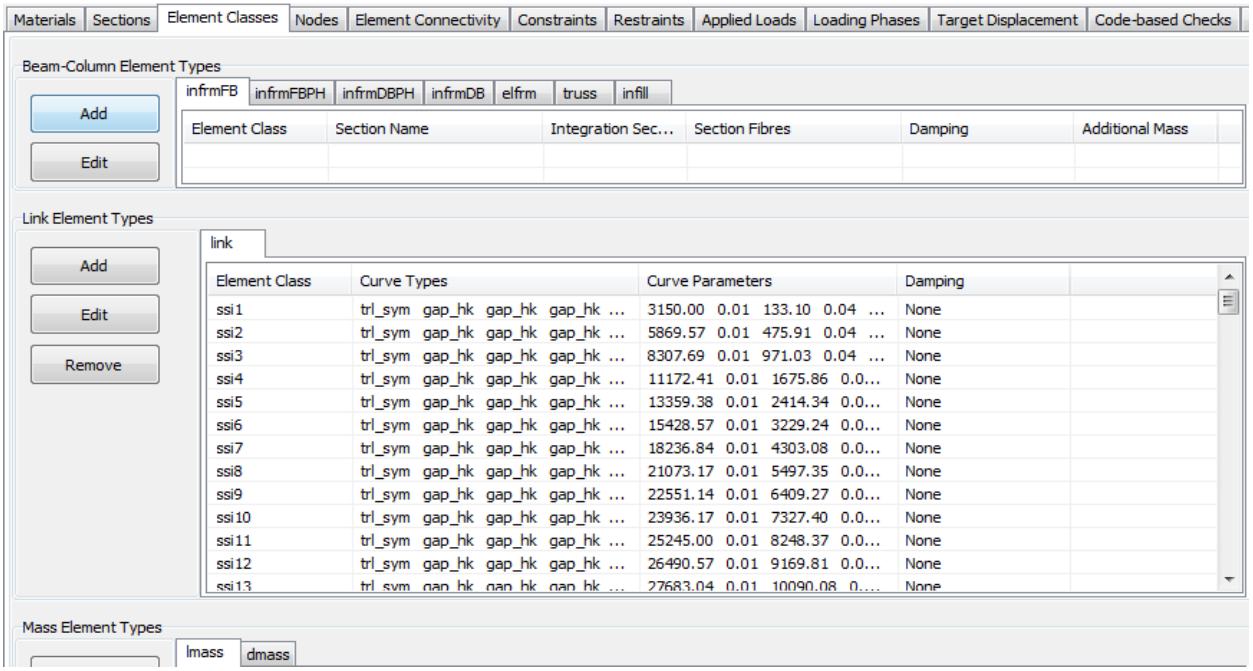

Figure A-15 Element Class in Seismostruct

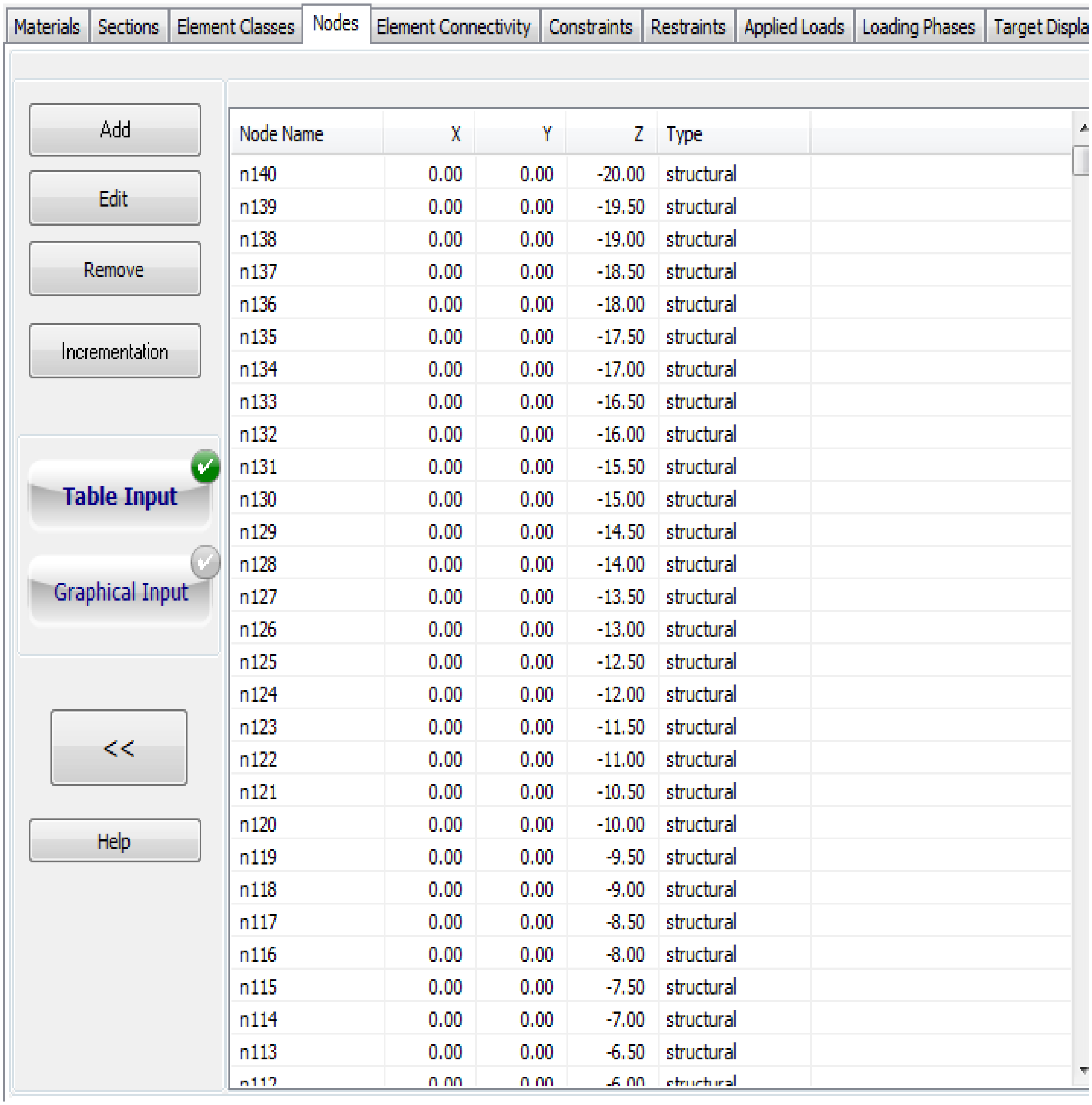

Figure A-16 Nodes and meshing illustration in seismostruct

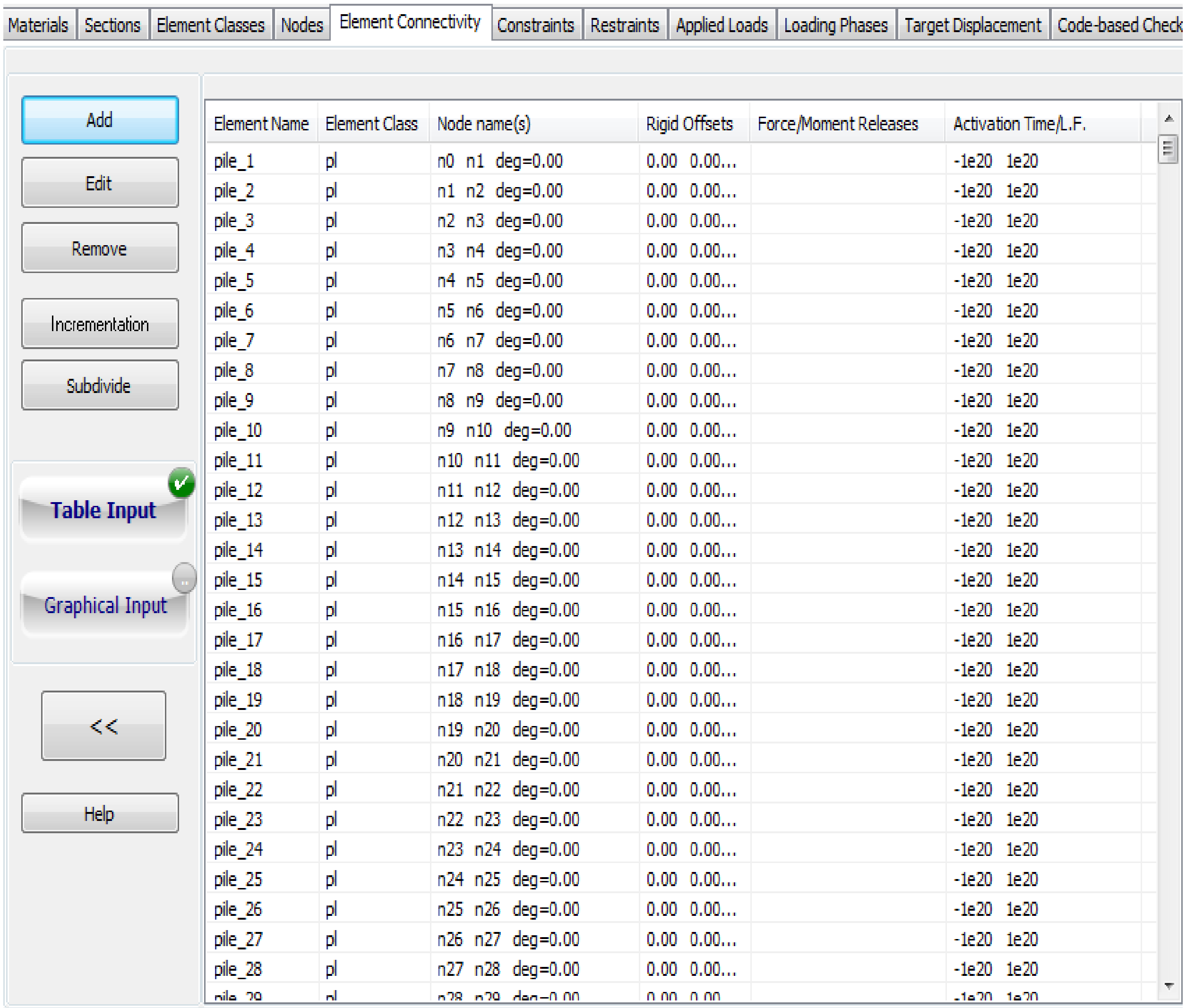

Figure A-17 Element connectivity to the nodes defined in seismostruct

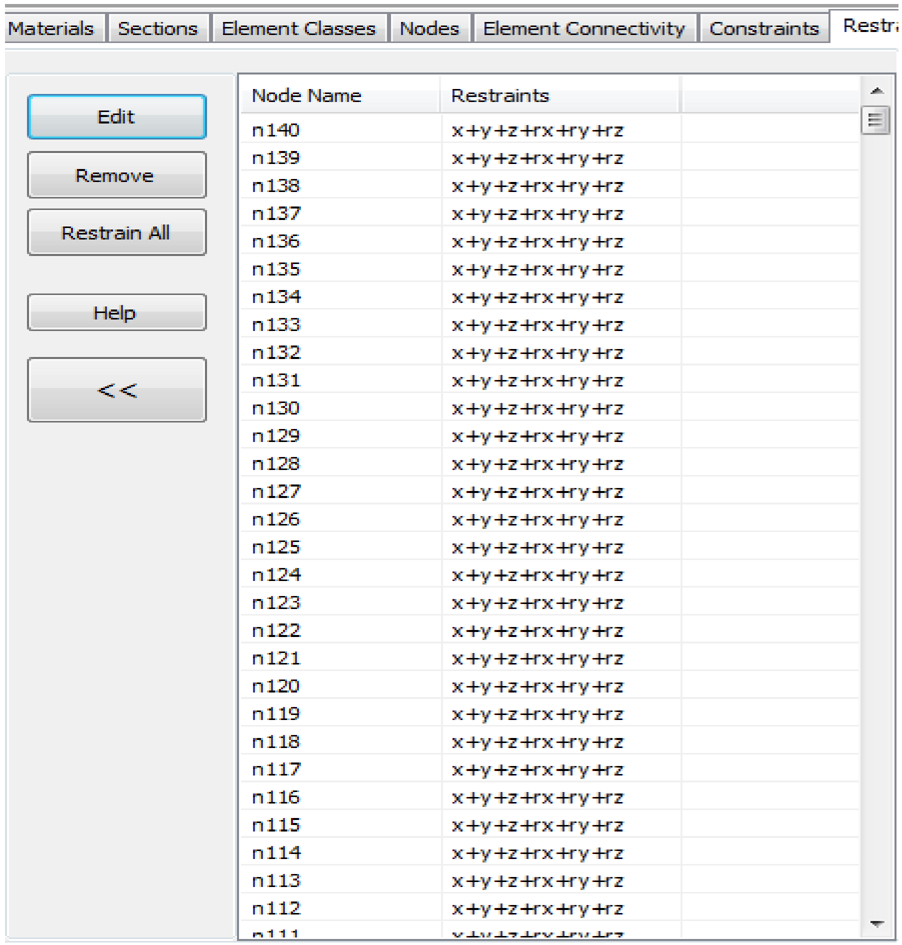

Figure A-18 Restrains In seismostruct

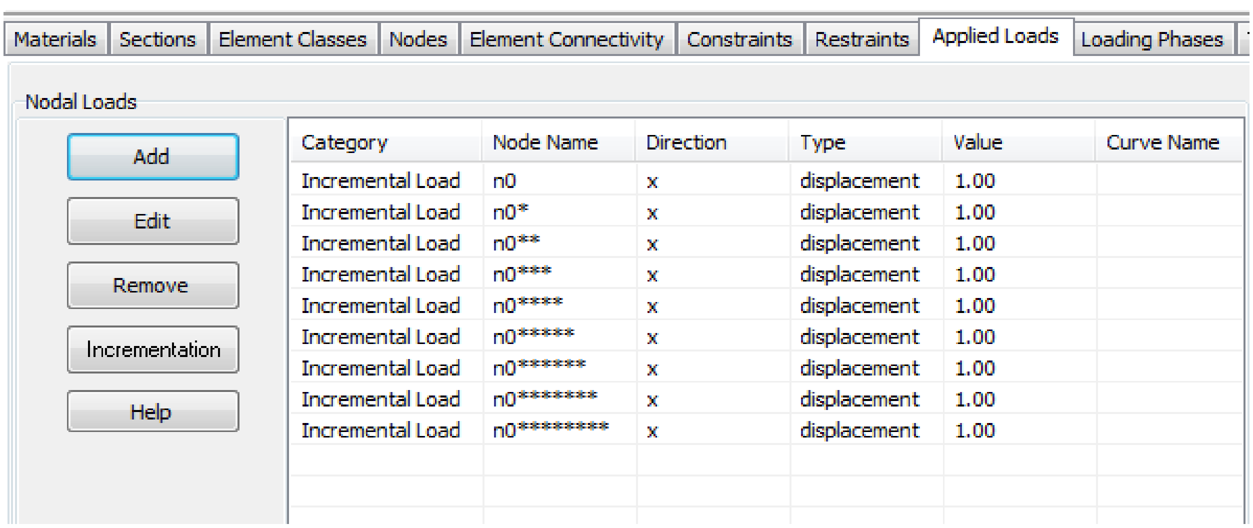

Figure A-19 Application of the load in Seismostruct

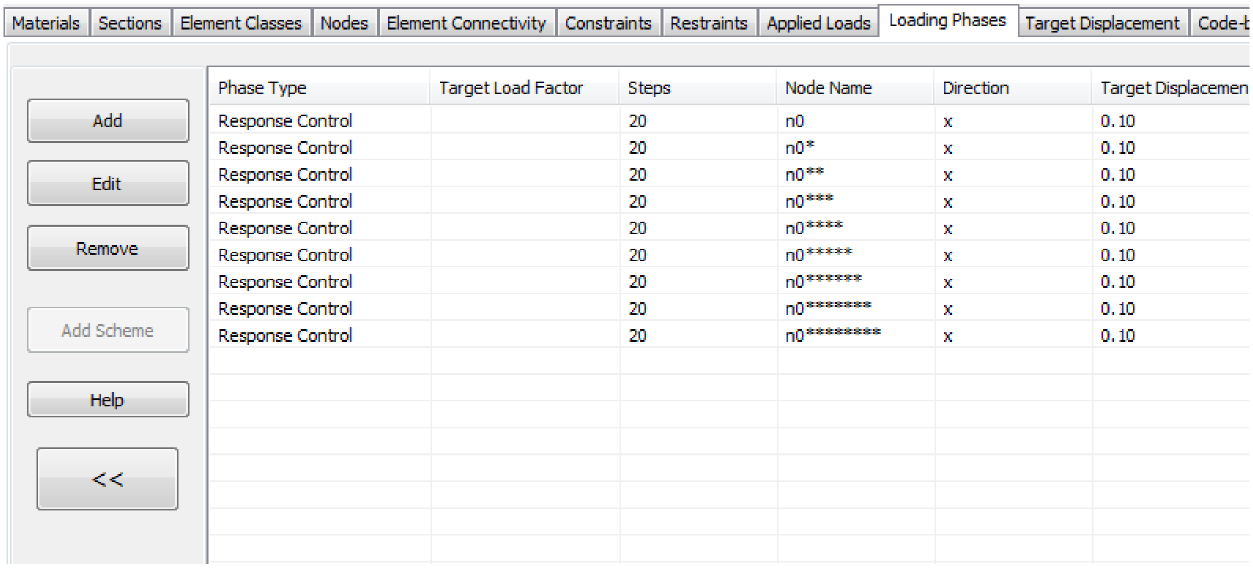

Phase Type	Target Load Factor	Steps	Node Name	Direction	Target Displacemen
Response Control		20	n0	x	0.10
Response Control		20	n0*	x	0.10
Response Control		20	n0**	x	0.10
Response Control		20	n0***	x	0.10
Response Control		20	n0****	x	0.10
Response Control		20	n0*****	x	0.10
Response Control		20	n0******	x	0.10
Response Control		20	n0*******	x	0.10
Response Control		20	n0********	x	0.10

Figure A-20 Loading phases in Seismostruct

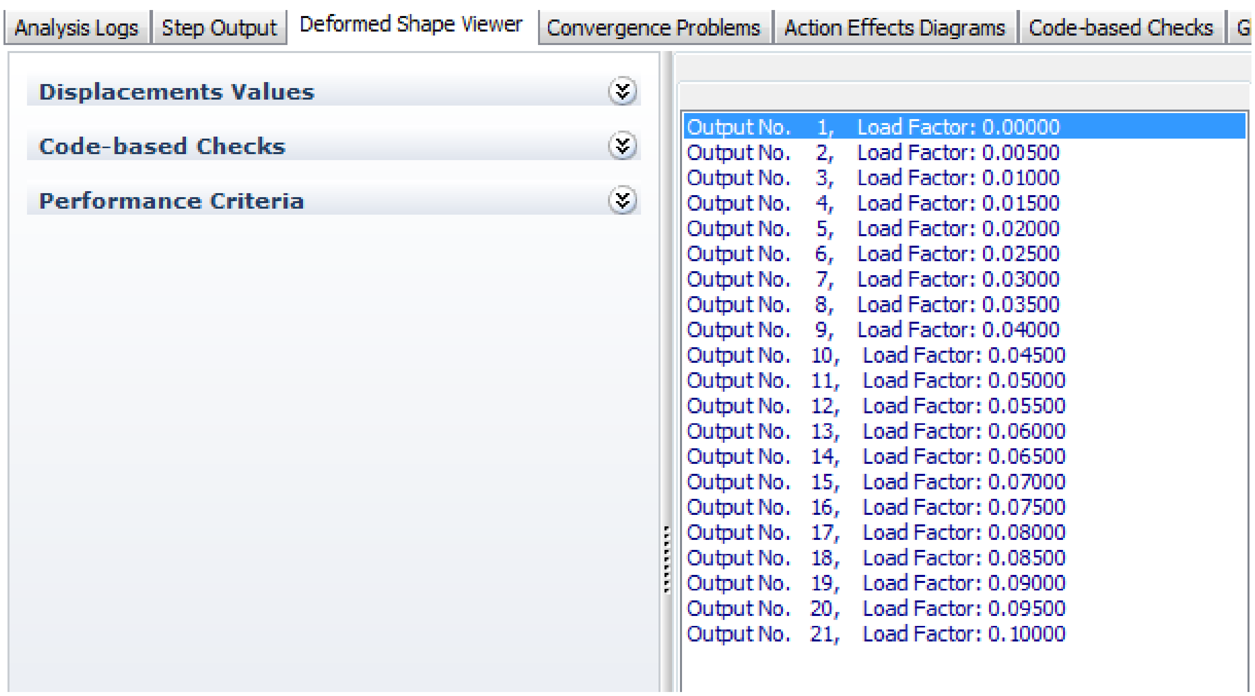

Figure A-21 Post Process and output result in Seismostruct